The Dissertation Committee for Chunxiao Zhu Certifies that this is the approved version of the following dissertation:

NMR Longitudinal Surface Relaxation Phenomena of Metal Oxide Nanoparticles in Porous Media

Committee:

Hugh C. Daigle, Supervisor

Steven L. Bryant

Carlos Torres-Verdin

David A. DiCarlo

Thomas E. Milner

NMR Longitudinal Surface Relaxation Phenomena of Metal Oxide Nanoparticles in Porous Media

by

Chunxiao Zhu

Dissertation

Presented to the Faculty of the Graduate School of

The University of Texas at Austin

in Partial Fulfillment

of the Requirements

for the Degree of

Doctor of Philosophy

The University of Texas at Austin

August 2017

Dedication

This is dedicated to my beloved parents, my dear husband, and little daughter.

Acknowledgements

This work was funded by University of Texas at Austin Nanoparticles for Subsurface Engineering Industry Affiliates Program member companies (Maersk Oil, Petrobras, Nissan Chemical America Corporation, Baker Hughes, Wintershall, and the Foundation CMG). I additionally acknowledge Nissan Chemical America Corporation for providing the zirconia nanoparticle dispersions; and Dr. Jimmie Baran of 3M for providing the silica nanoparticles. I thank Dr. David Medellin for providing Matlab support to obtain relaxation time of saturated Boise sandstone cores. The NMR inversion code used in this study was provided by UT Austin's Research Consortium on Formation Evaluation. I thank Dr. Hugo Celio at the Texas Materials Institute at the University of Texas at Austin for offering DLS ZetaSizer and TGA to test properties of nanoparticles, as well as performing XPS to check nanoparticles composition and presence of surface coating.

NMR Longitudinal Surface Relaxation Phenomena of Metal Oxide Nanoparticles in Porous Media

Chunxiao Zhu, Ph.D.

The University of Texas at Austin, 2017

Supervisor: Hugh Daigle

^{1}H Nuclear Magnetic Resonance (NMR) has long been applied in downhole logging and laboratory analyses to investigate pore size distributions of rocks through correlation with measured relaxation time distributions. However, due to the inherent chemical heterogeneity of pore surfaces in rock, the pore surface relaxivity, which links relaxation time and pore size, varies throughout the pore system. I seek to modify and control the surface relaxivity in natural porous media through coating of paramagnetic nanoparticles so that NMR measurements can be used to compute pore sizes directly.

I chose zirconia nanoparticle dispersions with opposite surface charge but similar size. The absence of surface coating on zirconia nanoparticles simplified the calculation of nanoparticle surface relaxivity and interactions between nanoparticles and pore walls. Glass bead packs and Boise sandstone cores were saturated with positively charged zirconia nanoparticle dispersions in which nanoparticles can be electrostatically adsorbed onto pore surfaces, while negatively charged zirconia nanoparticle dispersions were employed as a control group to provide the baseline of nanoparticle retention due to non-electrostatic attraction. When 1.114 vol. % positively charged zirconia nanoparticles dispersion was used to saturate a glass bead pack, 11.6% of the nanoparticles were adsorbed to the bead surfaces and modified the glass bead surface relaxivity.

I performed core flushing with DI water, pure acid and alkali, and compared properties of zirconia nanoparticles before and after exposure to Boise sandstone. After 2 pore volumes of core flooding, there was around 3% of negatively charged nanoparticles trapped in Boise sandstone core while around 30% to 40% of positively charged nanoparticles were retained in Boise sandstone cores. The results indicated that besides van der Waals attraction, electrostatic attraction is the driving force for retention of nanoparticles with positive surface charge in sandstone cores. Full coverage of nanoparticles onto sandstone surface was not achieved. The attachment of nanoparticles onto sandstone surface changed the mineral surface relaxivity. After contact with Boise sandstone, nanoparticles themselves exhibited increased relaxivity due to interactions between nanofluids and mineral surface under different pH conditions. The complicated interactions between nanofluids and pore surfaces make it difficult to predict sandstone surface relaxivity with attached nanoparticles.

Since adsorption of nanoparticles changed the pore surface relaxivity, it is crucial to know nanoparticle relaxivity and factors that may affect the relaxivity of nanoparticles. T_1 values of zirconia nanoparticle dispersions before and after mixing with various Fe(III) solutions were measured and compared. Adsorption of iron onto zirconia nanoparticles was confirmed based on measurements of aqueous Fe remaining in supernatants. Adsorbed iron increases zirconia nanoparticles' surface relaxivity, as the relaxation rate of zirconia nanoparticles increased with the amount of adsorbed Fe(III).

Besides adsorbed paramagnetic species, surface coatings also play a role in changing nanoparticle surface relaxivity. Since organic surface coatings usually give a small value of relaxivity, it is better to use a nanoparticle core with high relaxivity as to investigate the effect of organic surface coatings. I examined the relaxation properties of (3-Aminopropyl)triethoxysilane (APTES) coated Fe_3O_4 nanoparticles in mixtures with

different D_2O volume fractions. Fe_3O_4 nanoparticles exhibited decreased relaxivity with more APTES coating. The presence of D_2O affects proton-proton relaxation but not electron-proton relaxation. Comparison of relaxivity of APTES coated Fe_3O_4 nanoparticles with different coating amount and D_2O volume fractions indicated that at relatively high Fe concentration, when electron-proton interaction dominates surface relaxation, hydrogen atoms in the APTES did not significantly alter the surface relaxation mechanism of nanoparticles. At lower Fe_3O_4 concentration, proton-proton relaxation brought by APTES also played a role in the overall relaxation mechanism on nanoparticle surfaces, as more APTES coating showed lower apparent surface relaxivities with higher D_2O volume fractions in the mixture.

Table of Contents

List of Tables

List of Figures

Chapter 1

Introduction

1.1 MOTIVATION AND OBJECTIVES

In recent years, nuclear magnetic resonance (NMR) has been used to characterize a wide range of gaseous, liquid and solid materials. NMR is a phenomenon that occurs when nuclei of some atoms in a static magnetic field are exposed to a second oscillating electromagnetic field at a particular frequency. Some nuclear with spin will experience this phenomenon. NMR spectroscopy is used to study physical, chemical, and biological properties of materials. NMR is frequently used to measure the longitudinal (T_1) and transverse (T_2) relaxation times in fluid saturated porous media. NMR relaxation time distributions may be related to pore size distributions in porous media through calibration with other quantitative methods such as mercury injection capillary pressure (MICP) tests or 3-D imaging. Surface relaxivity is the parameter that relates relaxation time to pore size (Fleury, 2007), and is a function of the surface concentration of paramagnetic and/or magnetic sites on the pore surface (Kleinberg et al., 1994).

In natural porous media like rocks, the value of this important parameter is often unknown because the properties of rocks are heterogeneous, so NMR measurements can typically offer only relative pore size distributions (Nelson, 2009). We seek to modify and control surface relaxivity in natural porous media so that NMR measurements can be used to compute pore sizes directly. To control pore surface relaxivity, previous researchers have used paramagnetic materials to coat pore solid surfaces (Anand and Hirasaki, 2007) and magnetic particles to attach onto silica gel surfaces and pore surfaces (Bryar et al., 2000; Cheng et al., 2014).

There are many advantages of nanoparticles to be employed to accomplish our goal. The small size of nanoparticles relative to colloidal particles allows them to be transported freely through pores with the movement of the pore fluid. In addition, nanoparticles have relatively large mass compared to dissolved ions, which allows better control of adsorption and nanoparticle retention in porous media, and they have much lower potential for fluid-rock interactions than dissolved ions.

Due to the harsh subsurface environment in the oilfield (Carter et al., 2005), proper surface coating is widely employed to stabilize nanoparticles. However, care must be taken when using polymer-coated nanoparticles as contrast agents, as studies have reported that polymer coating affects the relaxivities of nanoparticles (Issa et al., 2011).

The use of paramagnetic nanoparticles as contrast agents to characterize porous media has focused on measurements of saturated porous media (Bryar et al., 2000; Yu, 2012; Cheng et al., 2014a), and questions regarding relaxation phenomena of nanoparticles and surface relaxivity alteration of pore walls remain to be answered. When nanoparticles are present in natural porous media like rocks, van der Waals attraction and electrostatic attraction can drive adsorption of nanoparticles onto pore surfaces (Caldelas, 2010), changing the pore surface relaxivity and hence the overall relaxation time of the dispersion-saturated rock. In addition, iron oxides and paramagnetic ions are commonly present on the pore surfaces of reservoir rocks (Carmichael, 1982), and after injection of nanoparticle dispersions into these reservoirs, it is possible that these chemical species may be adsorbed onto nanoparticles and alter the relaxivities of nanoparticles in the pore fluid and/or attached on pore surfaces. I seek to attach nanoparticles onto the pore surface to homogenize and control the pore surface relaxivity. This requires a detailed study of analyze relaxation properties of nanoparticles and pore surfaces in nanofluid-saturated porous media.

The main objectives of this dissertation are:

1. To attach nanoparticles onto sandstone surfaces via electrostatic attraction, thus changing and controlling pore surface relaxivity via adsorption of nanoparticles.
2. To quantify the relationship between adsorbed nanoparticles and alteration of surface relaxivity of sandstones.
3. To understand how the interactions between nanoparticles and sandstone surfaces under different pH conditions will affect adsorption and relaxivities of nanoparticles in porous media, and how this will be reflected in NMR measurements.
4. To study how surface coating may change nanoparticle relaxivities, which will provide useful insight for the future use of surface-coated nanoparticles in NMR measurements.

1.2 OUTLINE OF CHAPTERS

This dissertation contains 7 chapters.

Chapter 1 describes the problems and introduces the motivation and objectives of this project.

Chapter 2 reviews the methods and theories that have been applied to study relaxation of protons in pure fluids and in saturated porous media, the main force that drives adsorption of nanoparticles onto pore surfaces, possible interactions between nanoparticles' surfaces and pore surfaces, and alterations of nanoparticle properties due to surface coating.

Chapter 3 studies the relaxivities of nanoparticles and retention of nanoparticles on silica porous media (glass bead pack and Boise sandstone cores). Adsorption of positively

charged zirconia nanoparticles onto silica surface is confirmed. Silica pore surface relaxivities were altered due to attachment of nanoparticles.

Chapter 4 presents the changes in surface relaxivities of Boise sandstone cores after saturating with positively and negatively charged zirconia nanoparticles with different nanoparticle concentrations and pH values. Retention of nanoparticles in sandstone cores after core flooding was observed. The results also indicate alterations of zirconia nanoparticles' relaxivity after being flushed from Boise sandstone cores.

Chapter 5 studies the interactions of iron ions and uncoated zirconia nanoparticles and polyethylene glycol (PEG)-coated silica nanoparticles. Increased surface relaxivities of nanoparticles are shown to be associated with attached iron ions on nanoparticle surfaces.

Chapter 6 describes how 3-aminopropyl triethoxysilane (APTES) coating on Fe_3O_4 nanoparticles may reduce the relaxivities of nanoparticles and affect relaxation mechanisms on nanoparticle surface.

Chapter 7 summarizes this project and provides recommendations for future work.

Chapter 2

Background

2.1. PROTON NUCLEAR MAGNETIC RESONANCE IN POROUS MEDIA

The principle of NMR measurement is to use coils with strong currents which can generate a steady magnetic field that can polarize hydrogen nuclei (Abragam, 1961; Allen et al., 1998). Hydrogen is mainly present in the pore fluids in natural porous media, so proton NMR allows us to investigate the pore system and the fluids contained in it (Kleinberg et al., 1994).

The longitudinal relaxation time T_1 is the decay constant for recovery of nuclear spin magnetization perpendicular to the applied static field. As shown in Figure 2.1, when exposed to the static field of the NMR device, the nuclear spin magnetization is at its thermal equilibrium $M_{z,eq}$. At time 0, there is a second magnetic field with opposite direction (180°) to original magnetic field applied, which inverts the initial magnetization to $-M_{z,eq}$, as shown in Equation (2.1):

$$M_Z(0) = -M_{z,eq}. \quad (2.1)$$

After the 180° magnetic field pulse, under the original static field, the nuclear spin states are redistributed to reach the thermal equilibrium state distribution $M_{z,eq}$. During this redistribution, another magnetic field oriented perpendicular to the static field is applied at different inversion times TI, enabling measurement of the magnetization amplitude. The record of magnetization amplitude with different TI gives the profile shown in Figure 2.1. The decay constant is derived from Equation (2.2):

$$M_Z(t) = M_{Z,eq} - [M_{Z,\mathrm{eq}} - M_Z(0)]e^{-\frac{t}{T_1}} = M_{Z,\mathrm{eq}}[1 - 2e^{-\frac{t}{T_1}}]. \quad (2.2)$$

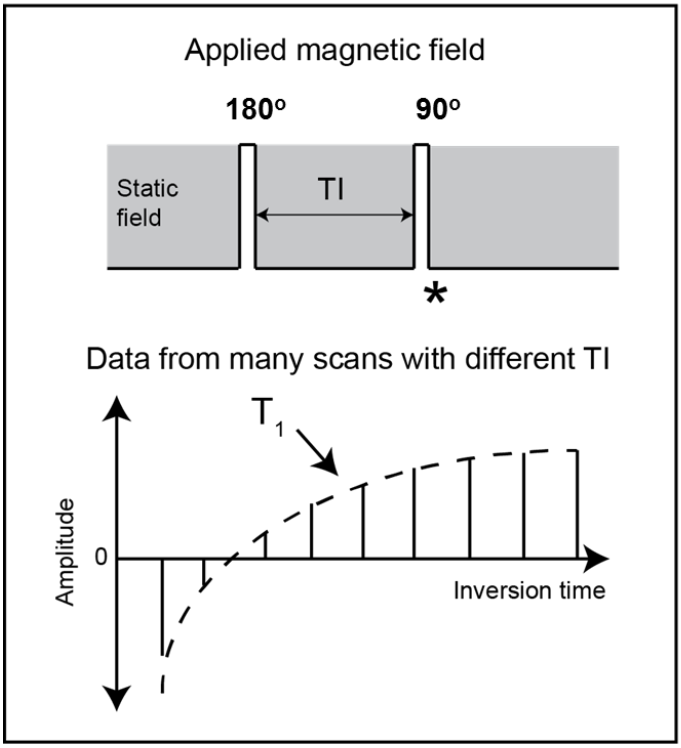

Figure 2.1 Mechanism of T_1 measurement in inversion recovery experiment. At the top is the applied magnetic field pulse sequence. A π pulse is followed by a π/2 pulse after TI (inversion time), then the resulting free induction decay's amplitude is recorded (asterisk). To compute T_1, with various values of TI, many measurements are made and the amplitude of free induction decay is fitted as function of TI employing Equation (2.2) (modified from Daigle et al., 2014).

Several mechanisms contribute to magnetic relaxation in porous media: bulk fluid relaxation, surface relaxation, and diffusion in local magnetic field gradients (Wong, 1999). Bulk fluid relaxation is due to dipole-dipole coupling among protons in the liquid (Bloembergen et al., 1948; Brownstein and Tarr, 1979). Surface relaxation is due to interactions between protons in the pore fluid and unpaired electrons in paramagnetic ions on the pore surface (Kleinberg et al., 1994), or protons on the pore surface (Washburn, 2014). Diffusion relaxation is due to diffusion of protons within local magnetic fields

generated by paramagnetic material in response to the applied static magnetic field. These three mechanisms act simultaneously to produce the measured magnetization decays.

T_1 relaxation is affected by bulk fluid relaxation and surface relaxation. In a single pore, the decay of magnetization is assumed to be single exponential, so the longitudinal relaxation rate $1/T_1$ can be denoted by the sum of different relaxation rates as described in Equation (2.3): sum of bulk fluid relaxation rate $1/T_{1,B}$ and surface relaxation rate $1/T_{1,S}$ (Carr and Purcell, 1954):

$$\frac{1}{T_1} = \frac{1}{T_{1,B}} + \frac{1}{T_{1,S}} \quad . (2.3)$$

Since the diffusion relaxation complicates the relationship between T_2 and pore size, I employ T_1 in this work.

Because the relaxation rate due to bulk fluid processes is much smaller than the surface relaxation rate, the relaxation of fluids confined in porous media is mainly controlled by fluid-grain surface interaction at the surface of pores. In most natural porous media, the pores are relatively small (order tens of microns and smaller), and diffusion of fluid molecules to grain pore surfaces is much faster compared to surface relaxation, so the overall relaxation time is controlled by relaxation at the pore surface (Brownstein and Tarr, 1979). In this case, the relaxation rate in a single pore is spatially uniform and single-exponential, does not depend on pore shape, and is proportional to surface-to-volume ratio as described in Equation (2.4):

$$\frac{1}{T_{1,S}} = \rho_1 \left(\frac{S}{V} \right)_{pore} , (2.4)$$

where ρ_1 is the longitudinal surface relaxivity of porous medium, S is porous medium surface area, and V is pore volume. In fluid saturated porous media, T_1 may be expressed by combining Equations (2.3) and (2.4) as

$$\frac{1}{T_1} = \frac{1}{T_{1,B}} + \rho_1 \left(\frac{S}{V} \right)_{pore} . \quad (2.5)$$

Thus, for each single pore there is a corresponding T_1, and the distribution of T_1 from NMR measurements will give pore size distribution in porous medium.

In rocks, due to the presence of paramagnetic materials on the pore surface, the overall relaxation rate of the pore surface can be explained as in Equation (2.6) (Kleinberg et al., 1994):

$$\frac{1}{T_{1,S}} = \rho_1 \left(\frac{S}{V} \right)_{pore} = \frac{c}{T_{1,M} + \tau_M} + \frac{1-c}{T_{1,N} + \tau_N} . \quad (2.6)$$

Here, c is mole fraction of adsorbed water molecules close enough to be relaxed by paramagnetic sites on the pore surface (surface ions in crystals, paramagnetic crystal defects, or adsorbed paramagnetic ions) and relaxed with relaxation time of $T_{1,M}$, and τ_M is the residence time of water molecules near paramagnetic sites. $T_{1,N}$ is relaxation time of adsorbed water molecules not relaxed by paramagnetic sites, and τ_N is the corresponding residence time of water molecules at surface.

Different species of paramagnetic sites may have various values of $T_{1,M}$ and τ_M, so Equation (2.6) can be re-written in a more general form as below. Here, c_i is the fraction of protons in water molecules relaxed by paramagnetic species i, h is the thickness of one monolayer of water, and n_i is surface fraction of paramagnetic sites i.

$$\frac{1}{T_{1,S}} = \rho_1 \left(\frac{S}{V} \right)_{pore} = \sum_{i=1}^{n} \frac{c_i}{(T_{1,M} + \tau_M)_i} + \frac{1 - \sum_{i=1}^{n} c_i}{T_{1,N} + \tau_N}$$

$$= h \left(\frac{S}{V} \right)_{pore} \left(\sum_{i=1}^{n} \frac{n_i}{(T_{1,M} + \tau_M)_i} + \frac{1 - \sum_{i=1}^{n} n_i}{T_{1,N} + \tau_N} \right) . \quad (2.7)$$

The surface relaxivity is hard to know and is often not a uniform, steady value (Ryu, 2009), and requires independent pore size measurements (e.g., microtomography images) to constrain.

2.2. NANOPARTICLES

2.2.1. Zeta potential model and theory

An important factor that controls the stability of nanoparticles in dispersions is zeta potential, which is used to quantify surface charge magnitude. It is the potential difference between the dispersion medium and the stationary layer of fluid attached to the dispersed particle. The sign and magnitude of zeta potentials of different materials will determine the electrostatic force between them, whether attractive when they have different signs of zeta potential (one is positive, the other is negative) or repulsive when they have the same sign of zeta potential. The repulsive forces are required to stabilize nanoparticles in dispersion against van der Waals attractive forces. Studies of adsorption of ionic surfactants on an ionogenic surface have shown that the adsorption is mainly controlled by the zeta potential (Keesom et al., 1998). The retention of surface-treated stabilized paramagnetic iron-oxide nanoparticles in sedimentary rocks is also controlled by the zeta potential of the nanoparticles in dispersion (Yu et al., 2010). Previous studies indicate that silica and most sedimentary rock grains have negative zeta potential when exposed to fluid with various pH values under laboratory conditions (Kim and Lawler, 2005). Therefore, nanoparticles with positive zeta potential are the best candidates for adsorption to silicate grain surfaces.

2.2.2 pH values affect nanoparticle zeta potential and size

In porous media, the electrostatic force is responsible for the retention of nanoparticles by adsorption on the pore surface (Overbeek, 1952). As shown in Figure 2.2, there is an electrical double layer (EDL) associated with the mineral surface. The outer

boundary of the EDL is the location where the particle's surface charge is neutralized by the nearest layer in the liquid containing ions of opposite charge to that of the surface (the counterions). The thickness of the EDL is determined by the concentration of electrolyte (Prides, 1994). Free electrolyte is in the pore fluid outside the EDL. The relative motion between the charged mineral surface and its EDL in pore fluid is localized along a shear plane within the EDL, and controls all electrokinetic phenomena such as the motion of particles and liquids in porous media under electric fields or chemical potential gradients, as well as electric fields and currents generated by motion of colloidal particles. Zeta potential is the electrical potential of the EDL (Overbeek, 1952).

The variation in zeta potential with electrolyte concentration has been studied for various minerals (Ishido and Mizutani, 1981; Morgan et al., 1989; Revil et al., 1999a,b). Silicate minerals have negative zeta potential ranging from -10mv to -130mv with different electrolyte concentrations ranging from 10^{-6} mol/L to 10^{-1} mol/L (Gaudin and Fuerstenau, 1955; Li and De Bruyn, 1966). As previously studied (Iler, 2004), silica surfaces contain two types of surface groups: $>Si_2O^0$ (surface siloxal group) and $>SiOH^0$ (surface silanol group). Here the symbol ">" indicates surface complexes. $>SiOH^0$ undergoes amphoteric reactions to generate positively charged surface groups ($>SiOH_2^+$) when pH is lower than 2, and negatively charged surface groups ($>SiO^-$) when pH is higher than 3 (Revil et al., 1999a,b). When silica minerals are exposed to electrolyte solutions, there are surface mineral reactions at silanol surface sites. In the left part of Figure 2.2, the pH value is between 3 and 8, the main surface groups are siloxane groups ($>Si_2O^0$), silanol groups (>SiOH), and silicic acid groups ($>SiO^-$), and the shear plane is on the mineral surface. In the right part of Figure 2.2, the pH value is higher than 8, and silicic acid chains generate longer filaments near the surface due to mineral surface dissolution. This builds a silica gel

layer that coats the solid mineral surface and the shear plane is located between the silica gel and aqueous phases (Revil et al., 1999a,b).

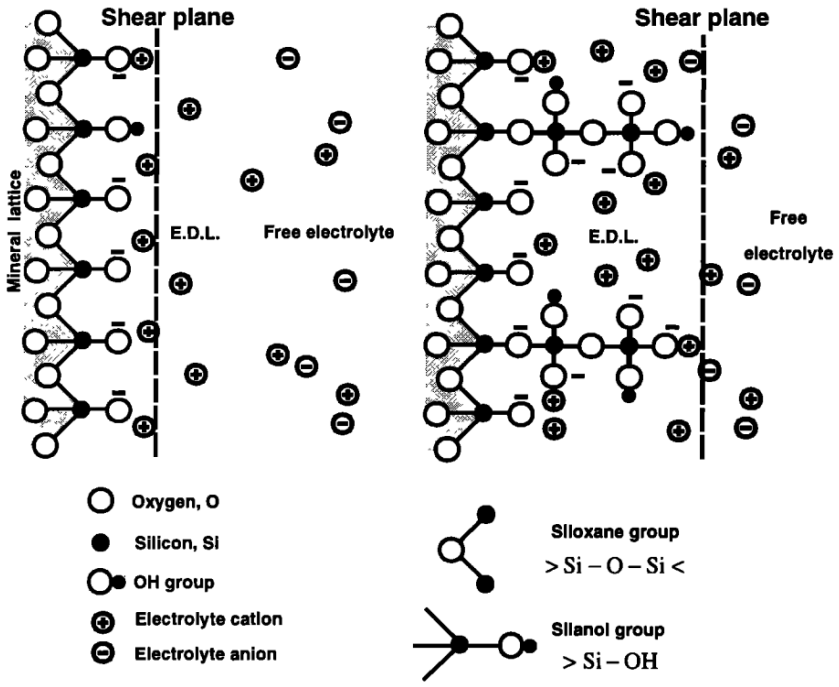

Figure 2.2 Simplified model of electric double layer (EDL) at a silica mineral surface in aqueous solution (Revil et al., 1999a).

It has been demonstrated that the pH value of a liquid affects nanoparticle zeta potential and aggregation (Godinez and Darnault, 2011). For small silica particles with diameters from 0.63 μm to 6.3 μm, zeta potential changes with pH values: zeta potential drops from -10 mV to -65 mV as pH increases from 2 to 10 (Nelson, 2009). The zeta potential of kaolinite is +0.7 mV at pH value of 2 and decreases to -54 mV at pH value of 10 (Vane and Zang, 1997; Daigle and Dugan, 2011). Reservoir brine pH is important to the zeta potential and aggregation behavior of nanoparticles (Yu et al., 2010; Daigle and Dugan, 2011). For pure commercial carbon black without surfactants, zeta potential is ~-

20 mV at pH ~6, and zeta potential drops to -40 mV when pH increases to 11 (Sis and Birinci, 2009). Even though nanoparticles are smaller than colloidal particles, similar pH-zeta potential behavior has been observed. When there are nonionic surfactants used to stabilize carbon black nanoparticles, zeta potential is -5mV when pH is ~3, and zeta potential decreases to -20mV when pH increases to 11 (Sis and Birinci, 2009). Lower pH values generally correspond to higher zeta potential, which could result in stronger repulsive forces between nanoparticles and inhibit nanoparticle aggregation.

2.2.3 Paramagnetism

Paramagnetism means the magnetic state of an atom with one or more unpaired electrons. The unpaired electrons can spin in either direction and thus generate magnetic moments in any direction. When they are placed in a magnetic field, they will be attracted by the magnetic field due to the electrons' magnetic dipole moments. Most paramagnetic materials are metals that are weakly attracted by magnets, and will not retain their magnetic properties after applied magnetic field disappears. Examples are aluminum, tin, and manganese. When paramagnetic materials are exposed to a magnetic field, they generate a secondary magnetic field that decreases the relaxation time of protons in the pore fluid. Paramagnetic nanoparticles mostly are rare earth oxides, hydroxides, and fluorides, which have been used as magnetic resonance imaging (MRI) contrast agents (Vuong et al., 2012). Now paramagnetic nanoparticles are widely used in NMR studies (Ryoo et al., 2012).

When there are paramagnetic nanoparticles present in pore fluid and attached on a grain surface, the contributions to the overall relaxation rate can be split more specifically from Equation (2.3). As shown in Figure 2.2, in part a, there is pure bulk pore fluid present in pores, with relaxation contributed by bulk fluid $T_{1,B}$ and pore surface $T_{1,S}$, corresponding to the two components in Equation (2.3). In part b, if nanoparticles are present only in the

pore fluid, they provide an additional relaxation contribution $T_{1,B\text{-}NP}$. If some nanoparticles move from bulk pore fluid to be adsorbed onto the pore surface, they provide an additional surface relaxation time $T_{1,S\text{-}NP}$. Hence the sum of these four relaxation contributions gives Equation (2.8):

$$\frac{1}{T_1} = \frac{1}{T_{1,B}} + \frac{1}{T_{1,B-NP}} + \frac{1}{T_{1,S}} + \frac{1}{T_{1,S-NP}} \quad . (2.8)$$

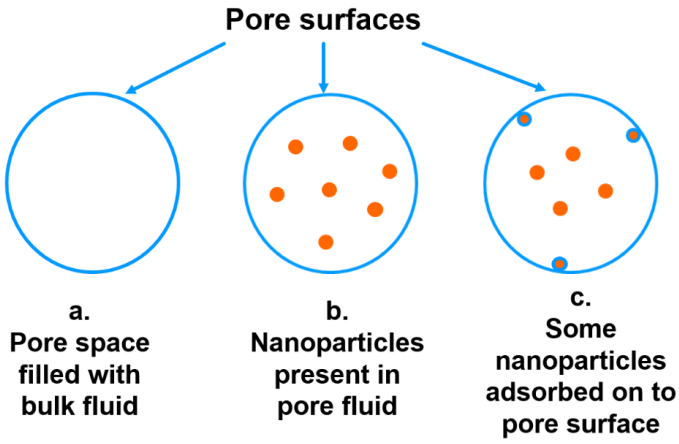

Figure 2.3 Mechanisms of relaxation of nanoparticle dispersion in a single spherical pore.

25 nm magnetite nanoparticles were used to coat fine and coarse sand at different surface concentrations (Anad and Hirasaki, 2007). The results indicate that the size and concentration of paramagnetic nanoparticles affect the degree to which they influence the proton relaxation times. Magnetite particles may be modeled as thin spherical shell of paramagnetic material.

2.3 Relaxation of Saturated Media Involving Nanoparticles

Based on previous work, the effect of paramagnetic nanoparticles on NMR measurements varies according to the nanoparticle locations, whether in bulk dispersion,

or adsorbed on a solid surface. Two models with different spatial scales may be used to quantify the effect of paramagnetic nanoparticles on longitudinal relaxation.

2.3.1 Dispersion scale

Model 1: Surface relaxation of nanoparticles surface with paramagnetic sites (Bryar et al., 2000; Zhu, et al., 2016)

We may also treat nanoparticle dispersions as a dilute porous medium in which solid nanoparticles are the matrix providing surface relaxation (Korb et al., 1997; McDonald et al., 2005; Zhu et al., 2015), and the bulk fluid in which the nanoparticles are dispersed provides the bulk fluid relaxation. The overall longitudinal relaxation rate $1/T_1$ of a nanoparticle dispersion is the sum of the contributions from bulk relaxation rate $1/T_{1,Fluid}$ and the nanoparticle surface relaxation rate $1/T_{1,NP}$ (e.g., Carr and Purcell, 1954), as displayed in Equation (2.9):

$$\frac{1}{T_1} = \frac{1}{T_{1,\mathrm{Fluid}}} + \frac{1}{T_{1,\mathrm{NP}}} \quad . (2.9)$$

$1/T_{1,\mathrm{Fluid}}$ can be calculated from experiments by measuring the relaxation time of the pure dispersing fluid. When diffusion of water molecules across the pores is fast enough to maintain uniform magnetization in the pores during signal decay, $1/T_{1,NP}$ is proportional to S/V, the ratio of total nanoparticle surface area (S) to total fluid volume (V) in the dispersion (Senturia and Robinson, 1970), with the constant of proportionality being the nanoparticles' surface relaxivity $\rho_{1,NP}$. In Equation (2.10), S_{pore} can be calculated from nanoparticles' volume V_{NP} and radius r_{NP} assuming that the nanoparticles are spherical. V_{pore} is fluid volume which equals total volume of suspension V_{Total} minus the nanoparticles' volume V_{NP}. The parameter χ is the ratio of the nanoparticles' volume to the fluid volume in the dispersion (Zhu et al., 2015):

$$\frac{1}{T_{1,NP}} = \rho_{1,NP}\left(\frac{S}{V}\right)_{pore} = \rho_{1,NP}\left(\frac{V_{NP}\dfrac{3}{r_{NP}}}{V_{Total}-V_{NP}}\right) = \rho_{1,NP}\left(\frac{3\chi}{r_{NP}}\right) \quad . \quad (2.10)$$

With various types of paramagnetic sites (surface ions in crystals, paramagnetic crystal defects, or adsorbed paramagnetic ions) on nanoparticle surfaces, the relaxation rate of nanoparticles has contributions from paramagnetic and non-paramagnetic parts (Kleinberg et al., 1994) as shown in Equation (2.11): c_i is fraction of water molecules get close enough and relaxed by paramagnetic locations on surface, T_{1M} is the intrinsic relaxation time for each paramagnetic site, τ_M is the corresponding residence time of water molecules, h is thickness of one monolayer of water molecule, n_i is surface fraction of paramagnetic sites on nanoparticle surface. When surface concentrations of paramagnetic sites n_i increase, the overall relaxation rate of nanoparticle will increase accordingly.

$$\frac{1}{T_{1,NP}} = \rho_{1,NP}\left(\frac{S}{V}\right)_{pore} = \sum_{i=1}^{n}\frac{c_i}{(T_{1M}+\tau_M)_i} + \frac{1-\sum_{i=1}^{n}c_i}{T_{1N}+\tau_N}$$

$$= h\left(\frac{S}{V}\right)_{pore}\left(\sum_{i=1}^{n}\frac{n_i}{(T_{1M}+\tau_M)_i} + \frac{1-\sum_{i=1}^{n}n_i}{T_{1N}+\tau_N}\right) \quad . \quad (2.11)$$

If ρ_i is the inherent relaxivity of the different kinds of paramagnetic relaxation sites on the solid surface, n_i is surface concentration of paramagnetic species (Bryar et al., 2000), and ρ_N is the relaxivity of the non-paramagnetic sites, the overall relaxivity $\rho_{1,NP}$ of nanoparticles with surface coating can be computed using Equation (2.12):

$$\rho_{1,NP} = \sum_{i=1}^{n} n_i\rho_i + \left(1-\sum_{i=1}^{n}n_i\right)\rho_N = \rho_N + \sum_{i=1}^{n} n_i\left(\rho_i-\rho_N\right) \quad . \quad (2.12)$$

2.3.2 Molecular Scale

Model 2: Surface relaxation on surfaces with adsorbed paramagnetic species (McDonald et al., 2005)

The dominant mechanism of longitudinal surface relaxation is interactions with paramagnetic relaxation centers on the pore wall (Korb et al., 1997). Since the size of water molecules is much smaller than the porous medium grains, the pore surface is relatively flat in the reference frame of the water molecules. As shown in Figure 2.4, during the surface residence time τ_s in which the water molecule is close enough to the surface to interact with paramagnetic ions, the motion of the water molecules may be represented by a two-dimensional random walk in which the water molecules jump between relaxing sites on the solid surface with a characteristic time τ_m (translational correlation time) ($\tau_s >> \tau_m$). After τ_s the water molecule leaves the surface and returns back to pore fluid. The longitudinal relaxation time of protons in the surface relaxing layer may be expressed as

$$\frac{1}{T_{1,M}} = \frac{2}{9}\gamma_I^2\gamma_S^2\hbar^2 S(S+1)[J_L^0(\omega_I - \omega_S) + 3J_L^1(\omega_I) + 6J_L^2(\omega_I + \omega_S)] \quad , (2.13)$$

where the spectral density functions J_L are different from those in Equation (2.11) and are computed as in Equation (2.13). Here, σ_s is surface density of paramagnetic species and δ is the distance of minimum approach, which is taken as the radius of a water molecule.

$$J_L^{0,1,2}(\omega) = \frac{3}{40}\frac{\pi\sigma_s}{\delta^4}\tau_m \ln\left[\frac{1+\omega^2\tau_m^2}{(\frac{\tau_m^2}{\tau_s^2}) + \omega^2\tau_m^2}\right]. \quad (2.14)$$

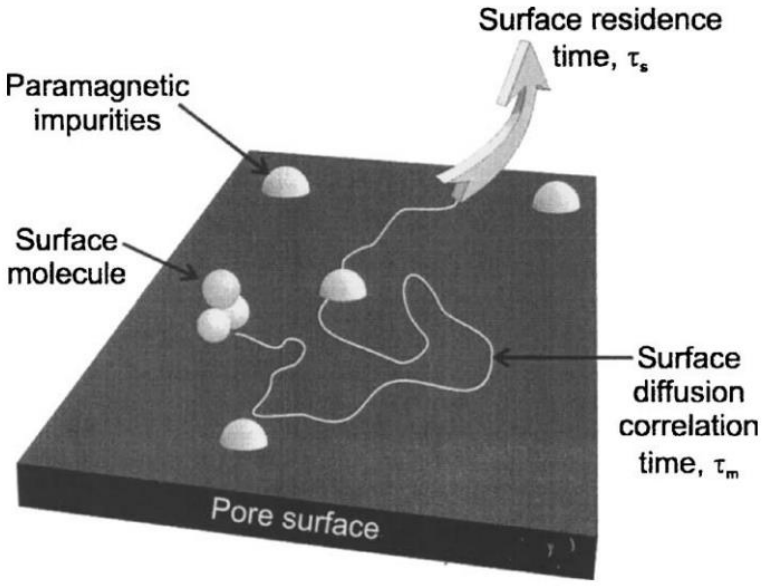

Figure 2.4 Schematic of mechanism of a two-dimensional random walk of water molecules coordinated with paramagnetic relaxation sites on the pore surface (McDonald et al., 2005).

Previous studies of surface relaxation in porous media modified with paramagnetic materials (iron or manganese precipitated from solution) have shown that the adsorption of paramagnetic materials can increase surface relaxivity by factors of 6 to 50 (Kenyon and Kolleeny, 1995).

If we treat the adsorbed paramagnetic nanoparticles on mineral surfaces as a uniform layer with a given surface concentration of paramagnetic relaxation sites, the relaxation rate of that layer is the difference between overall relaxation rate and pore fluid relaxation rate, and can be easily derived from Equation (2.3).

Chapter 3

Nuclear Magnetic Resonance Investigation of Pore Surface Relaxivity Alteration with Presence of Paramagnetic Nanoparticles[1]

3.1 INTRODUCTION

^{1}H Nuclear magnetic resonance (NMR) is widely used to characterize a wide range of gaseous, liquid and solid materials. NMR relaxation time distributions may be related to pore size distributions in porous media through calibration with other quantitative methods such as mercury injection capillary pressure (MICP) tests or 3-D imaging. To obtain pore size distribution, paramagnetic nanoparticles are employed as contrast agents.

25 nm magnetite nanoparticles were employed to saturate fine and coarse sand at different surface concentrations by Anand and Hirasaki (2008). Their results indicate that the size and concentration of paramagnetic nanoparticles affect the degree to which they influence the proton relaxation times. More recent work has shown that superparamagnetic nanoparticles in porous media change the NMR signal by shortening transverse relaxation times (Cheng et al., 2014a,b).

An important factor that controls the stability of nanoparticles in dispersions is the zeta potential, which is used to quantify surface charge magnitude. In porous media, electrostatic forces are also responsible for the retention of nanoparticles by adsorption on the pore surface (Overbeek, 1952). Studies of adsorption of ionic surfactants on an ionogenic surface have shown that the adsorption is mainly controlled by the zeta potential (Keesom et al., 1988). The retention of surface-treated stabilized paramagnetic iron-oxide nanoparticles in sedimentary rocks is also controlled by the zeta potential of the nanoparticles in dispersion (Yu et al., 2010). Previous studies indicate that silica and most

[1]This chapter is based on: Zhu, C., Daigle, H., & Bryant, S. (2015, September). Nuclear magnetic resonance investigation of surface relaxivity modification by paramagnetic nanoparticles. In *SPE Annual Technical Conference and Exhibition*. Society of Petroleum Engineers. I was the primary author.

sedimentary rock grains have negative zeta potential when exposed to fluid with various pH values under laboratory conditions (Kim and Lawler, 2005). Therefore, nanoparticles with positive zeta potential are the best candidates for adsorption to silicate grain surfaces.

Previous studies such as Anand and Hirasaki's work focused on characterization of transverse relaxation regimes in sandstones corresponding to paramagnetic particles' concentration and size, and provided a way to quantitatively understand the relaxation of paramagnetic particles in sandstone due to diffusion in internal magnetic field gradients. However, the surface relaxivity of pore surface was not studied. We chose zirconia nanoparticles provided from Nissan Chemical America, because (1) these nanoparticles do not have surface coating, which may interfere with the relaxivity of nanoparticles; (2) they are stabilized and dispersed under 2 different pH conditions, giving opposite surface charge; and (3) they have similar size. In this paper, we measured longitudinal relaxation time distribution which solely depends on bulk relaxation and surface relaxation. The objectives of our work are: 1) to understand how dispersed zirconia nanoparticles affect proton relaxation in bulk fluid, and 2) how adsorbed zirconia nanoparticles change the surface relaxivity of porous media. We measured relaxation time and particle sizes of zirconia nanoparticle dispersions at different concentrations, characterized the relationship of relaxation rate of zirconia nanoparticles and particle sizes and concentrations, and estimated nanoparticles' surface relaxivity. We measured and compared relaxation time of DI water and zirconia nanoparticles under three conditions: the original bulk dispersion, saturating a silica porous medium, and as effluent flushed from the silica porous medium. Our results indicated adsorption of nanoparticles onto pore surface leaves fewer nanoparticles in the pore space and affects surface relaxation at the pore wall.

3.2 THEORY

In order to analyze nanoparticles' relaxation time under different conditions, well studied equations that characterized nanoparticles with simplified assumptions and models can be used.

3.2.1 Bulk Relaxation of Paramagnetic Nanoparticle Dispersions

The bulk relaxation behavior of paramagnetic nanoparticle dispersions is similar to the relaxation behavior of a dilute porous medium in which solid nanoparticles are the matrix providing surface relaxation (Korb et al., 1997; McDonald et al., 2005). The fluid within the dispersion has a characteristic bulk relaxation rate $1/T_{1,Fluid}$. Paramagnetic ions on the surface of the nanoparticles create relaxation sites that contribute an additional surface relaxation rate $1/T_{1,NP}$ (Korb et al., 1997). We assume that the decay of magnetization in the dilute medium is single exponential, so the longitudinal relaxation rate $1/T_1$ can be denoted by the sum of different relaxation rates (e.g., Carr and Purcell, 1954):

$$\frac{1}{T_1} = \frac{1}{T_{1,\mathrm{Fluid}}} + \frac{1}{T_{1,\mathrm{NP}}} \quad . (3.1)$$

The bulk fluid relaxation rate is easy to obtain from experiments by measuring the relaxation time of pure fluid. The surface relaxation rate generated by dispersed nanoparticles can be modeled and computed as a 2D random walk (McDonald et al., 2005). The dominant mechanism of longitudinal surface relaxation is interactions with paramagnetic relaxation centers on the nanoparticle surfaces (Korb et al., 1997). Since water molecules are much smaller than the nanoparticles, the nanoparticle surfaces are relatively flat in the reference frame of the water molecules. The longitudinal relaxation rate of protons near the paramagnetic nanoparticle surfaces may be expressed as (McDonald et al., 2005):

$$\frac{1}{T_{1,NP}} = \frac{2}{9}\delta\left(\frac{S}{V}\right)\gamma_I^2\gamma_S^2\hbar^2 S(S+1)\left[J_L^0(\omega_I-\omega_S)+3J_L^1(\omega_I)+6J_L^2(\omega_I+\omega_S)\right], \quad (3.2)$$

where δ is the water molecular diameter, S/V is specific surface area of the pore space, γ_I and γ_S are the gyromagnetic ratios of the protons and electrons, respectively, and γ_S =658.21γ_I, $\hbar$ is the reduced Planck's constant, S is the spin of paramagnetic ions in the nanoparticles, and ω_S and ω_I are Larmor angular frequencies of electrons and protons, respectively. The Fourier spectral density functions J are given by

$$J_L^{0,1,2}(\omega) = \frac{3}{40}\frac{\pi\sigma_s}{\delta^4}\tau_m \ln\left[\frac{1+\omega^2\tau_m^2}{\left(\frac{\tau_m^2}{\tau_s^2}\right)+\omega^2\tau_m^2}\right], \quad (3.3)$$

where τ_s is surface residence time in which the water molecule is close enough to the surface to interact with paramagnetic ions, τ_m is the translational correlation time that is a measure of the time a proton is coordinated with each relaxation site, and σ_s is the surface density of relaxation sites. The motion of the water molecules may be represented by a two-dimensional random walk in which the water molecules jump between relaxing sites on the solid surface with a characteristic time τ_m (translational correlation time) ($\tau_s >> \tau_m$).

The surface density σ_s can be calculated from known properties of paramagnetic nanoparticles as

$$\sigma_s = X\eta\rho_b\xi, \quad (3.4)$$

where X is the fraction of paramagnetic atoms in nanoparticles with non-zero spins, η is the number of paramagnetic atoms per gram of dry material of nanoparticles, ρ_b is the density of the solid nanoparticles, and ξ is the distance between paramagnetic atoms in the nanoparticle crystal structure.

Equation (3.2) may be simplified by introducing the longitudinal surface relaxivity ρ_1, which relates $1/T_{1,NP}$ to S/V as $1/T_{1,NP} = \rho_1(S/V)$. Since S/V is the ratio of total

nanoparticle surface area to total fluid volume in the dispersion, it may be computed from nanoparticle radius r_{NP} and volume fraction χ as

$$\frac{1}{T_{1,\mathrm{NP}}} = \rho_{1,\mathrm{NP}} \left(\frac{S}{V} \right)_{pore} = \rho_{1,\mathrm{NP}} \left(\frac{V_{NP} \dfrac{3}{r_{NP}}}{V_{Total} - V_{NP}} \right) = \rho_{1,\mathrm{NP}} \left(\frac{3\chi}{r_{NP}} \right) \quad , (3.5)$$

where χ is assumed to represent volume of nanoparticles per unit volume of fluid in the dispersion.

3.2.2 Relaxation of Nanoparticle Dispersions in Porous Media

When nanoparticle dispersions enter a porous medium, it is possible for nanoparticles to attach to the porous medium surface (Anand and Hirasaki, 2008), thus affecting the surface relaxation of the porous medium. Some nanoparticles will remain in the dispersion within the pore space. Again assuming single exponential decay in a single pore, the overall relaxation rate can be described as

$$\frac{1}{T_1} = \frac{1}{T_{1,\mathrm{Bulk}}} + \frac{1}{T_{1,\mathrm{Surface}}} = \left(\frac{1}{T_{1,\mathrm{Fluid}}} + \frac{1}{T_{1,\mathrm{NP-in-pore}}} \right) + \left(\frac{1}{T_{1,\mathrm{Medium-surface}}} + \frac{1}{T_{1,\mathrm{NP-on-surface}}} \right) , (3.6)$$

where $T_{1,\mathrm{Bulk}}$ is the relaxation time of bulk dispersion in pore space, $T_{1,\mathrm{Surface}}$ is the surface relaxation time at pore wall, $T_{1,\mathrm{NP\text{-}in\text{-}pore}}$ is the relaxation time of nanoparticles remained in pore space, $T_{1,\mathrm{Medium\text{-}surface}}$ is the surface relaxation time of the porous medium, and $T_{1,\mathrm{NP\text{-}on\text{-}surface}}$ is the relaxation time of nanoparticles adsorbed onto pore surface. Adsorbed nanoparticles will alter both bulk dispersion relaxation time (by reducing the nanoparticle concentration in the dispersion) and surface relaxation time at the pore wall.

Similarly, in a porous medium saturated with nanoparticle dispersions, when pores are treated as spheres with radius of r_{pore}, the overall surface relaxation rate can be linked with pore size using a modified surface relaxivity $\rho_{1,\mathrm{eff}}$. $\rho_{1,\mathrm{eff}}$ arises from the scenario in which some of the nanoparticles in dispersion are removed from the pore space and

attached to the solid pore wall. With N_{NP} nanoparticles adsorbed onto one spherical pore, $\rho_{1,\text{eff}}$ is related to the relaxivities of the adsorbed nanoparticles and the pore wall. On pore surface, the altered surface relaxivity may be determined by considering the surface area that is covered by the projection of an adsorbed nanoparticle onto the pore surface. $\rho_{1,\text{eff}}$ is calculated from the areally weighted average of medium surface relaxivity $\rho_{1,\text{Medium-surface}}$ and attached N_{NP} nanoparticles relaxivity $\rho_{1,\text{NP}}$:

$$\frac{1}{T_{1,\text{surface}}} = \rho_{1,\text{eff}} \left(\frac{S}{V}\right)_{pore} = \rho_{1,\text{eff}} \frac{3}{r_{pore}}, \quad (3.7)$$

$$\rho_{1,\text{eff}} = \frac{N_{NP}\pi r_{NP}^2}{4\pi r_{pore}^2}\rho_{1,\text{NP}} + \frac{4\pi r_{pore}^2 - N_{NP}\pi r_{NP}^2}{4\pi r_{pore}^2}\rho_{1,\text{Medium-surface}}, \quad (3.8)$$

$$\rho_{1,\text{Medium-surface}} = \frac{1}{T_{1,\text{Medium-surface}}}\left(\frac{V}{S}\right)_{pore} = \frac{1}{T_{1,\text{Medium-surface}}}\frac{r_{pore}}{3}. \quad (3.9)$$

The relaxation rate of the bulk nanoparticle dispersion $1/T_{1,\text{NP-in-pore}}$ with M_{NP} nanoparticles remaining in the pore can be calculated from the original relaxation rate of the bulk dispersion $1/T_{1,\text{NP}}$ with (M_{NP}+N_{NP}) nanoparticles:

$$\frac{1}{T_{1,\text{NP-in-pore}}} = \frac{1}{T_{1,\text{NP}}}\left(\frac{M_{NP}}{M_{NP}+N_{NP}}\right). \quad (3.10)$$

3.3 METHODS

We used zirconia nanoparticles dispersed in water (ZR-30AL) with 30 wt% of colloidal zirconium oxide (ZrO_2) stabilized with 0.9 wt% HNO_3 from Nissan Chemical America Corporation. The specific gravity was 1.36 and the pH value was 3.2. The original ZR-30AL was diluted with DI water to obtain dispersions with various zirconia

nanoparticles, ranging from 0.3 wt% of ZrO_2 to 15 wt% of ZrO_2. 6 wt% of ZrO_2 in dispersion (ZR-6AL) was used for further saturation of silica porous media. The nanoparticles had positive surface charge, with an average zeta potential of +32.5 mV. Nanoparticle diameters were between 110 and 130 nm measured by a Dynamic Light Scattering (DLS) ZetaSizer (Malvern Nano ZS).

We also used a 40 wt% dispersion of colloidal ZrO_2 (ZR-40BL) from Nissan Chemical America Corporation. These nanoparticles were dispersed in water and stabilized with 1 wt% $C_4H_{12}N.HO$. The specific gravity was 1.53 and pH was 9.2. The original ZR-40BL dispersion was diluted with DI water to reduce the weight concentration of zirconia nanoparticles to a wide range from 0.4 wt% to 20 wt%. The 6 wt% of ZrO_2 in dispersion (ZR-6BL) was used to saturate silica porous media. The nanoparticles in the ZR-6BL dispersion had negative surface charge with average zeta potential of -38.8 mV. Nanoparticle diameters were between 70 and 90 nm. Figure 3.1 shows the Transmission Electronic Microscope (TEM) images of these particles.

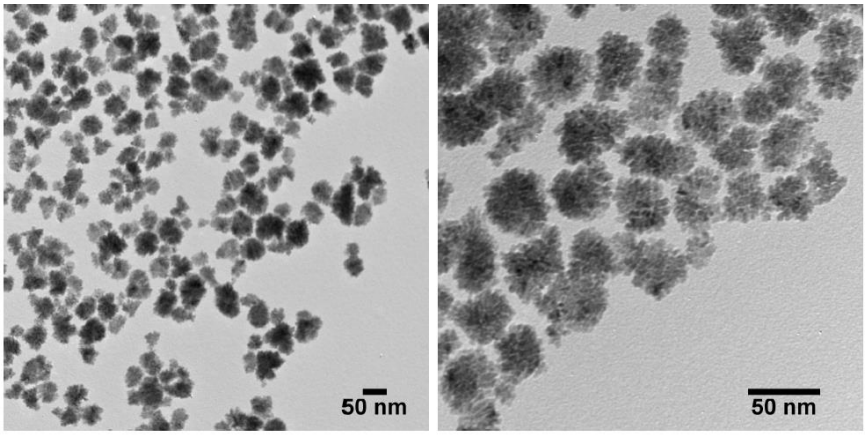

Figure 3.1 TEM image of zirconia nanoparticles in ZR-BL dispersion.

The Malvern Nano ZS was used to measure size distribution and surface zeta potential of zirconia nanoparticles at different concentrations in ZR-AL and ZR-BL. Size and zeta potential calibrations were performed with calibration standard dispersions before each measurement. 0.450 mL of zirconia nanoparticle dispersion was placed in a disposable cell to measure size distribution. The size distribution and average value of measured size were recorded. A 1.0 mL plastic syringe was used to inject 1 mL of nanoparticle dispersion into a disposable folded capillary cell to measure zeta potential. The average volume and distribution of zeta potentials were recorded. Measurements of each dispersion sample were performed three times and the mean value and standard deviation were recorded.

NMR measurements were performed at room temperature (20°C) using a 2 MHz GeoSpec2 benchtop NMR core analysis instrument from Oxford Instruments with an operating frequency of 2.15 MHz The external magnetic field B_0 was 0.05047 Tesla. We used an inversion recovery measurement to determine the distribution of longitudinal relaxation times (T_1).

In order to check nanoparticles' retention in porous media, density of zirconia nanoparticles dispersions ZR-6AL and ZR-6BL before and after saturating porous media were computed. The mass of 1 mL of dispersion was measured by Mettler Toledo mass balance. Measurements were repeated 5 times at room temperature, and average values were used.

Glass beads with diameter of 2 mm were soaked in ethanol to remove dust and other surface impurities for 10 hours, and then dried in an oven for 14 hours at 135°C. Glass beads were packed in plastic cylinder to form a column with 1.5" (3.81 cm) in diameter and 4" (10.16 cm) in length. The porosity of glass bead pack was determined as 38% based on NMR measurements with DI water as the saturating fluid. Three plastic tubes containing

the glass bead packs were oriented vertically, and different saturating fluids were injected from the bottom of bead pack at constant flow rate of 0.5 mL/min using a Teledyne ISCO D-Series hydraulic pump. The bottom valves were closed once fluid was observed running out through the top outlet.

The three Boise Sandstone samples (BS1, BS2, BS3) used in this study were 1.5" (3.81 cm) in diameter and 3" (7.62 cm) in length. All core samples were oven-dried for 14 hours at 135°C. The porosity of the core samples was computed approximately 29% according to NMR measurements with DI water as the saturating fluid. All dried core samples were placed in a sealed container and vacuumed with a Welch vacuum pump for 4 hours. After vacuuming, the saturating fluid was sucked into the sealed container until the core sample was fully immersed. The core samples were kept immersed in the saturating fluid under vacuum for 1 additional hour to ensure complete saturation.

To test and check whether there were nanoparticles adsorbed on pore surface, after measuring the T_1 distribution of the saturated porous media we flooded the media with DI water from bottom to top at a constant flow rate of 0.5 ml per minute. Core flooding was performed until 1.2 pore volumes (PV) were injected. The first 0.7 PV of effluent was collected from the top outlet of the bead packs and core samples. The T_1 value and nanoparticle sizes were measured and compared with that of the original fluids.

Error bars for the longitudinal relaxation rate were computed from the standard deviation of the longitudinal relaxation time obtained from the Matlab inversion. The signal and noise were extracted from the raw NMR data in the time domain. Random noise with the same properties (magnitude, mean value and standard deviation) of noise extracted from raw NMR data was added to the time domain signal. With the added noise, there was a slightly different magnetization buildup curve compared to the curve obtained directly from the raw data. A linear inversion regression was then applied to the buildup curve with

added noise to compute the T_1 value. After repeating this process 100 different times, 100 buildup curves were generated and used to calculate associated T_1 values. Based on these 100 computed T_1 values, the standard deviation of T_1 was recorded and used to compute the errors in longitudinal relaxation rate.

3.4 RESULTS

3.4.1 Zirconia Nanoparticles Characterization

We measured the size and zeta potential of zirconia nanoparticles at different concentrations in ZR-AL and ZR-BL. As shown in Table 3.1, zirconia nanoparticles in diluted dispersions with less stabilizer tend to aggregate and showed bigger nanoparticle size than well-stabilized nanoparticle dispersions. Zeta potential of nanoparticles in ZR-AL and ZR-BL at highest concentration were not displayed since dispersions were so dense that results were too noisy.

Table 3.1 DLS ZetaSizer measured size and zeta potential of zirconia nanoparticles in ZR-AL and ZR-BL at different concentrations.

ZR-AL			
Concentration (wt%)	Concentration (vol%)	Average Size (nm)	Average Zeta potential (mV)
15.0	3.034	110	N.A
6.0	1.114	113	32.5
3.0	0.542	115	29.8
0.6	0.106	118	35.3
0.3	0.053	128	36.2
ZR-BL			
Concentration (wt%)	Concentration (vol%)	Average Size (nm)	Average Zeta Potential (mV)
20	4.259	80.5	N.A
8.0	1.513	84.6	-36.3
4.0	0.729	85.2	-32.1
0.8	0.142	88.1	-32.8
0.4	0.071	88.3	-34.0

3.4.2 Bulk Relaxation Rate $1/T_1$ of Zirconia Nanofluids

We measured the bulk relaxation rate of DI water, ZR-AL, and ZR-BL with different concentrations. Those fluids were placed in glass tubes and T_1 was measured. According to Equation (3.1), the relaxation rate of zirconia nanoparticles $1/T_{1,NP}$ can be obtained by deducting the pure liquid longitudinal relaxation rate $1/T_{1,Liquid}$ from the overall longitudinal relaxation rate $1/T_1$. Here $1/T_{1,Liquid}$ is the relaxation rate of DI water, which was determined as 0.385 s^{-1}. We calculated the $1/T_{1,NP}$ values of zirconia nanoparticle dispersions with different concentrations. In Figure 3.2, $1/T_{1,NP}$ shows a linear relationship with $3\chi/r_{NP}$ in both ZR-AL and ZR-BL dispersions. Zirconia nanoparticle surface relaxivity in ZR-AL was computed as 1.427 ± 0.014 μm/s as indicated in Figure 3.2a) according to Equation (3.5) using the slope of the weighted least squares regression line in Figure 3.2. Similarly, ZR-BL has relaxivity as 1.095 ± 0.024 μm/s. According to the equations in Appendix A, error bars in $1/T_{1,NP}$ associated with each point were obtained from the standard deviations of $1/T_1$ and $1/T_{1,Liquid}$, which were computed from the standard deviations of T_1 and $T_{1,Liquid}$ obtained from Matlab as illustrated in section 3.3. The raw NMR data for zirconia nanoparticle dispersions with different nanoparticle concentrations are displayed in the Appendix. We additionally determined the correlation times τ_m and τ_s in Equations (3.2 and 3.3) according to parameter values listed in Table 3.2 by optimizing the measured $1/T_{1,NP}$ values at different nanoparticle concentrations. For ZR-AL dispersions we found τ_m = 0.233 ns and τ_s = 2.524 ns, and for ZR-BL dispersions we found τ_m = 0.251 ns and τ_s = 1.528 ns. Figs. 3a and 3b show the predicted nanoparticle relaxation rate from Equations (3.2 and 3.3) versus the measured relaxation rate in ZR-AL and ZR-BL, respectively. There is excellent match between fitted and measured values.

Table 3.2 Parameter values used in calculation of τ_m and τ_s.

Parameter	Value used in Equations (3.2 and 3.3)
B_0	0.05047 T
δ	7×10^{-10} m
γ_I	2.675×10^{8} $s^{-1}\cdot T^{-1}$
$\gamma_s=(658.21\times\gamma_I)$	1.761×10^{11} $s^{-1}\cdot T^{-1}$
$\hbar$	1.055×10^{-34} J·s
S	2.5
$\omega_I=(\gamma_I\times B_0)$	1.348×10^{7} s^{-1}
$\omega_s=(\gamma_s\times B_0)$	8.874×10^{8} s^{-1}
σ_s	1.028×10^{18} m^2

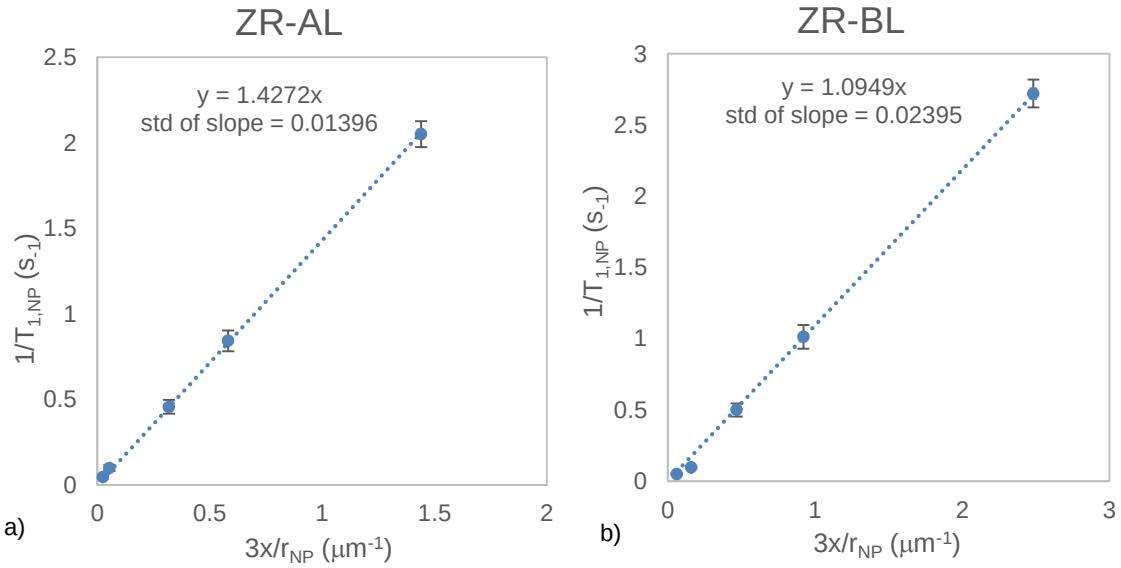

Figure 3.2 Measured $1/T_1$ of zirconia nanoparticles with different nanoparticle fluid volume ratio χ and size r_{NP} in a) ZR-AL dispersions, and b) ZR-BL dispersions fit the theory of Equations (3.2 and 3.3) well for suitable values of τ_m and τ_s. Values and standard deviations of slopes are obtained via weighted least squares linear regression.

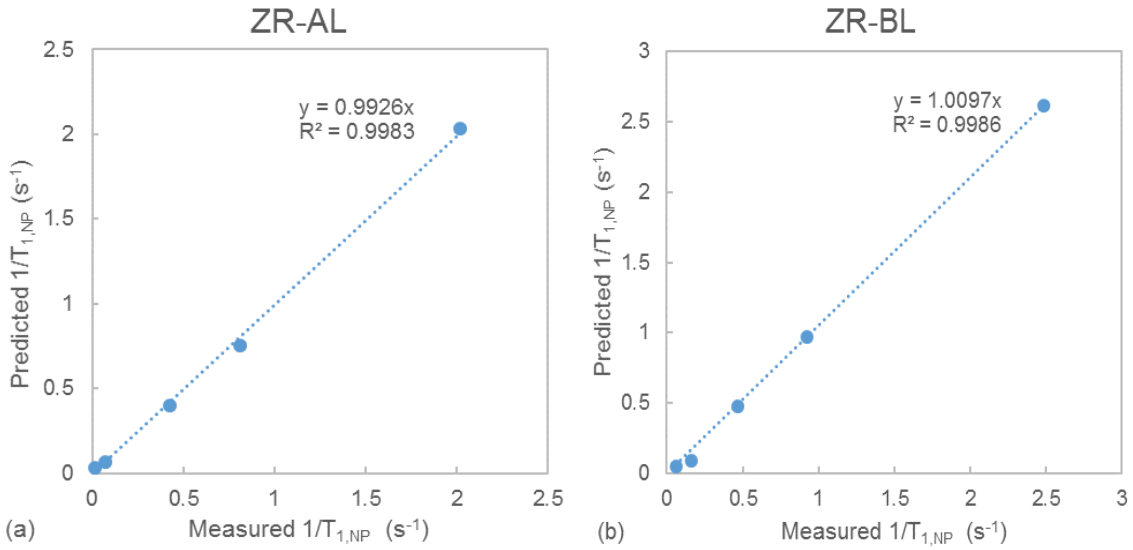

Figure 3.3 Predicted $1/T_{1,NP}$ from Equations (3.2) and (3.3) versus measured $1/T_{1,NP}$ in a) ZR-AL dispersions, and b) ZR-BL dispersions.

3.4.3 Fluids with Glass Bead Packs

Evidence of Adsorption

The recorded densities of the original ZR-6AL fluid and effluent with 0.7 PV were 1.0631 g/cm^3 and 1.0557 g/cm^3, respectively; measured densities of ZR-6BL before and after contact with glass bead pack were 1.0633 g/cm^3 and 1.0632 g/cm^3, respectively. Figure 3.4 shows the measured relaxation rates of DI water, ZR-6AL and ZR-6BL in three states: as bulk fluids before injecting into the glass bead pack, as the saturating fluid within the glass bead pack, and as effluent flushed from the glass bead pack. The bulk relaxation rates of DI water, ZR-6AL and ZR-6BL were 0.357, 1.166, and 1.234 s^{-1}, respectively. When saturating the glass bead pack, the relaxation rates were 0.408, 1.122, and 1.292 s^{-1}, respectively. Finally, when the fluids were flushed out of the glass bead pack the relaxation rates were 0.357, 0.850, and 1.237 s^{-1}, respectively. Error bars were calculated from the standard deviation of the longitudinal relaxation time (T_1) of the nanoparticle dispersions

before, during, and after contact with the 2 mm glass bead pack by linear regression of raw data with added noise as described previously.

The $1/T_1$ value of DI water increased inside the glass bead pack because of the presence of glass bead surfaces providing additional surface relaxation. The DI water effluent had the same value of bulk $1/T_1$ as before saturating the glass bead pack, as expected. The $1/T_1$ value of ZR-6BL also increased in the bead pack relative to the bulk value due to additional surface relaxation on the glass bead surfaces. Effluent ZR-6BL and the original bulk ZR-6BL showed similar $1/T_1$ values (1.234 s^{-1} and 1.235 s^{-1}) and nanoparticle sizes (84.8 nm and 85.1 nm), suggesting that the zirconia nanoparticle concentration in the ZR-6BL effluent was the same as that in the original dispersion. The measured density of the fluid did not change, confirming the absence of adsorption. Since the nanoparticles in ZR-6BL were negatively charged, we hypothesize that the electrostatic repulsion between the nanoparticles and glass bead surfaces prevented adsorption.

In contrast to the DI water and ZR-6BL, the $1/T_1$ value of ZR-6AL decreased inside the bead pack relative to the original dispersion, and the ZR-6AL effluent had a smaller $1/T_1$ than the original dispersion. The smaller $1/T_1$ in the bead pack result is counterintuitive because the additional surface relaxation contributed by the glass bead surfaces should have increased the relaxation rate. The explanation is that nanoparticles adsorbed onto the bead surfaces, reducing their concentration in the aqueous phase. The evidence of adsorption comes from the smaller $1/T_1$ of the effluent, which strongly indicates smaller nanoparticle concentration in the effluent than in the original dispersion. Moreover, the effluent density was smaller than the density of the original fluid, also consistent with nanoparticle adsorption on the beads. Since nanoparticles in ZR-6AL were positively charged, we hypothesize that electrostatic attraction caused adsorption of positively charged nanoparticles onto the negatively charged glass bead surface. This is consistent

with previous studies that have shown that the retention of surface-treated stabilized paramagnetic iron-oxide nanoparticles in sedimentary rocks is controlled by the zeta potential of the nanoparticles in dispersion (Yu et al., 2010). Evidently, the reduction in $1/T_1$ caused by depletion of nanoparticles in the aqueous phase in the pore space dominates the increase in $1/T_1$ brought from bead surfaces. The other effect of adsorption in this experiment is on the surface relaxation rate, which is described next.

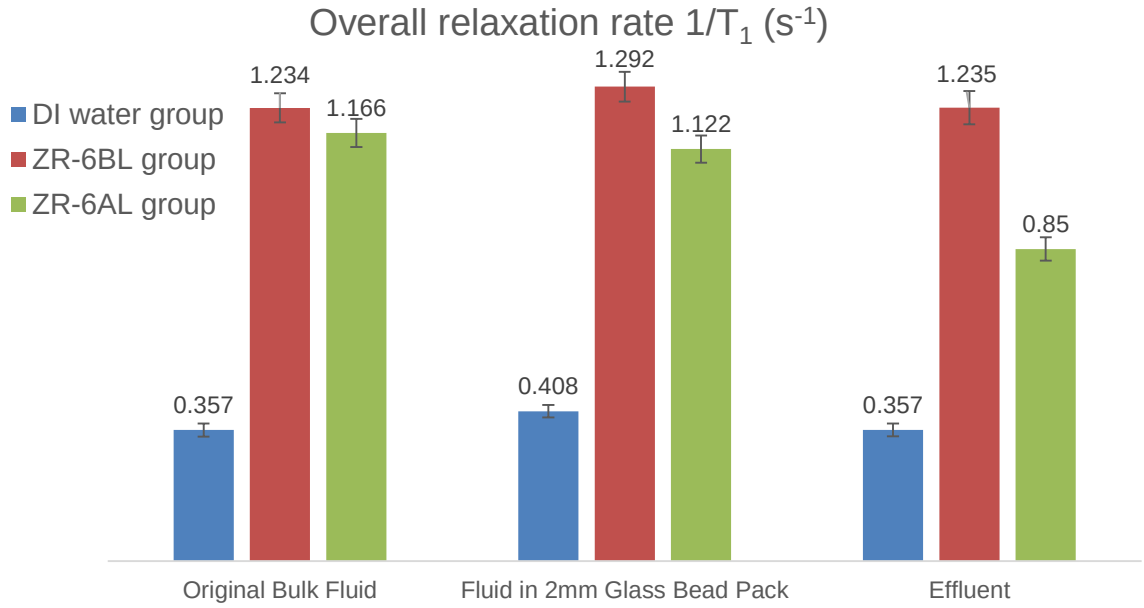

Figure 3.4 Comparison of $1/T_1$ values of DI water, ZR-6AL and ZR-6BL as prepared bulk phase; when present in pore space of bead pack; as bulk phase withdrawn from bead pack.

Adsorbed Nanoparticles

Based on relaxation rate of DI water and DI water in the glass bead pack, we were able to compute the glass bead surface relaxation rate $1/T_{1,\text{Medium-surface}}$, 0.051 s^{-1} based on Equation (3.6). In bead pack with 2 mm glass beads and 38% porosity, we assumed that the pores could be represented as spheres with the radius of a maximum inscribed sphere in body-centered cubic packing, which yielded r_{pore} of 0.613 mm. According to Equation

(3.9), the glass bead surface relaxivity $\rho_{1,\text{Medium-surface}}$ was 10.42 μm/s. The fact that the glass beads had a larger surface relaxivity than the nanoparticles (1.43 μm/s) was probably due to the presence of paramagnetic impurities in the glass beads, as has been noted in other studies using these particular beads (e.g., Daigle et al., 2014).

To compute the theoretical maximum adsorption amount of nanoparticles onto the glass bead surface, we assume that the conditions such as zeta potential, pH value, temperature, and other driving forces such as van der Waals attraction are favorable for each positively charged nanoparticle to attach onto negatively charged glass bead surface. A simple geometric method is used. With the assumption that nanoparticles form a dense packing in a monolayer on the glass bead surface, each nanoparticle covers a projected area (πr_{NP}^2) on the bead surface. A hexagonal packing of equal circles in 1 dimension is used to compute the maximum surface fraction of the glass bead surface that can be occupied by adsorbed nanoparticles (Chang and Wang, 2010). In the ZR-6AL group, we assumed that the number of nanoparticles remaining in the bulk fluid was M_{NP} and that the number of adsorbed nanoparticles on the glass bead surface was N_{NP}. Given that the glass bead pore radius is computed as 613 μm, and the volume fraction of nanoparticles in ZR-6AL is 1.114 %, the total number of nanoparticles with size about 113 nm in dispersion ($M_{NP}+N_{NP}$) in a single spherical pore is estimated as 1.42×10^9. N_{NP}, M_{NP} and $\rho_{1,\text{eff}}$ were computed from solving Equations (3.6, 3.7, 3.8 and 3.10). According to Equation 3.8, the maximum surface fraction of nanoparticles is 0.9069, and the corresponding fraction of nanoparticles in the system attached onto the glass bead surface is computed as 30.0%. When fully covered by a monolayer of zirconia nanoparticles, the surface relaxivity of the glass bead is 2.265 μm/s, and the overall relaxation rate is 0.934 s^{-1}. As shown in Figure. 3.5, with a fixed total number of nanoparticles in one pore, the overall relaxation rate of the saturated pore ($1/T_1$) decreases with adsorption of nanoparticles onto the glass bead surface. The

experimental data are consistent with the trend expected for adsorption of nanoparticles in a close-packed monolayer on the bead surface.

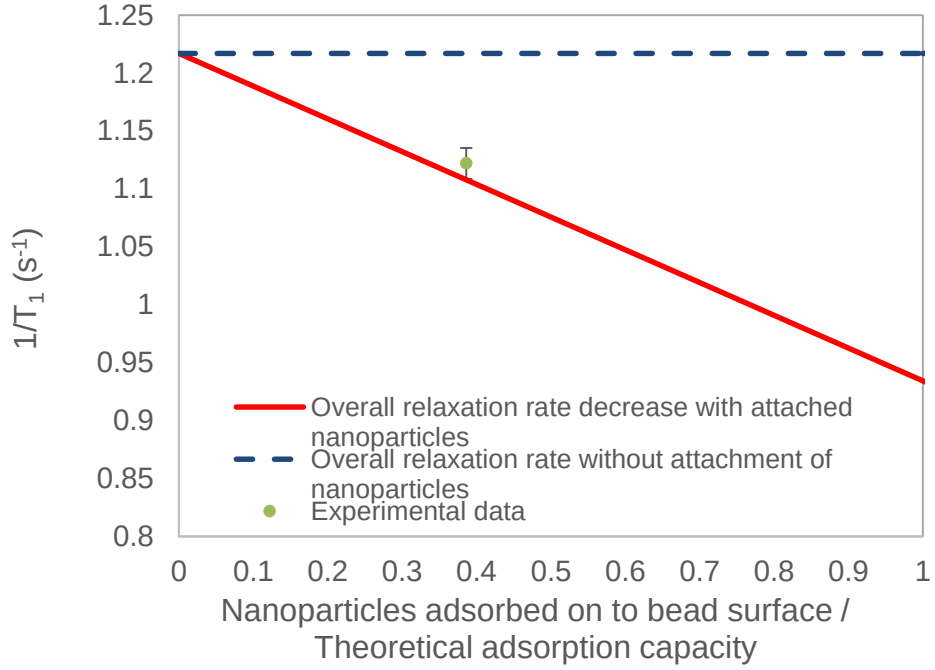

Figure 3.5 Calculated relaxation rate of saturated glass bead pack with adsorbed ZR-6AL nanoparticles. Black line indicates no adsorption, the overall relaxation rate remains as 1.217 s^{-1}; red line shows how overall relaxation rate of ZR-6AL saturated glass bead pack decreases with more attached nanoparticles; green dot is computed from density measurement of effluent and original fluid and corresponding relaxation rate of saturated bead pack.

Based on density measurement, we computed that approximately 11.6% of the nanoparticles in the original dispersion adsorbed onto glass bead surface and modified the surface relaxivity $\rho_{1,eff}$ to 7.27 μm/s. The smaller relaxivity also contributes to the smaller value of $1/T_1$ in the ZR-6AL fluid-saturated bead pack, though in this experiment the reduced aqueous phase concentration is the dominant effect. The measured relaxation rate of glass bead pack after core flushing with 1.2 PV of DI water was 0.498 s^{-1}, which is faster than that of glass bead pack saturated with DI water (0.408 s^{-1}), this may due to part of

nanoparticle desorption during core flushing. Recall Equations (3.5 and 3.8), when nanoparticles are in fluid, the surface area that proton would access it the whole sphere surface ($4\pi r_{NP}^2$), while adsorbed nanoparticles on pore surface only provide projected area (πr_{NP}^2) on pore surface for proton to relax. Relative amount of desorbed nanoparticles was 14%, after 1.2 PV of DI water flushing, effective pore surface relaxivity was 6.05 μm/s with remained 86% of adsorbed nanoparticles, there was 15.4% change in pore surface relaxivity due to core flooding.

3.4.4 Fluids with Boise Sandstone Core Samples

Evidence of adsorption

DI water, ZR-6AL, and ZR-6BL were used to saturate three Boise sandstone cores labeled as BS1, BS2, and BS3, respectively. We then measured the T_1 distributions of the three saturated core samples. Figure 3.6 is obtained from a linear inversion calculation based on NMR raw data displayed in the Appendix. Figure 3.6 shows and compares T_1 distribution of Boise sandstone cores BS1, BS2, and BS3 saturated with DI water, ZR-6AL, and ZR-6BL, respectively. Assuming that the three cores had similar pore structure and size, different saturating fluids altered relaxation time to different extents: core sample BS2 saturated with ZR-6BL showed the shortest peak T_1 (443.2 ms), core sample BS3 saturated with ZR-6AL gave an intermediate peak T_1 (424.3 ms), and the DI water-saturated core sample (BS1) displayed the longest peak T_1 value (1165 ms). The differences can be explained by different degrees of surface relaxivity alteration in the different core samples. Note the apparent variation in total porosity (the area under each curve) among the three samples; this is probably due to differences in hydrogen index due to different stabilizers in the nanoparticle dispersions as well as the presence of the nanoparticles themselves, which would tend to lower the hydrogen index of the pore fluid.

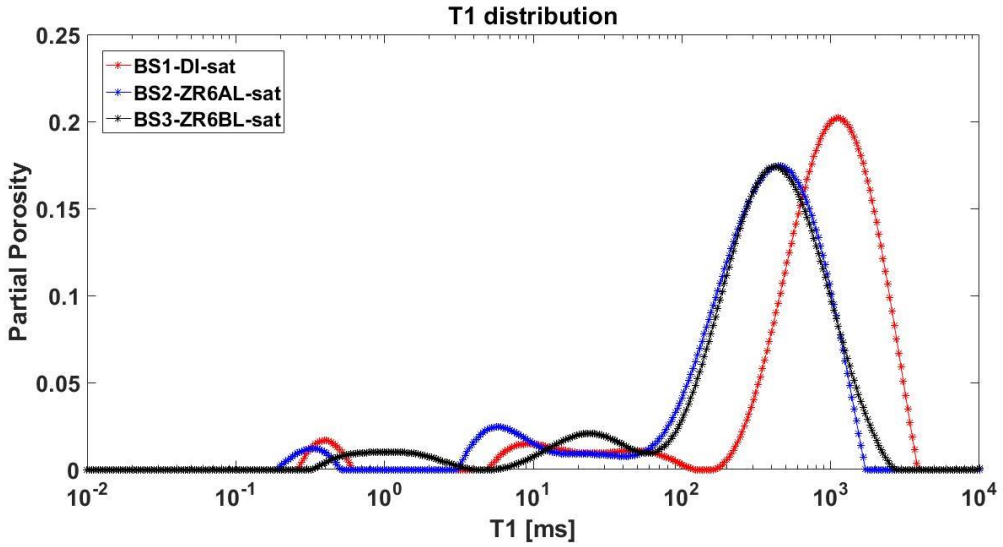

Figure 3.6 T_1 distribution of Boise sandstone cores saturated with DI water, ZR-6AL, and ZR-6BL.

The bulk relaxation rates, nanoparticle sizes and density of the original fluids before saturating Boise sandstone cores and the effluents are displayed in Table 3.3. Based on density measurements (values not shown here), there were less nanoparticles in effluents than in original fluids. Thus some of the nanoparticles introduced into the cores during vacuum saturation remained in the core after the injection of 1.2 PV of DI water. This is expected for the positively charged ZR-6AL nanoparticles and the negatively charged sand grains in the core. For the negatively charged ZR-6BL nanoparticles, this is presumably the consequence of mechanical retention or van der Waals attraction. Measured nanoparticle size in effluents were slightly larger than that in original fluids. According to Figure 3.2, larger nanoparticle size and smaller nanoparticle concentration should result in a smaller relaxation rate if nanoparticle relaxivity remained constant. However, the measured relaxation rates of the effluents did not decrease correspondingly. In fact the relaxation rate increased for the ZR-6AL fluid. Because ZR-6AL contains HNO_3 to

stabilize nanoparticles, it is possible that acid dissolved iron or other minerals from the sandstone. The presence of these species in the effluent would relax protons faster and thus counterbalance the effect of reduced nanoparticle concentration. This complicates the relationship between nanoparticle concentration and measured relaxation rate.

Table 3.3 NMR measured relaxation rate and nanoparticle size of nanofluids before, in and after contact with Boise sandstone core.

Original Fluids	DI water	ZR-6BL	ZR-6AL
Relaxation rate $1/T_1$ (s^{-1})	0.348	1.294	1.202
Nanoparticle size (nm)	N/A	84.8	113
Fluids in Boise sandstone core	DI water	ZR-6BL	ZR-6AL
Relaxation rate $1/T_1$ (s^{-1})	0.858	2.26	2.36
Relaxation rate change due to Boise sandstone $1/T_1$ (s^{-1})	0.51	0.966	1.158
Effluents	DI water	ZR-6BL	ZR-6AL
Relaxation rate $1/T_1$ (s^{-1})	0.353	1.293	1.209
Nanoparticle size (nm)	N/A	90.1	115

Adsorbed Nanoparticles

As shown in Table 3.3, when saturating Boise sandstone, the relaxation rates of DI water, ZR-6BL and ZR-6AL increased by 0.51 s^{-1}, 0.966 s^{-1} and 1.158 s^{-1}, respectively. The magnitude of change was much larger when nanoparticles were present. With saturation of zirconia nanoparticles, Boise sandstone surface relaxivity may have changed, but the value was difficult to determine since there apparently were complicated reactions between nanoparticles and the sandstone surface. We calculated the surface relaxation rate of Boise sandstone from the DI water measurement using Equation (3.6) as 0.51 s^{-1}. To compute the surface relaxivity of Boise sandstone, we assumed that the pore radius was 145 μm based on micro-CT images (Krohn, 1988). From Equation (3.9) we obtained Boise sandstone surface relaxivity as 24.65 μm/s when DI water present. Based on Equation (3.6), in ZR-6BL saturated Boise sandstone, we expected no adsorption of nanoparticles

due to electrostatic repulsion, hence $1/T_{1,\text{NP-on-surface}}$ should be zero. If assumed medium surface relaxivity as 24.65 μm/s, to give overall relaxation rate as 2.36 s^{-1} in ZR-6BL saturated Boise sandstone core, nanoparticle dispersion in pore fluid should have relaxation rate as 1.85 s^{-1}, which is higher than original ZR-6BL relaxation rate (1.294 s^{-1}). From Equation (3.5), the corresponding relaxivity of nanoparticles would be 1.561 μm/s, which is in consistence with our previous guess based on effluent relaxation rate and density measurements. Increased relaxivity of nanoparticles may be caused by dislodged materials that relax proton faster from sandstone surface. If constant relaxivity of nanoparticles in ZR-6BL was assumed, Boise sandstone surface should give an increased surface relaxivity as 51.52 μm/s. However, in ZR-6AL saturated Boise sandstone, when assume fixed relaxivity of nanoparticles (1.427 μm/s) in ZR-6AL, based on Figure 3.2 we calculated higher nanoparticle concentration in effluent than in original dispersion, which conflicted with mass conservation. Thus, nanoparticle relaxivity might have changed after contact with Boise sandstone. To get the best estimate of the changed surface relaxivity of nanoparticles and sandstone surface, we assumed the relevant amount of adsorbed zirconia nanoparticles was 11.6% according to the results in siliceous glass bead packs. Effective sandstone surface relaxivity was computed as 55.16 μm/s, nanoparticle surface relaxivity was changed to 1.60 μm/s during interactions with Boise sandstone minerals. Characterization of nanoparticles in effluent is presented with more details in Chapter 4.

3.5 DISCUSSIONS

Recent NMR works have been focused on measurements of porous media saturated with nanofluids (Anand and Hirasaki, 2008; Yu, 2012; Cheng et al., 2014a,b), did not study the effects of nanoparticles brought to pore surface relaxivity. How and to what extent will the pore surface relaxivity be altered by adsorbed paramagnetic nanoparticles remained

unknown. In this work, we try to answer this question by adding different paramagnetic nanoparticles in pore fluid, and made three measurements: i) a nanoparticle-free fluid measurement (DI water) to get pore wall effect; ii) the fluid-saturated measurement under conditions for which the change in aqueous concentration is the dominant effect (this demonstrates surface adsorption occurred); iii) displace the nanoparticle dispersion with DI water and isolate the effect of the controlled relaxivity of the pore walls.

This work is a step toward the engineered control of surface relaxivity of porous media, which in turn would enable more robust inference of pore size distributions from NMR measurements, especially in logging tools. In our experiments, the known value of pore size and surface relaxivity of silica porous media enabled us to estimate adsorbed zirconia nanoparticles and modified surface relaxivity. To realize the end goal of being able to predict pore size distributions directly from NMR measurements with no prior knowledge of pore sizes, further work is necessary to understand the link between zeta potential differences between nanoparticles and substrates, quantity adsorbed, and overall relaxivity alteration. Once such model is generated and tested, we can use it to simulate, predict and control concentration of adsorbed nanoparticles on pore surface to fix effective surface relaxivity to the pre-decided value, followed by the calculation of pore size from measured relaxation time distribution. The results presented here show promise for this technique and serve as a proof of the concept that surface relaxivity can be modified in a predictable manner.

More generally our work helps to understand behavior of nanoparticles in porous media and will be used in future studies of the pore-scale characteristics in rocks. In particular, our work highlights the complicated interplay between nanoparticles and rock surfaces that affect measurements of bulk properties. Understanding these complicating factors is essential to future applications that depend on coating grain surfaces or fluid

interfaces with nanoparticles, such as enhanced oil recovery, imaging oil-water contacts, and determining interfacial surface areas.

3.6 CONCLUSIONS

We studied the influence of zirconia nanoparticles on NMR response in bulk fluid dispersion and in porous media. The bulk relaxation rate of nanoparticle dispersions is proportional to nanoparticle-pure fluid volume ratio and inversely proportional to nanoparticle size. In nanofluid-saturated porous media (glass bead packs, outcrop sandstone), electrostatic attraction between grain surfaces and nanoparticles was the main driving force for adsorption of nanoparticles onto grain surfaces. The two types of nanoparticles used in this study differed only in their zeta potential (one being positive, the other negative), and only the positively charge particles adsorbed appreciably onto the negatively charged silica surfaces of the porous medium. Porous media surface relativities were altered only by the presence of adsorbed paramagnetic nanoparticles. When 1.114 vol. % positively charged zirconia nanoparticles dispersion was used to saturate a glass bead pack, 11.6% of the nanoparticles were adsorbed to the bead surfaces and modified the glass bead surface relaxivity from 10.42 μm/s to 7.27 μm/s.

Under theoretically favorable conditions where all ZR-6AL nanoparticles are driven to attach onto the glass bead surface and generate a monolayer with dense packing, the maximum fraction of nanoparticles that can be attached is 30.0%, occupying 0.9069 of glass bead surface. The surface relaxivity is altered to 2.265 μm/s, and the overall relaxation rate is 0.934 s^{-1}. In this study, the fraction of retained nanoparticles is 11.6%, which is much lower than the theoretical maximum value of 30.0%. Note that we did not consider the hydration layer on the nanoparticles themselves, which may affect attachment of nanoparticles onto bead surface.

DI water flushing was able to wash out 14% of adsorbed nanoparticles from siliceous surface, change of surface relaxivity due to core flushing was 15.4%. In contrast, negatively charged zirconia nanoparticles did not alter the relaxivity of the beads. When positively charged zirconia nanoparticle dispersions were used to saturate a Boise sandstone core, both pore surface and nanoparticle relaxivity were altered. With the assumption of fixed relaxivity of nanoparticles in ZR-6AL, retained nanoparticles in Boise sandstone would be negative, and thus invalidate that assumption. With assumed 11.6% of positive nanoparticles' adsorption, Boise sandstone surface relaxivity was modified from 24.65 μm/s to 55.16 μm/s, and nanoparticle surface relaxivity changed from 1.43 μm/s to 1.60 μm/s However, mechanical retention of negatively charged nanoparticles in the Boise sandstone may have caused additional relaxation effects such as increased surface relaxivity to 1.561 μm/s or increased nanoparticle relaxivity from 24.65 μm/s to 51.52 μm/s. Our work indicated there is a way to control pore surface relaxivity by adsorbed paramagnetic nanoparticles and served as the foundation to generate a model to link relaxation time distribution and pore size by altered pore surface relaxivity. But in the subsurface environment in the oilfield where temperature, pressure, and pH are different from those of our experiment, the behavior and stability of nanoparticles may be different from our observation in this study. In addition, the hydration layer present on nanoparticles may also play a role in affecting attachment of nanoparticles onto the pore surface. Further work is needed to constrain these effects.

Chapter 4

Paramagnetic nanoparticles as NMR contrast agents in sandstone: Importance of nanofluid-rock interactions[2]

4.1 INTRODUCTION

In porous media, the nuclear magnetic resonance (NMR) relaxation time distribution is mainly controlled by interactions near the pore-grain interface for wetting phase fluids (Foley et al., 1996). Fluid molecules in the pore space have the chance to interact with pore surface by diffusion, where they are temporarily adsorbed (Korringa et al., 1962). On the pore surface, generally there are two types of adsorption sites: one magnetic, including paramagnetic and ferromagnetic, and the other diamagnetic. Magnetic sites enhance relaxation due to the strong coupling between nuclear magnetic moments and unpaired electrons and thus control relaxation rate. Magnetic sites in natural rocks are paramagnetic ions, and most of them are iron (Carmichael, 1982). The concentration of paramagnetic ions varies with natural sedimentary rocks, so pore surface relaxivity varies from rock to rock and even within the rock at the pore scale. To control pore surface relaxivity, we investigated the adsorption of paramagnetic nanoparticles onto pore surface. Nanoparticles offer advantages over the ferric ions that have been employed in previous work (Anand and Hirasaki, 2008) since sorption of ions is more difficult to monitor and quantify, while nanoparticles have several independent mechanisms for attachment: van der Waals forces, electrostatic attraction, and a tunable chemical affinity for functional groups or compounds at the rock surface.

Transport and retention behavior of paramagnetic nanoparticles in sedimentary rocks have been studied by Oldenburg et al. (2000), Prodanović et al. (2010) and Yu et al.

[2]This chapter is based on: Zhu, C., Daigle, H., & Bryant, S. L. (2016). Paramagnetic nanoparticles as nuclear magnetic resonance contrast agents in sandstone: Importance of nanofluid-rock interactions. *Interpretation*, *4*(2), SF55-SF65. I was the primary author.

(2014). When stable nanoparticles with virtually zero surface charge and or with negative charge were individually dispersed in sandstone pores, even though there was no electrostatic attraction between nanoparticles and silica surface, attachment of nanoparticles onto pore surface was observed by Yu et al. (2010). The main retention mechanism is reversible adsorption on pore wall: van der Waals attraction could drive attachment of nanoparticles onto solid surface, and such attachment can be reversed due to Brownian diffusion (Rodriguez Pin et al., 2009 and Yu et al., 2010). Nanoparticles that are unstable tend to aggregate to form clusters when van der Waals attraction overcomes electrostatic repulsion, which leads to nanoparticle retention when the size of the clusters become larger than pore throats (Wang et al., 2008). Positively charged nanoparticles tend to attach onto negatively charged mineral surfaces by electrostatic attraction (Zhu et al., 2015).

Previous work in Chapter 3 has indicated that positively charged zirconia nanoparticles adsorb onto glass bead surfaces and decreased the surface relaxivity of the glass beads due to smaller relaxivity of the nanoparticles, while negatively charged nanoparticles are not retained in glass bead packs and do not affect the pore surface relaxivity (Zhu et al., 2015). However, in Boise sandstone, due to the complicated interactions between the nanoparticle dispersion and mineral surface, the surface relaxivities of the pore surface and the nanoparticles both change but in opposite directions. The purpose of our present work is therefore to analyze the interactions of paramagnetic nanoparticle dispersions and sandstone surface that lead to surface relaxivity alteration, as well as the factors that control such interactions. In our work we analyzed longitudinal relaxation time (T_1) measurements since the diffusion relaxation additionally complicates the relationship between transverse relaxation time (T_2) and pore size (e.g., Kleinberg and Horsfield, 1990). We measured longitudinal relaxation time, pH, zeta potential, and

nanoparticle size of zirconia nanoparticle dispersions with different surface charge under various pH values. We then saturated Boise sandstone cores with the different dispersions, and performed corefloods to displace the dispersions, and collected the effluents. T_1, pH value, zeta potential, and nanoparticle sizes in effluent samples were measured and compared with the original dispersions to investigate possible interactions between nanoparticle dispersions and pore surfaces. To isolate the effects of the nanoparticle dispersion fluids from the effects of the nanoparticles themselves, we used pure deionized (DI) water, nitric acid, and TMAH as control groups in corefloods. We found that nanoparticles were able to decrease Boise sandstone surface relaxivity by attachment onto pore surface. In addition, we found that pH was an important parameter in determining zeta potential and stability of nanoparticles, and influenced adsorption of nanoparticles on pore walls. Our work showed that rock's relaxivity can be changed by attachment of nanoparticles. This can serve as the foundation to generate a model to link relaxation time distribution and pore size by altered pore surface relaxivity.

4.2 THEORY OF RELAXATION CALCULATION

4.2.1 Relaxivity of nanoparticles in bulk fluid

We analyzed the longitudinal relaxation of nanoparticle dispersions by considering them as dilute porous media composed of spherical nanoparticles and dispersion fluid. Assuming that surface relaxation takes place in the fast diffusion regime (Brownstein and Tarr, 1979), the nanoparticle surface relaxivity $\rho_{1,NP}$ can be computed from Equation (4.1), where pore surface area S that water molecules can access to equals the surface area of nanoparticle spheres, pore fluid volume V is computed as total dispersion volume V_{Total} minus nanoparticle volume V_{NP}, χ is volume of nanoparticles per unit volume of fluid in the dispersion:

$$\frac{1}{T_{1,\mathrm{NP}}} = \rho_{1,\mathrm{NP}}\left(\frac{S}{V}\right)_{pore} = \rho_{1,\mathrm{NP}}\left(\frac{V_{NP}\dfrac{3}{r_{NP}}}{V_{Total}-V_{NP}}\right) = \rho_{1,\mathrm{NP}}\left(\frac{V_{NP}}{V_{Total}-V_{NP}}\right)\left(\frac{3}{r_{NP}}\right) = \rho_{1,\mathrm{NP}}\left(\frac{3\chi}{r_{NP}}\right) \quad , (4.1)$$

Nanoparticle surface relaxation rate $1/T_{1,\mathrm{NP}}$ can be obtained from the relaxation rates of the nanoparticle dispersion $1/T_1$, and pure dispersion fluid $1/T_{1,\mathrm{Fluid}}$ according to Equation (4.2). While it is well established that salinity affects aggregation properties of nanoparticles (Fernández-Toledano et al., 2006) and so would have an effect on the NMR response of the nanoparticles in porous media. Higher salinity leads to more aggregation, less effective transportation and slower relaxation rate of nanoparticles. We did not perform experiments at elevated salinity because we wanted to minimize any potential aggregation.

$$\frac{1}{T_1} = \frac{1}{T_{1,\mathrm{Fluid}}} + \frac{1}{T_{1,\mathrm{NP}}} \quad . (4.2)$$

We assume that the relaxation rates from different processes are additive (e.g., Carr and Purcell, 1954).

4.2.2 Retained nanoparticles in Boise sandstone cores

When nanoparticle dispersions enter a porous medium, it is possible for nanoparticles to attach to the porous medium surface (Anand and Hirasaki, 2008), thus affecting both the bulk dispersion relaxation time and the surface relaxation time at the pore wall. Suppose some number N_{NP} of nanoparticles move from the pore space to the pore surface, while M_{NP} nanoparticles remain in the pore space. According to our previous study (McDonald et al., 2005 and Zhu et al., 2015), the relaxation rate of nanoparticles in bulk dispersion ($1/T_{1,\text{NP-in-pore}}$) with M_{NP} nanoparticles remaining in the pore can be

calculated from the original relaxation rate of the bulk dispersion $1/T_{1,\mathrm{NP}}$ with (M_{NP}+N_{NP}) nanoparticles:

$$\frac{1}{T_{1,\mathrm{NP-in-pore}}} = \frac{1}{T_{1,\mathrm{NP}}}\left(\frac{M_{NP}}{M_{NP}+N_{NP}}\right). \quad (4.3)$$

With assumed single exponential decay in a single pore (Brownstein and Tarr, 1979), the overall relaxation rate is the sum of relaxation rates of the bulk dispersion in pore space and the surface relaxation rate of the pore wall. As shown in Figure 4.1, in a porous medium saturated with nanoparticle dispersion, relaxation occurs in the pure dispersion fluid and at the surfaces of nanoparticles still in dispersion, as well as on the pore surface and on the surfaces of nanoparticles adsorbed to the pore wall. The overall relaxation rate in the pore is given by

$$\frac{1}{T_1} = \frac{1}{T_{1,\mathrm{Bulk}}} + \frac{1}{T_{1,\mathrm{Surface}}} = \left(\frac{1}{T_{1,\mathrm{Fluid}}} + \frac{1}{T_{1,\mathrm{NP-in-pore}}}\right) + \left(\frac{1}{T_{1,\mathrm{Medium-surface}}} + \frac{1}{T_{1,\mathrm{NP-on-surface}}}\right), \quad (4.4)$$

where $1/T_1$ is the measured relaxation rate of porous media saturated with nanoparticle dispersion, $1/T_{1,\mathrm{Bulk}}$ is the relaxation rate of nanoparticle dispersion in pore, $1/T_{1,\mathrm{Surface}}$ is the relaxation rate of pore surface, $1/T_{1,\mathrm{Fluid}}$ is the relaxation time of pure fluid in nanoparticle dispersion, $1/T_{1,\mathrm{NP\text{-}in\text{-}pore}}$ is the relaxation rate of nanoparticles in dispersion located in pores, $1/T_{1,\mathrm{Medium\text{-}surface}}$ is the intrinsic relaxation rate on the pore surface in the absence of nanoparticles, and $1/T_{1,\mathrm{NP\text{-}on\text{-}surface}}$ is the relaxation rate of adsorbed nanoparticles on pore surface.

Adsorbed nanoparticles will alter both the bulk dispersion relaxation time (by reducing the nanoparticle concentration in the dispersion) and the surface relaxation time at the pore wall. With N_{NP} nanoparticles adsorbed onto one spherical pore, $\rho_{1,\mathrm{eff}}$ is related to the relaxivities of the adsorbed nanoparticles and the pore wall. We know that the nanoparticles were not perfect spheres, and the surface of the glass beads and Boise

sandstone at the nanometer scale may have irregularities that, when combined with the irregular shape of the nanoparticles, would result in a finite contact area between the nanoparticles and grains. Therefore, we believe that it is unlikely that the nanoparticles were in point contact with the grain surfaces in both the case of the glass beads and Boise sandstone. In addition, small interstices between the adsorbed nanoparticles and the silica surface may relax protons at a much faster relaxation time (1~50 ms) as shown in Figure 4.4 and Figure 4.6 due to restrictions in Brownian motion of protons in and out of these interstices. Since the silica grain radius is much larger than nanoparticle radius, we use the projected area of the nanoparticles on the silica surface to compute the contributed relaxation of nanoparticles with relaxivity of $\rho_{1,\mathrm{NP}}$, and the remaining accessible silica surface area provides a relaxivity of $\rho_{1,\text{Medium-surface}}$. $\rho_{1,\text{Medium-surface}}$ can be calculated according to the intrinsic relaxation rate on the pore surface in the absence of nanoparticles $1/T_{1,\text{Medium-surface}}$ and pore radius r_{pore}. $\rho_{1,\mathrm{eff}}$ is calculated from the areally weighted average of medium surface relaxivity $\rho_{1,\text{Medium-surface}}$ and attached NNP nanoparticles relaxivity $\rho_{1,\mathrm{NP}}$, as indicated in Equations (4.5-4.7).

$$\frac{1}{T_{1,\text{surface}}} = \rho_{1,\mathrm{eff}}\left(\frac{S}{V}\right)_{pore} = \rho_{1,\mathrm{eff}}\frac{3}{r_{pore}} \quad \text{for spherical pores,} \quad (4.5)$$

$$\rho_{1,\mathrm{eff}} = \frac{N_{NP}\pi r_{NP}^2}{4\pi r_{pore}^2}\rho_{1,\mathrm{NP}} + \frac{4\pi r_{pore}^2 - N_{NP}\pi r_{NP}^2}{4\pi r_{pore}^2}\rho_{1,\mathrm{Medium-surface}}, \quad (4.6)$$

$$\rho_{1,\mathrm{Medium-surface}} = \frac{1}{T_{1,\mathrm{Medium-surface}}}\left(\frac{V}{S}\right)_{pore} = \frac{1}{T_{1,\mathrm{Medium-surface}}}\frac{r_{pore}}{3}. \quad (4.7)$$

Here r_{pore} is the radius of an assumed spherical pore, $4\pi r_{pore}^2$ indicates the total pore surface of porous media made from packed sphere grains, and πr_{NP}^2 measures the area occupied by one nanoparticle attached to the pore wall.

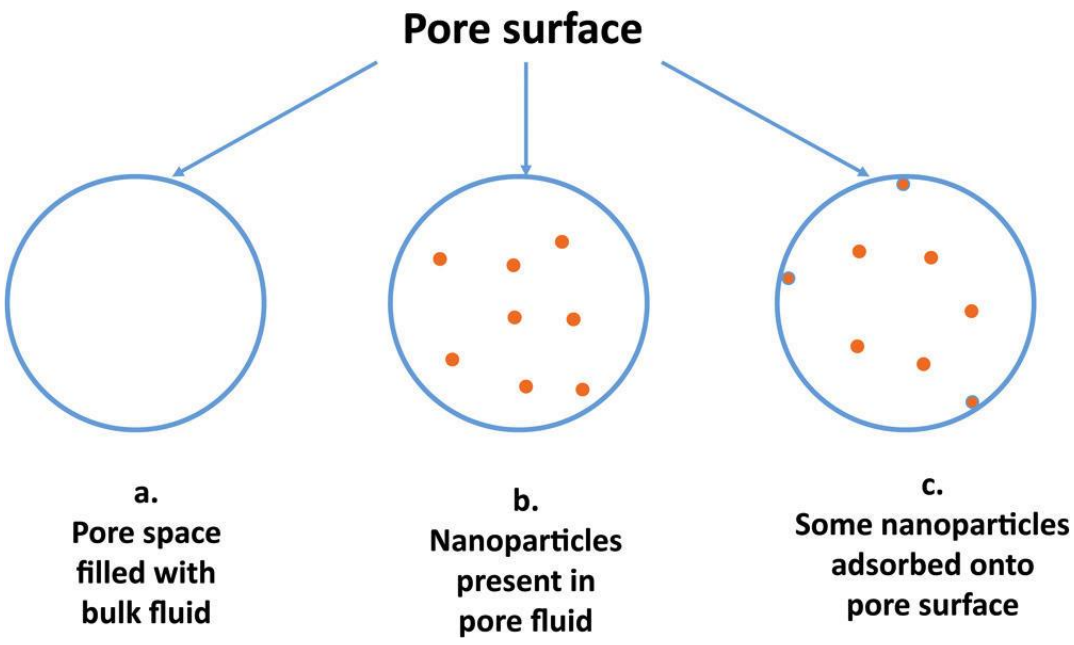

Figure 4.1 Mechanisms of relaxation of nanoparticle dispersion in a single spherical pore. Sizes of the pore space and nanoparticles are not to scale: (a) When only pure bulk fluid is present in the pore space, the overall relaxation rate $1/T_1$ is the sum of $1/T_{1,\text{fluid}}$ and $1/T_{1,\text{medium-surface}}$; (b) when nanoparticles are in pore fluid, $1/T_1$ increases by an increment $1/T_{1,\text{NP-in-pore}}$; and (c) some nanoparticles are adsorbed onto the pore surface, and the measured $1/T_1$ equals the summation of $1/T_{1,\text{fluid}}$, $1/T_{1,\text{NP-in-pore}}$, $1/T_{1,}$medium-surface, and $1/T_{1,\text{NP-on-surface}}$. Note that $1/T_{1,\text{NP-in-pore}}$ is smaller than in panel (b) because fewer nanoparticles are present in the bulk fluid.

4.3 METHODS

We used two types of zirconia nanoparticle dispersions from Nissan Chemical America Corporation. The first was ZR-30AL, with 30 wt% positively charged zirconia (ZrO_2) nanoparticles with HNO_3 as stabilizer. The second was ZR-40BL, with 40 wt% negatively charged zirconia nanoparticles with $C_4H_{12}N.HO$ (Tetramethylammonium

Hydroxide: TMAH) as stabilizer. DI water was used to dilute the original zirconia nanoparticle dispersions into 6 wt% and 7.5 wt%, which we denote as ZR-6AL, ZR-7.5AL, ZR-6BL, and ZR-7.5BL. pH values were measured with a pH probe and nanoparticle sizes were measured by dynamic light scattering (DLS). To provide control groups, we prepared HNO_3 solution with the same pH value of ZR-6AL (3.2), and TMAH solution with same pH value of ZR-6BL (9.1).

A Malvern Nano ZS ZetaSizer was used to measure particle size distribution and surface zeta potential of the zirconia nanoparticles. Size and zeta potential calibrations were performed with calibration standard dispersions before each measurement. 450 μL of nanoparticle dispersion was placed in a disposable cell to measure particle size distribution. Fisher Scientific 1.0 mL plastic syringe was used to inject 0.9 mL of nanoparticle dispersion into a disposable folded capillary cell for zeta potential measurement. The average value and distribution of sizes and zeta potentials were recorded. Each sample was measured three times and the mean value was chosen to be presented.

NMR measurements were performed at room temperature (20°C) using a 2 MHz GeoSpec2 benchtop NMR core analysis instrument from Oxford Instruments with an operating frequency of 2.15 MHz The external magnetic field B_0 was 0.05047 Tesla. Inversion recovery measurement was used to determine the distribution of longitudinal relaxation times (T_1). Signal noise ratio (SNR) was set to 100 for each NMR measurement.

To obtain nanoparticle concentration, we determined the density of nanoparticle dispersions ZR-6AL, ZR-7.5AL, ZR-6BL, and ZR-7.5BL, DI water, HNO_3 and TMAH original fluids and effluents after saturating porous media. The mass of known volume of dispersion was measured by Mettler-Toledo mass balance with a precision of 0.0001 g. Measurements were repeated 5 times at room temperature, and average values were used. Nanoparticle concentration was computed from the density of an effluent sample and that

of the corresponding pure dispersion fluids. This method for determining nanoparticle concentration assuming that the concentration of other fluid components (notably the dissolved solids) is invariant, and in particular that the acid and base neutralization reactions in the core do not change the fluid density.

We measured pH with a Thermo Scientific Orion Versa Star pH benchtop meter. The meter was calibrated with standard pH buffers at pH 4.01, 7.00 and 10.01. The pH probe was triple rinsed with DI water before measurements of different fluid samples.

We used ten Boise sandstone samples Core #1-#13 in this study, each 1" (2.54 cm) in diameter and 3" (7.62 cm) in length. All core samples were oven-dried for 24 hours at 135°C. All dried core samples were saturated with various fluids by vacuum pump. Our preliminary results indicated that ZR-6AL and ZR-7.5AL dispersion remained stable after contact with Boise sandstone, while nanoparticles in ZR-6BL and ZR-7.5BL dispersion coagulated and most of nanoparticles were retained in Boise sandstone due to large cluster size since the ZR-6BL and ZR-7.5BL effluent showed pH value close to 7. Since ZR-6BL and ZR-7.5BL nanoparticles are stable in dispersion only at pH >8.8, Cores #8, #9, #13 and #13 were pretreated with strong TMAH at pH 13.416 and put into oven to dry for 24 hours at 135°C before saturating with ZR-6BL and ZR-7.5BL. After the pre-treatment, TMAH residues were able to stay on sandstone surface and provide strong alkaline condition. To isolate the effect of dried strong alkali left on pore surface, we also pretreated Core #4 and #5 with strong TMAH at pH 13.4 for same procedure before saturated with TMAH fluid with pH of 9.1. All saturating fluids for 10 cores were introduced by vacuum pump. To saturate the cores, oven-dried cores were placed in a vacuum container for 4 hours, after which the saturating fluid was injected and vacuumed for another 1 hour.

To test whether nanoparticles were adsorbed on pore surface, after measuring the T_1 distribution of the saturated core plug we flooded the plug with DI water at a constant

flow rate of 0.5 ml per minute. Effluent was collected from the bottom outlet of the vertically mounted core samples. To identify the effect of pH on the interactions between nanoparticles and the pore surface, we also flushed all pore fluids (with and without nanoparticles) with pure solutions at the same pH value. DI water was also used as flushing fluid as a control. The T_1 value, nanoparticle size, zeta potential and concentration were measured and compared with that of the original fluids.

We used mass balance to measure nanoparticle concentrations. There are three main reasons that we did not use UV-VIS to measure normalized concentration: The first reason is that our NP concentrations in the original fluid and effluents were relatively high and out of the range in which UV-VIS displays a linear relationship with concentration. The second reason is that we collected very small volumes of effluent at each time, such as 0.4 ml, which was not enough for the UV-VIS measurement which requires at least 1 ml. Finally, we wanted to collect all effluents and measure the T_1 value and Fe concentration in the effluents, and dilution to make the UV-VIS measurement would have altered the experimental results.

To identify and isolate the contribution of nanoparticles to the overall relaxation rate in effluent samples, we additionally centrifuged nanoparticles from the effluents we collected. Zirconia nanoparticle dispersion effluents were placed in 15ml Fisher Scientific plastic centrifuge tubes and centrifuged at 10000 rpm for 30 minutes using Beckman Avanti J-E centrifuge and rotor JA-10. Supernatant fluid was collected to measure T_1, density, and iron concentration.

We used Varian Liberty Series II Axial ICP-OES to measure dissolved iron concentration in original fluids and effluents after removal of nanoparticles. Wavelengths for Fe were picked as 234.350 nm, 238.204 nm, and 259,940 nm, 1 mg/L, 2 mg/L, 5 mg/L, 8 mg/L, 10 mg/L, 20 mg/L, 50 mg/L, 80 mg/L and 100 mg/L iron standard solutions were

used for calibration. Concentrations of iron in samples were measured and calculated based on a calibration range from 0 mg/L to 100mg/L. Measurements were performed in triplicate and we reported the average value of the three values as the iron concentration in each sample.

4.4 RESULTS

Different Boise sandstone cores were saturated with DI water, HNO_3, TMAH, ZR-6AL, ZR-7.5AL, ZR-6BL, and ZR-7.5BL, and the saturating fluids were flushed with DI water, HNO_3, and TMAH. Table 4.1 displays the 13 Boise sandstone cores along with their respective saturating and flushing fluids. The T_1 distributions of fluids before, during and after exposure to the Boise sandstone cores were measured and compared.

Table 4.1 List of Boise Sandstone Cores with saturating and flushing fluids.

Core #	Saturated with Fluid	Flushed with Fluid
1	DI	DI
2	HNO_3 (pH 3.1)	DI
3	HNO_3 (pH 3.1)	HNO_3 (pH 3.1)
4*	TMAH (pH 9.1)	DI
5*	TMAH (pH 9.1)	TMAH (pH 9.1)
6	ZR-6AL (pH 3.1)	DI
7	ZR-6AL (pH 3.1)	HNO_3 (pH 3.1)
8*	ZR-6BL (pH 9.1)	DI
9*	ZR-6BL (pH 9.1)	TMAH (pH 9.1)
10	ZR-7.5AL (pH 3.1)	DI
11	ZR-7.5AL (pH 3.1)	HNO_3 (pH 3.1)
12*	ZR-7.5BL (pH 9.1)	DI
13*	ZR-7.5BL (pH 9.1)	TMAH (pH 9.1)

*Cores were pre-soaked in TMAH at pH 13.41 to maintain significant negative surface charge.

4.4.1 Pure fluids in cores: effect of pH

Figure 4.2 displayed below is obtained from Matlab via linear inversion of raw NMR data shown in the Appendix B. Figure 4.2a) shows the measured T_1 distribution of

Boise sandstone cores #1 to #5 saturated with corresponding fluids. Core #1, saturated with DI water, displayed a modal (peak) T_1 value of 0.557 s and was used as a reference sample against which to check for surface relaxivity alteration caused by pure solutions at different pH values and addition of nanoparticles. Figure 4.2b) exhibits T_1 distribution of Cores #1-#5 after 2 pore volume flushing with selected fluids. T_1 peak value of Cores #1-#5 after core flooding are 0.534 s, 0.480 s, 0.465 s, 0.424 s, and 0.444 s respectively. After core flooding, T_1 values were slightly shorter comparing to those of saturated cores before flushing.

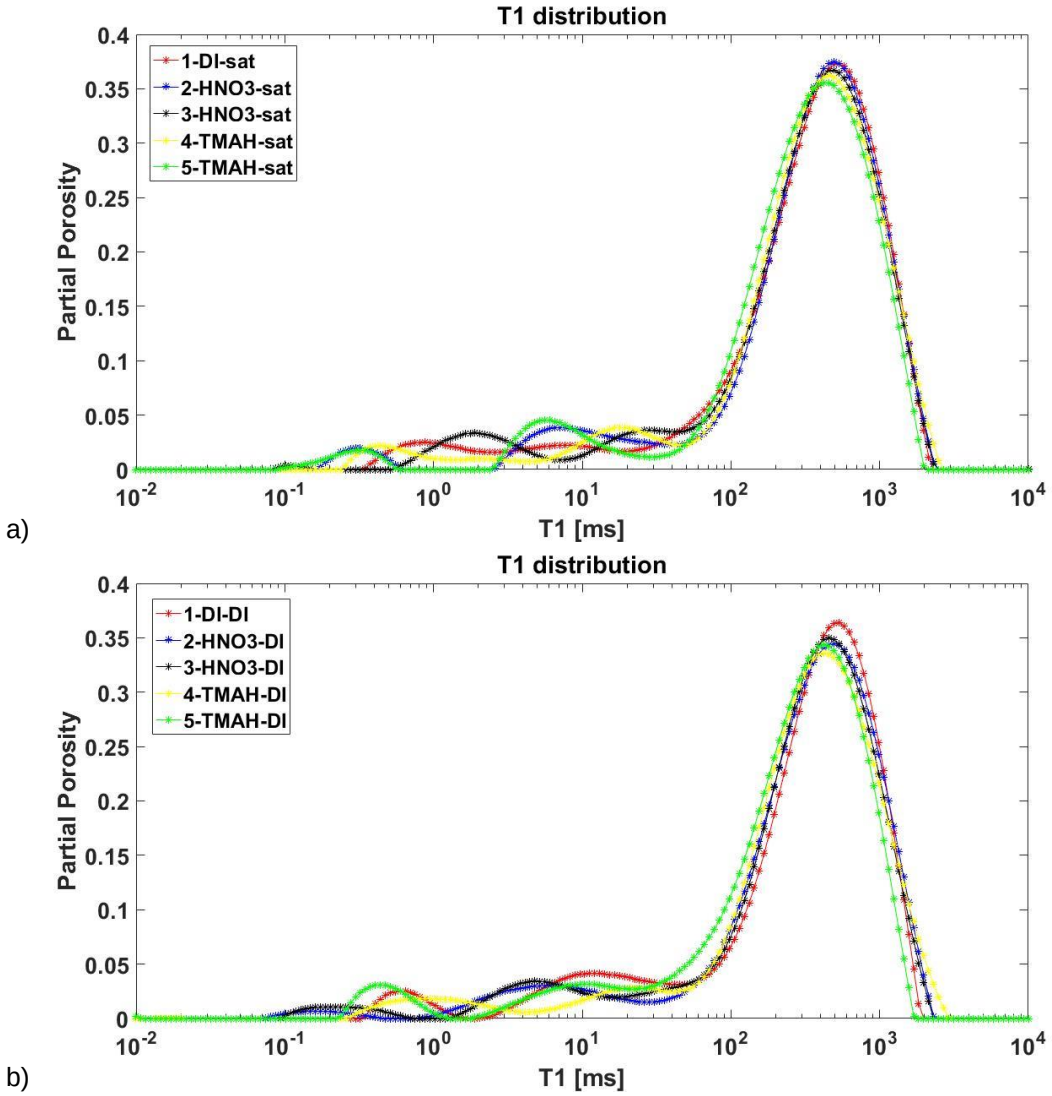

Figure 4.2 The T_1 distribution of a) Boise sandstone cores saturated with pure fluids at different pH values: Core #1 saturated with DI water at pH 7, Core #2 and #3 saturated with HNO_3 at pH 3.1, Core #4 and #5 are pretreated with strong TMAH at pH 13.4, and saturated with TMAH at pH 9.1; b) Boise sandstone Cores #1-#5 after 2 pore volume flooding with selected fluids.

Table 4.2 T_1 and pH values of original fluids and effluents.

Core #	1	2	3	4	5
Original Fluid T_1 (s)	2.743	2.625	2.625	2.659	2.659
Core Saturated with Fluid T_1 (s)	0.557	0.503	0.502	0.452	0.469
EffluentT_1 (s)	2.630	2.571	2.607	2.183	2.051
Sandstone Surface Relaxation Rate (s^{-1})	1.430	1.606	1.610	1.833	1.758
Sandstone Surface Relaxivity (μm/s)	5.05	5.67	5.69	6.48	6.21
Original Fluid Iron conc. (mg/L)	0	0.020	0.020	0.245	0.245
Effluent Iron conc. (mg/L)	0.071	0.046	0.053	3.594	2.953
Original Fluid pH	7.0	3.1	3.1	9.1	9.1
Effluent pH	7.1	6.9	6.7	9.9	10.0

Table 4.2 summarizes the T_1 values of bulk fluid DI water, HNO_3 at pH 3.1 and TMAH at pH 9.1 after pretreated with strong TMAH at three stages of the experiment: before entering a core, while within a core and after being displaced from a core. We recorded the peak T_1 value of each core saturated with different fluids, the sandstone surface relaxation rate was calculated correspondingly based on Equation (4.4). Using the T_1 values of original DI water and sandstone Core#1 saturated with DI water, the Boise sandstone surface relaxation rate was computed from Equations (4.4 and 4.5) as 1.43 s^{-1} when saturated with DI water. Assuming a median pore radius of 10.6 μm based on Boise sandstone pore structure studied by Arawole (2015), the Boise sandstone surface relaxivity was calculated as 5.05 μm/s. Mild acid at pH 3.1 increased surface relaxivity slightly to around 5.7 μm/s and after pretreatment with strong alkali, saturation of mild alkali at pH 9.1 also increased sandstone surface relaxivity to around 6.3 μm/s.

Each fluid's and effluent's pH values were recorded as well. The pH value of DI water increased slightly from 7 to 7.1 after contact with Core #1. In Core #2 and Core #3, the pH of the HNO_3 effluents increased from 3.1 to values close to 7, indicating that most of H^+ in acid were either attached to negatively charged sandstone surface or reacted with the mineral surfaces. After contact with Core #4 and Core #5, which were pretreated with

TMAH at pH 13.4, the effluent from the saturating fluid (TMAH) at pH 9.1 increased to pH of 10, probably due to residue of strong TMAH left on sandstone surface that was dried out was washed into effluent.

Iron concentration in HNO_3 increased from 0.02 mg/L to 0.046 mg/L ~ 0.053 mg/L after contact with Boise sandstone, indicated that acid dissolved some irons. TMAH at pH 9.1 showed increased iron concentration from 0.25 mg/L to 3.0 mg/L ~ 3.6 mg/L. Presence of more irons in effluents results in shorter relaxation time.

4.4.2 Nanoparticle dispersions in cores

Negatively charged nanoparticle dispersion in Boise sandstone

Figure 4.3 shows the normalized nanoparticle concentration in the effluents with respect to the concentration in the original ZR-6BL and ZR-7.5BL dispersions (6 wt% and 7.5 wt%) when flushed with DI water in Core #8 and #12 and with TMAH at pH 9.1 in Core #9 and #13. Comparison of the mass of nanoparticles in the effluents and original fluids indicated little retention of nanoparticles in Boise sandstone cores, with about 2.8% and 2.3% of the ZR-6BL and ZR-7.5BL nanoparticles retained in Core #9 and #13 when flushed by TMAH, and approximately 3.4% and 3.0% of nanoparticles in ZR-6BL and ZR-7.5BL trapped in Core #8 and #12 after DI water flushing.

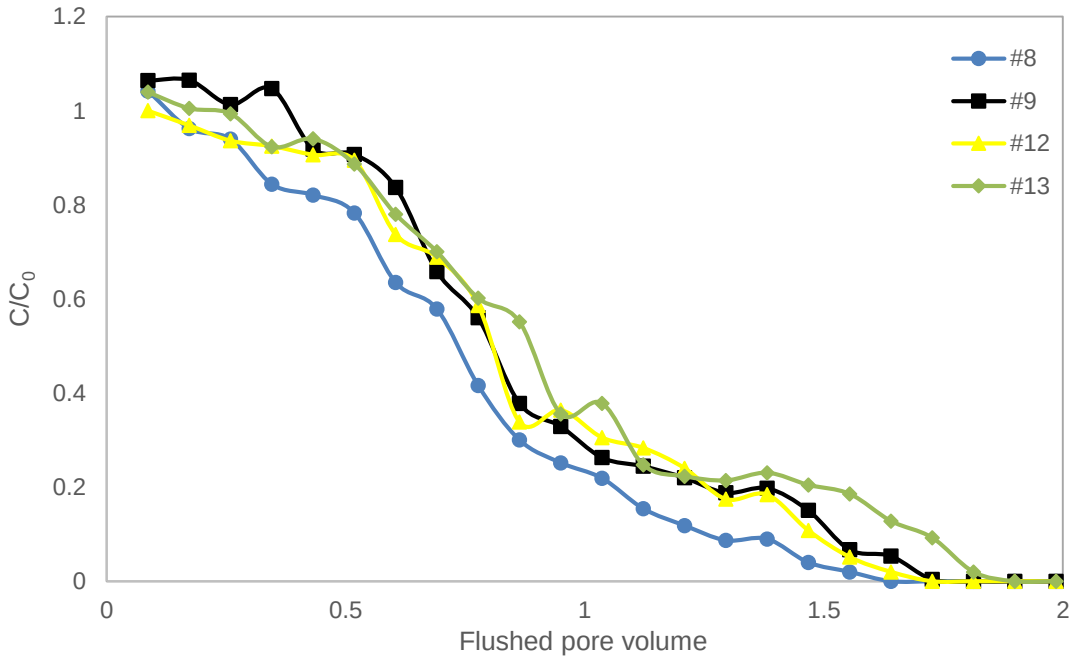

Figure 4.3 Normalized effluent nanoparticle concentration with respect to nanoparticle concentration in original ZR-6BL and ZR-7.5BL dispersion (6 wt% and 7.5 wt%) as a function of pore volume flushing in Cores #8, #9, #12, and #13. Two pore volumes of DI was injected into Cores #8 and #12; 2 pore volumes of water and TMAH at pH 9.1 were used to flush Core #9 and #13. The T_1 value for the effluent (see Table 4.3) was obtained by measuring the first 0.7 pore volumes commingled.

As shown in Figure 4.4, a) before core flooding, Boise sandstone Cores #4, #8, #9, #12, and #13 were saturated respectively with TMAH at pH 9.1, ZR-6BL, ZR-6BL, ZR-7.5BL and ZR-7.5BL. The corresponding T_1 peak values are 0.452 s, 0.115 s, 0.108 s, 0.0803 s, and 0.0724 s; b) after flushing 2 pore volumes, Cores #8, #9, #12 and #13 had T_1 peak values (0.378 s, 0.307 s, 0.274 s, and 0.268 s, respectively) close to 0.424 s of Core #4. This suggests comparable surface relaxivity to that exhibited by Core #4, which was pretreated with the same strong alkali used to pretreat Cores #8, #9, #12, and #13. The retained 2.3% to 3.4% of nanoparticles in Cores #8, #9, #12, and #13 after flushing may contribute to the shortening of the T_1 peak value relative to that of Core #4. Therefore, this

surface relaxivity alteration was likely a direct result of the pretreatment; retained nanoparticles in the porous media after core flooding played a role in speeding up the overall relaxation rate. Figure 4.4 was obtained from Matlab processing of raw data displayed in Appendix B via linear inversion.

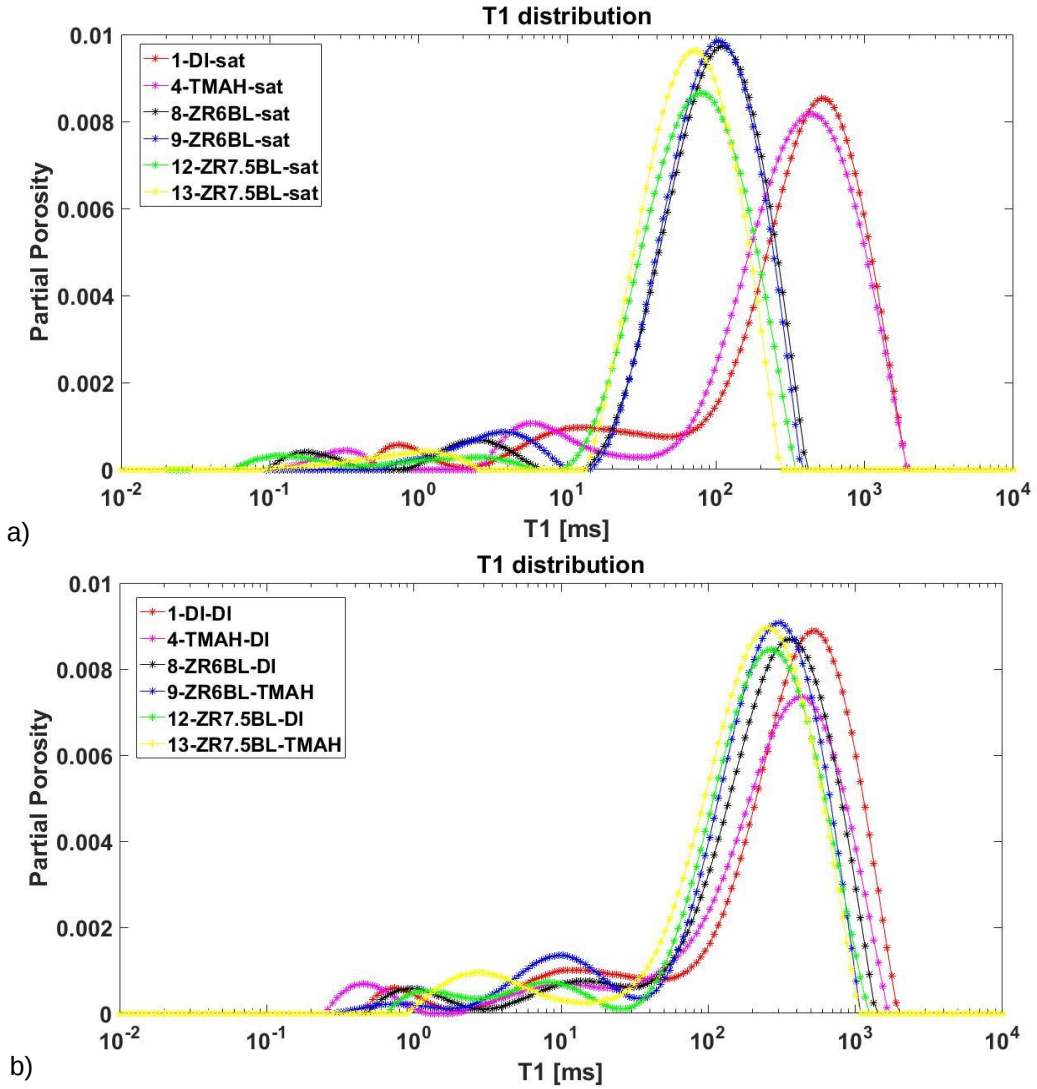

Figure 4.4 The T_1 distribution of Boise sandstone Cores #1, #4, #8, #9, #12, and #13 a) saturated with TMAH at pH 9.1, ZR-6BL, ZR-6BL, ZR-7.5BL, and ZR-7.5BL, respectively and b) after flushing with two pore volumes of DI water and TMAH at pH 9.1. Figures are obtained from Matlab via linear inversion, number of point for T_1 distribution was set to 200.

Table 4.3 T_1 of ZR-6BL and ZR-7.5BL dispersions before, during and after contact with Boise sandstone, along with pH value and nanoparticle size, zeta potential relaxation rate and relaxivity in original dispersion and effluents.

Core #	8	9	12	13
Original Fluid T_1 (s)	0.878	0.832	0.733	0.733
Core Saturated with Fluid T_1 (s)	0.115	0.108	0.803	0.724
Effluent T_1 (s)	0.121	0.0855	0.058	0.061
Effluent pure dispersion fluid without nanoparticles T_1 (s)	1.44	1.65	1.10	1.37
Original Fluid pH	9.1	9.1	9.1	9.1
Effluent pH	9.5	9.6	9.7	9.9
Iron concentration in Original Fluid without nanoparticles (mg/L)	0.015	0.015	0.018	0.018
Iron concentration in Effluent without nanoparticles (mg/L)	2.91	1.58	3.04	2.83
Nanoparticle Relaxation Rate in Original Fluids (s^{-1})	0.774	0.774	1.000	1.000
Nanoparticle Relaxivity in Effluents (μm/s)	12.34	16.19	17.49	18.82
Nanoparticle Size in Original Fluids (nm)	72.4	72.4	72.7	72.7
Nanoparticle Size in Effluents (nm)	78.0	77.4	78.4	79.0
Nanoparticle Relaxation Rate in Effluents (s^{-1})	7.60	11.09	16.32	15.66
Nanoparticle Relaxivity in Original Fluids (μm/s)	1.095	1.095	1.095	1.095
Nanoparticle Zeta Potential in Original Fluids (mV)	-28.9	-28.9	-29.3	-29.3
Nanoparticle Zeta Potential in Effluents (mV)	-26.1	-25.8	-26.2	-26.2

As shown in Table 4.3, the T_1 of ZR-6BL decreased from 0.878 s to 0.121 s and 0.0855 s after contact with sandstone Cores #8 and #9; similarly, T_1 of ZR-7.5BL dropped from 0.733 s to around 0.06 s after being flushed from Cores #12 and #13. This is inconsistent with small amount of nanoparticle retention in the cores (2.3% to 3.4%), which would have increased the relaxation times slightly. When ZR-6BL was saturating the sandstone Core #9, T_1 was around 0.108 s, which is longer than that of the effluents: 0.0855 s. For ZR-7.5BL saturated Core #12, T_1 peak value was 0.0803 s, while effluent from Core

#12 has shorter T_1 as 0.058 s. It is possible that this is a result of nanoparticle adsorption on the mineral surfaces as explained in Chapter 3.

The T_1 of the first 0.7 pore volumes of effluent collected from Cores #8, #9, #12 and #13 were 0.121 s, 0.0855s, 0.058s and 0.061 s, respectively. The T_1 of the effluents after removal of nanoparticles by filtration shown in Table 4.3 (1.44 s, 1.65 s, 1.10 s and 1.37 s) were shorter than the effluent T_1 from Cores #4 (2.183 s) and Core #5 (2.051 s) displayed in Table 4.2. But the difference cannot explain the significant drop in T_1 of effluents from ZR-BL saturated cores. This suggests that the much faster relaxation seen in the effluents was mainly caused by the nanoparticles themselves rather than the dispersion fluid. For pure fluid in ZR-6BL and ZR-7.5BL effluents after removal of nanoparticles, iron concentrations were 1.6 mg/L to 3.0 mg/L, smaller than that in TMAH effluent (3.0 mg/L to 3.6 mg/L). It is possible that irons with positive charge tends to attach on negatively charged nanoparticles and were removed in the centrifuge procedure. More iron present will result in shorter relaxation time, this is consistent with T_1 measurements mentioned above. Another possibility is that there were other magnetic species such as Mn in the effluent that sped up the relaxation, but we did not measure concentration of Mn in this study.

After deduction of the pure dispersion fluid's contribution to the overall relaxation rate, the nanoparticle relaxation rate in the effluents increased by a factor more than 10. Given the computed nanoparticle concentration based on Figure 4.3, according to Equations (4.1 and 4.2), the relaxivity of the nanoparticles increased from 1.10 μm/s (Zhu et al., 2015) to 12.3 μm/s ~ 16.2 μm/s (in effluents wash from Core #8 and #9) and 17.5 μm/s ~ 18.8 μm/s (in effluents from Core #12 and #13) after contacting with strong alkali-treated Boise sandstone cores. The dramatic increase in nanoparticle relaxivity was possibly due to interactions between nanoparticle dispersion and Boise sandstone surface.

Alkaline solution with pH larger than 8 brought mineral surface dissolution (Revil et al., 1999a, b), paramagnetic materials such as iron cations were exposed and attached to negatively charged nanoparticles. Attached iron onto nanoparticles in ZR-6BL will help increase nanoparticle relaxivity. With the same nanoparticle concentration in the nanofluids before core flooding, nanoparticles in effluents flushed by DI water had lower relaxivities than nanoparticles in effluents flushed by TMAH at pH 9.1. It is possible that this is due to the higher pH creating a more negative surface charge on the nanoparticles, promoting more adsorption of metal cations.

Due to the procedures used to pre-treat Cores #8, #9, #12, and #13, there might be residual TMAH on the sandstone surface after oven drying. This would tend to increase the pH of the ZR-6BL after contact with Boise sandstone cores. Nanoparticles in the ZR-6BL and ZR-7.5BL effluents remained stable, with zeta potential increasing slightly by 3 m V ~ 4 mV and size increasing by 5 nm ~ 6 nm.

Positively charged nanoparticle dispersion in Boise sandstone

Figure 4.6a) exhibits T_1 profile of Cores #2, #6, #7, #10 and #11 saturated with HNO_3, ZR-6AL, ZR-6AL, ZR-7.5AL, and ZR-7.5AL, respectively. Normalized nanoparticle concentration in effluents with respect to the concentration of the original ZR-6AL and ZR-7.5AL dispersions (6 wt% and 7.5 wt%) as a function of flushed pore volume in Cores #6, #7, #10 and #11 are displayed in Figure 4.5. Based on these measurements we determined that 40% and 37% of the nanoparticles were retained in Core #6 and #10 after flushing with 2 pore volumes of DI water, and 35% and 31% of the nanoparticles were retained in Core #7 and #11 after flushing with 2 pore volumes of HNO_3. After flushing, Boise sandstone cores were put in the NMR probe to measure the T_1 distributions. As shown in Figure 4.6b), with nanoparticles retained in Core #6, #7, #10, and #11, the T_1

peak values were 0.424 s, 0.322 s, 0.361 s, and 0. 250 s, respectively. The values are shorter than that of Core #2 after core flooding: 0.480 s. Figure 4.6 is obtained from Matlab processing linear inversion of NMR raw data displayed in the Appendix B.

Table 4.4 T_1 of ZR-6AL and ZR-7.5AL dispersions before, during and after contact with Boise sandstone, along with pH value and nanoparticle size, zeta potential relaxation rate, and relaxivity in original dispersion and effluents.

Core #	6	7	10	11
Original Fluid T_1 (s)	0.794	0.794	0.676	0.676
Core Saturated with Fluid T_1 (s)	0.284	0.299	0.251	0.235
Effluent T_1 (s)	0.439	0.178	0.360	0.169
Effluent pure dispersion fluid without nanoparticles T_1 (s)	2.271	1.880	2.210	1.872
Original Fluid pH	3.1	3.1	3.1	3.1
Effluent pH	4.5	4.4	4.3	4.3
Iron concentration in Original Fluid without nanoparticles (mg/L)	0.022	0.022	0.023	0.023
Iron concentration in Effluent without nanoparticles (mg/L)	0.035	0.049	0.037	0.047
Nanoparticle Relaxation Rate in Original Fluids (s^{-1})	0.895	0.895	1.115	1.115
Nanoparticle Relaxation Rate in Effluents (s^{-1})	1.84	5.07	2.33	5.38
Nanoparticle Size in Original Fluids (nm)	101	101	101	101
Nanoparticle Size in Effluents (nm)	109	108	104	106
Nanoparticle Relaxivity in Original Fluids (μm/s)	1.427	1.427	1.427	1.427
Nanoparticle Relaxivity in Effluents (μm/s)	4.68	10.08	4.29	8.95
Nanoparticle Zeta Potential in Original Fluids (mV)	32.1	32.1	32.5	32.5
Nanoparticle Zeta Potential in Effluents (mV)	20.1	22.4	21.0	21.9

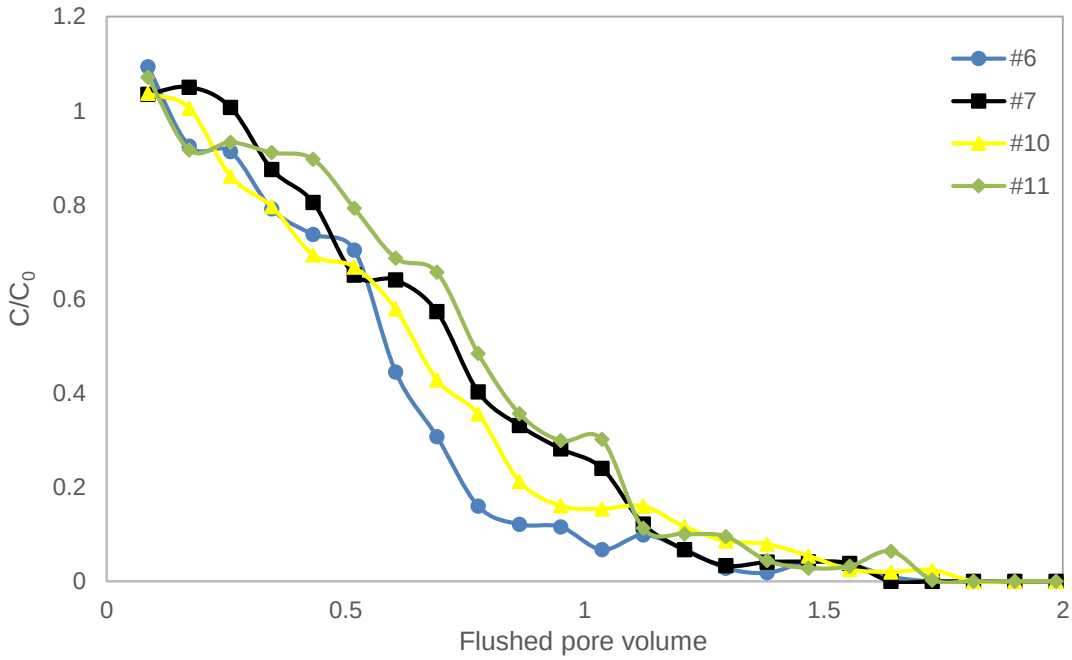

Figure 4.5 Normalized effluent nanoparticle concentration with respect to nanoparticle concentration in the original ZR-6AL and ZR-7.5AL dispersions (6 wt% and 7.5 wt%) as a function of pore volume flushed in Cores #6, #7, #10 and #11. Two pore volumes of selected fluid was injected into Cores #6, #7, #10 and #11, which were originally saturated with ZR-6AL and ZR-7.5AL. The T_1 value for the effluent (see Table 4.4) was obtained by measuring the first 0.7 pore volumes commingled.

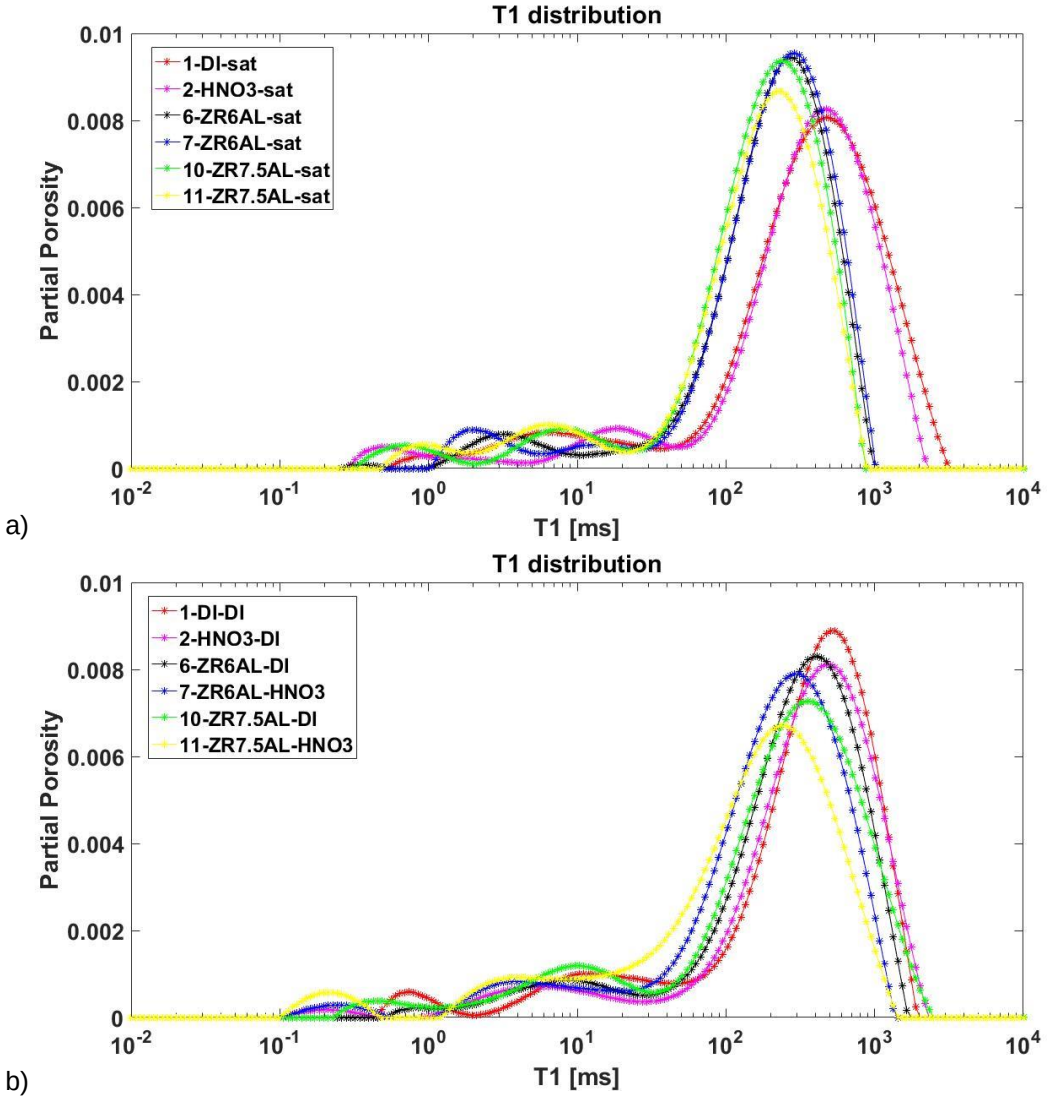

Figure 4.6 The T_1 distributions of Boise sandstone Cores #1, #2, #6, #7, #10 and #11 a) saturated with HNO_3, ZR-6AL, ZR-6AL, ZR-7.5AL, and ZR-7.5AL, respectively, and b) Cores #4, #6, #7, #10 and #11 after flushing with two pore volumes of selected fluids. Figures are obtained from Matlab via linear inversion, number of point for T_1 distribution was set to 200.

Table 4.4 summarizes nanoparticle relaxation rate, nanoparticle size and zeta potential, and T_1 of ZR-6AL and ZR-7.5AL dispersions before and after flooding in Boise sandstone. T_1 of ZR-6AL decreased from 0.794 s to 0.4398 s and 0.178 s after contact with

to sandstone Cores # 6 and #7, T_1 of ZR-7.5AL dropped from 0.676 s to 0.360s and 0.169 s in the first 0.7 pore volume effluents displaced from Core #10 and #11. After removing nanoparticles from effluent, the pure dispersion fluid showed shorter T_1 (2.271 s, 1.880 s, 2.210 s and 1.872 s) than the effluents from Core #2 (2.571 s) and Core #3 (2.607 s). The difference may be due to additional interactions between the Boise sandstone surface and the acidic nanoparticle dispersion that resulted in more paramagnetic species dissolved into fluid. After subtracting the pure dispersion fluid's contribution to the overall relaxation rate, we found that the nanoparticle relaxation rate in the effluents increased by a factor of 2~6. Given the computed nanoparticle concentrations based on Figure 4.3, according to Equations (4.1 and 4.2), the relaxivity of ZR-6AL increased from 1.43 μm/s (Zhu et al., 2015) to 4.68 μm/s, 10.08 μm/s, 4.29 μm/s, and 8.95 μm/s after flooding the Boise sandstone Cores #6, #7, #10, and #11 respectively. ZR-AL nanoparticles flushed by DI water have relaxivities lower than 5 μm/s, while ZR-AL nanoparticles flushed by HNO_3 have higher relaxivity of 9 to 10 μm/s. It is possible that at lower pH, more paramagnetic ions can be removed from the pore surface and be available to adsorb onto nanoparticles.

After being exposed to the sandstone pore surface, the pH value of the effluents increased by less than 1.5, and the pH difference is much smaller than the acidic fluid (no nanoparticles) used in Core #2 and Core #3 in which the pH value increased from 3 to around 7. It is possible that some of the abundant H^+ in the ZR-6AL and ZR-7.5AL dispersions attached to the negatively charged sandstone surface or reacted chemical with impurities on mineral surface. Since H^+ is the stabilizer in ZR-6AL and ZR-7.5AL, H^+ were ionically bonded at the nanoparticle surface and within the Stern layer. Due to the large surface area to volume ratio of the nanoparticles, less H^+ was available to be attached to the sandstone surface when nanoparticles were present, and the pH of the effluents was relatively larger than that of the pure HNO_3 effluents after contact with Core #2 and Core

#3. Nanoparticle zeta potential dropped from 32 mV to 20 m V ~ 22 mV, and nanoparticle size remained similar to that in the original dispersion.

4.5 DISCUSSIONS

4.5.1 General observations

After saturating Boise sandstone cores with pure fluids at different pH, effluents from Cores #1 to #5 showed shorter T_1 compared to that of the original fluid. The decrease in T_1 of DI water after contact with Boise sandstone is probably due to the presence of dissolved paramagnetic species or mobilized fine mineral particles in the sandstone core (Keating and Knight, 2008). Cores #2 and #3, which were saturated with HNO_3, displayed enhanced surface relaxivity and increased relaxation rate $1/T_1$ in the effluents. A possible explanation is that acid contains more H^+ which can react with impurities such as Fe_2O_3 on sandstone surface, and dissolve more paramagnetic materials in pore fluid. Iron concentrations in effluents from Core #2 and Core #3 were relatively higher than original fluids (0.05 mg/L in effluent versus 0.02 mg/L in original fluids). For Cores #4 and #5 which are pretreated with strong TMAH, relaxivity of sandstone surface increased from 5.05 μm/s to larger than 6 μm/s. This is probably due to mineral surface dissolution that occurs when silica cores are saturated with alkaline solution at pH higher than 8 (Revil et al., 1999a,b). In this situation, paramagnetic ions such as iron in sandstone could be exposed to pore fluid and dislodged into pore fluid, thereby speed up relaxation in pore fluid (Foley et al., 1996). Effluents from Cores #4 and #5 showed increased Fe concentration comparing to that in original fluids (3.0 mg/L ~ 3.5 mg/L comparing to 0.25 mg/L)

Effluents of both ZR-6AL, ZR-7.5AL, ZR-6BL, and ZR-7.5BL had much shorter relaxation time than the original dispersions despite the fact that part of nanoparticles have

been captured in sandstone cores, which should have slowed relaxation in the effluent. The ways in which sandstone surface relaxivity changed with presence of zirconia nanoparticles dispersions depended both on the dispersion pH and the surface charge of the nanoparticles.

4.5.2 Negatively charged nanoparticles dispersion in Boise sandstone

Given the negative surface charge of nanoparticles in the original fluids and effluents, there was an electrostatic repulsive force between the nanoparticles and the sandstone surface. Nanoparticle retention occurred due to reversible adsorption on pore surface caused by van der Waals attraction. Brownian diffusion would finally release attached nanoparticles from pore wall when flushed with a pure fluid containing no nanoparticles (Yu et al., 2010). According to Equations (4.3, 4.4, 4.5, 4.6, and 4.7) and altered sandstone surface relaxivity as 6.3 μm/s by strong alkali, 13% ~ 19% of ZR-6BL nanoparticles were initially attached to sandstone surface due to van der Waals attraction and more than 82% ~ 88% of the attached nanoparticles were removed due to Brownian motion. For cores saturated with ZR-7.5BL, 15% ~ 21% of ZR-7.5BL nanoparticles were initially attached to sandstone surface due to van der Waals attraction, while Brownian motion removed about 80% ~ 86% of the attached nanoparticles.

Along with mineral surface dissolution under strong alkaline condition, it is possible that after interactions with Boise sandstone surface, the stabilizer TMAH was consumed during interactions with silica surface, less stabilizer in pore fluid brought more pure nanoparticles exposed to the bulk fluid and provided more paramagnetic relaxation sites for protons. Slightly increased nanoparticle size and zeta potential in effluents does indicate less stability of the nanoparticles, which may due to less stabilizer remained. Attached iron cations onto nanoparticle surface also played a role in increase nanoparticle surface relaxivity.

The theoretical maximum amount of ZR-BL that can attach onto Boise sandstone may be computed using a geometrical method by assuming that attached nanoparticles form a dense pack in a monolayer and occupy a projected area of πr_{NP}^2 on the pore surface. According to a hexagonal packing of equal circles, the highest surface fraction that can be occupied by the projected area of the nanoparticles is 0.9069. In Boise sandstone saturated with ZR-6BL, I assume that the pores can be simplified as spheres with a median radius of 10.6 μm. With nanoparticle size around 72 nm and volume fraction of 1.114%, number of nanoparticles in ZR-6BL inside a single pore is calculated as 2.73×10^5. Based on Equations (4.3, 4.4, 4.5, 4.6, and 4.7), the largest number of nanoparticles that can possibly adsorbed onto the pore surface is 3.15×10^5, where 90.69% of grain surface is covered by attached nanoparticle monolayer. The corresponding surface relaxivity is about 8.98 μm/s to 10.7 μm/s depending on the surface relaxivity of the attached nanoparticles. Our experimental results indicated that, with 2.8% and 3.4% of 2.73×10^5 ZR-6BL nanoparticles retained in a single pore of Cores #9 and #8, there are 2.2% and 2.7% of sandstone pore surface covered by trapped nanoparticles. Similarly, in ZR-7.5BL saturated Boise sandstone cores, there are 2.73×10^5 nanoparticles inside a single pore with radius 10.6 μm, highest possible percentage of attached nanoparticles is 89.7% (3.15×10^5 nanoparticles) when 0.9069 of pore surface is covered by monolayer of attached nanoparticles. The resulting surface relaxivity would be 16.5 μm/s to 17.7 μm/s in this case. With 2.3% and 3.0% of ZR-7.5BL (7843 and 10230 nanoparticles) retained in Cores #13 and #12, assuming monolayer packing of trapped nanoparticles onto pore surface, the surface fractions covered by nanoparticles are 2.3% and 3.0%, respectively.

Assuming a monolayer packing of attached ZR-BL nanoparticles, with the lowest and highest relaxivities determined from effluents, the relaxivity range of the Boise sandstone pore surface covered with retained nanoparticles is calculated and displayed by

lines in Figure 4.7. Theoretical The experimental data fall within the predicted range. Source of error bars are NMR noise and errors in obtaining longitudinal relaxation rate ($1/T_1$) of flushing fluid by linear regression of raw data. The scatter observed in the experimental data points indicates that the nanoparticles may have variable relaxivity between these bounds, or the pore size in each Boise sandstone cores is not exactly the same as 10.6 μm. When comparing cores contacted with same nanofluids, surface relaxivities of Cores # 8 and #12 flushed by DI water were close to the lower bound while the relaxivity values of Cores #9 and #13 after flushing with TMAH were closes to the upper bound.

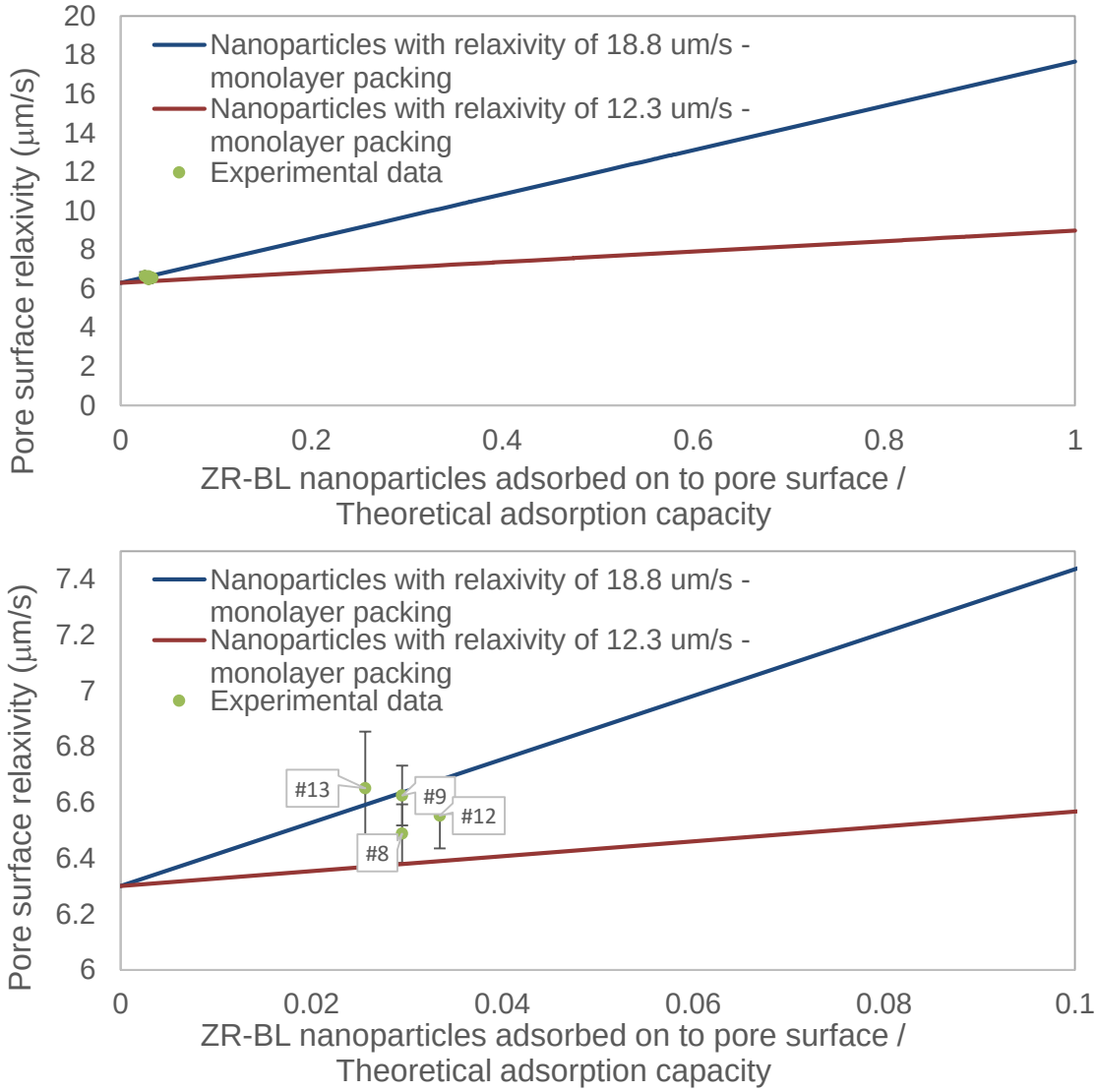

Figure 4.7 Computed possible boundaries (two lines) of Boise sandstone pore surface relaxivities covered by different fraction of ZR-BL nanoparticles with 12.3 µm/s and 18.8 µm/s. Experimental determined sandstone pore surface relaxivities from flushed Boise sandstone cores and corresponding retained nanoparticle fraction are indicated by scattered points. Diagram at the bottom shows zoomed in view with x-axis ranges from 0 to 0.1 and y-axis ranges from 6 to 7.5.

4.5.3 Positively charged nanoparticles dispersion in Boise sandstone

Core flooding with DI water in Core #6 and Core #10 (37% and 40%) trapped more fraction of positively charged nanoparticles than in Core #7 and Corex cc #11 (35% and 31%) flushed by HNO_3 at pH 3.1. It is possible that since SiO_2 zeta potential drops from -10 mV to -65 mV as pH increases from 2 to 10 (Li and De Bruyn, 1966), sandstone surface tends to be more negative at higher pH and attract more positively charged nanoparticles. Based on Equations (4.3, 4.4, 4.5, 4.6, and 4.7), 49% ~ 52% of nanoparticles in ZR-6AL were initially attached onto Cores #6 and #7 driven by electrostatic attraction, Boise sandstone surface relaxivity was altered to about 5 μm/s ~ 6.7 μm/s. Around 45% ~ 50% of ZR-7.5AL were attached onto Cores #10 and #11 before core flooding. Boise sandstone surface relaxivity changed from 5.05 μm/s to around 5.4 μm/s as a result of the attached nanoparticles. The surface relaxivity of the zirconia nanoparticles in effluents increased from 1.43 μm/s to more than 4 μm/s (washed with DI water) and approximately 9 μm/s (washed with HNO_3). After interactions between the nanoparticle dispersion and the mineral surface, pore fluid pH increased, decreasing the positive charge on nanoparticle surface and weakening the bond between nanoparticles and pore surface, causing around 20% ~ 30% of adsorbed nanoparticles to desorb back into the fluid. Similar with ZR-BL, increased surface relaxivity may due to less stabilized condition where part of H^+ were attached onto sandstone surface or reacted with impurities, leaving more paramagnetic relaxation sites on pure nanoparticles that were accessible to protons. Changes in nanoparticle size and drops in zeta potential again indicated less stability of the nanoparticles in dispersion.

We used the same geometric method that was used to calculate largest fraction of ZR-BL can be adsorbed on the sandstone surface. In Boise sandstone cores saturated with ZR-6AL, with nanoparticle radius of 101 nm, there are 1.03×10^5 nanoparticles in a

spherical pore with radius 10.6 μm. The theoretical maximum number of ZR-AL nanoparticles that can be adsorbed on the pore surface is 1.60×10^5 to cover 90.69% of the sandstone pore surface area. The corresponding surface relaxivity is about 4.77 μm/s to 9.67 μm/s depending on the surface relaxivity of attached nanoparticles. Experimental data showed that there were 35% and 40% of ZR-6AL (36050 and 41200 nanoparticles) trapped in Boise sandstone Cores #7 and #6, surface fractions covered by attached nanoparticles are 20.45% and 23.38% respectively assuming monolayer packing. Similarly, in Boise sandstone cores saturated with ZR-7.5AL, the number of nanoparticles with radius as 51 nm inside a pore with radius 10.6 μm is 1.25×10^5, the highest theoretical amount of attached nanoparticles is 1.60×10^5 when 0.9069 pore surface is occupied by nanoparticles. The resulting surface relaxivity would be 4.42 μm/s to 7.74 μm/s in this case. According to experimental results, there were 31% and 37% of nanoparticles (38750 and 46250 nanoparticles) retained in Cores #11 and #10, covering 21.99% and 26.42% of pore surface via monolayer packing.

In Figure 4.8, Boise sandstone surface relaxivities determined experimentally are indicated by scattered points. Error bars are computed from determination of the longitudinal relaxation rate ($1/T_1$) of flooding fluid by linear regression of raw data and noise. The expected surface relaxivity bounds were computed assuming a monolayer packing of attached ZR-AL nanoparticles with relaxivities of 4.29 μm/s and 10.08 μm/s. The ZR-AL nanoparticles flushed with DI water from Cores #6 and #10 have relaxivity close to 5.9 μm/s, while the ZR-AL nanoparticles flushed with HNO_3 from Cores #7 and #11 have relaxivity around 6.4 μm/s. The experimental data form Cores #6 and #10 are located closer to the lower bound, while the computed relaxivities of Cores #7 and #11 are closer to the upper bound. As before, it is possible that the nanoparticles inside the core had relaxivity values between the bounds I assumed here.

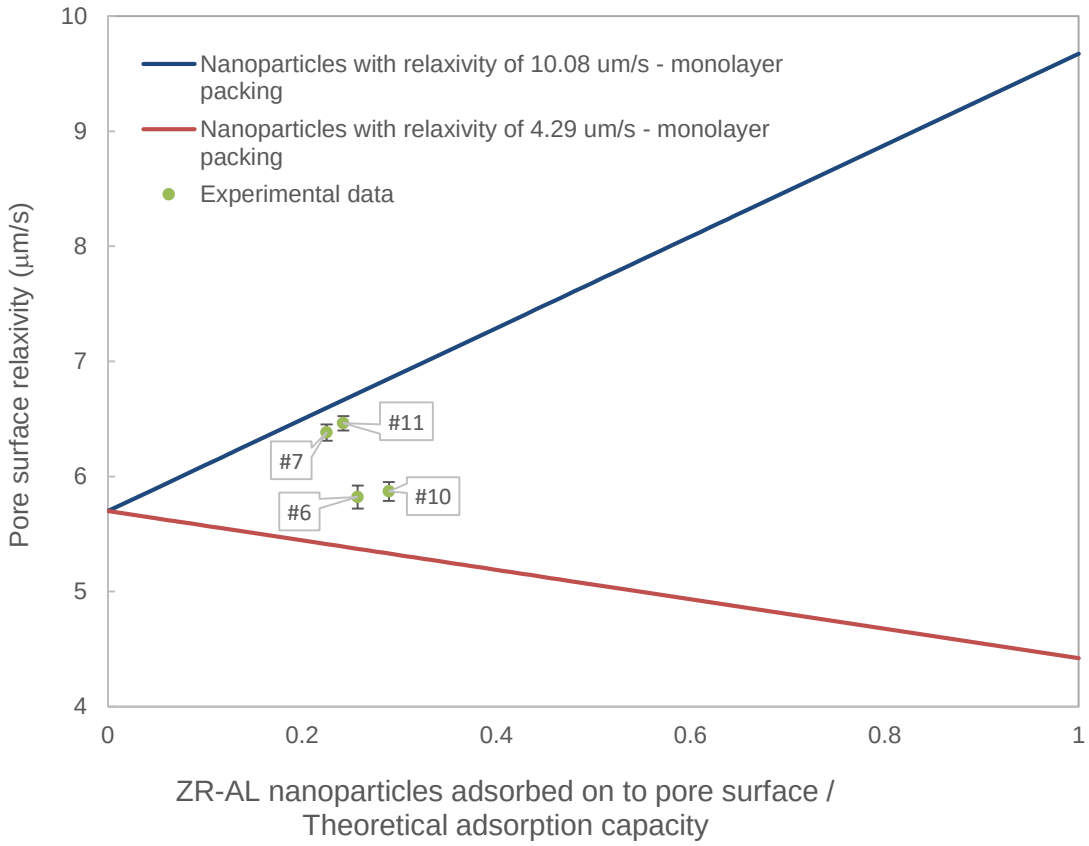

Figure 4.8 Computed possible boundaries (two lines) of Boise sandstone pore surface relaxivities covered by different fraction of ZR-AL nanoparticles with 4.29 µm/s and 10.08 µm/s. Experimental determined sandstone pore surface relaxivities from flushed Boise sandstone cores and corresponding retained nanoparticle fraction are indicated by scattered points.

In the future, we will inject NP dispersions with positive surface charge that do not require changing the pH in the sandstone pores. In our experiments, we only pretreated the sandstone with strong alkali to allow stability of negatively charged nanoparticles, and the behavior of these nanoparticles is treated as a control group with zero adsorption. Therefore this treatment would likely not be required in the field.

4.6 CONCLUSIONS

Our study showed that nanoparticle dispersions in Boise sandstone cores altered sandstone surface relaxivity, in a complicated way depending on nanoparticles' surface charge and pH condition of the dispersions. During contact with 6 wt% and 7.5 wt% positively charged zirconia nanoparticles at pH 3.1, Boise sandstone surface relaxivity changed from 5.05 μm/s to 5 μm/s ~ 6.7 μm/s due to 45% ~ 51% adsorbed nanoparticles onto pore surface. In Boise sandstone pores with pore walls pretreated with TMAH at pH 13.4, sandstone surface relaxivity increased to more than 6 μm/s due to strong alkaline condition, nanoparticle dispersion at pH 9.1 with 6 wt% and 7.5 wt% negatively charged zirconia nanoparticles temporally increased sandstone surface relaxivity to 7 μm/s ~ 10 μm/s when approximately 13% ~ 21% of negatively charged nanoparticles were attached to silica surface driven by Van der Waals attraction. However, after coreflooding, most attached negatively charged nanoparticles were removed by Brownian diffusion, Boise sandstone surface relaxivity remained more than 6 μm/s as result from strong alkaline environment.

In this experiment, with a pore radius as small as 10.6 μm, the specific surface area of Boise sandstone is much larger than that of the 2 mm glass bead pack, which has pore radius around 613 μm. This provides more surface area for nanoparticle attachment. In the 2 mm glass bead pack, only up to 30% of ZR-6AL can attach to the bead surface and form a dense monolayer packing of nanoparticles, while in Boise sandstone, the upper limit is 100% for ZR-6AL. The theoretical maximum amount of adsorbed nanoparticles onto the pore surface is limited by the density of the hexagonal packing of equal circles: nanoparticles can only occupy up to 0.9069 of the pore surface via the projected area. In this limit, the sandstone surface contributes a negligible amount to the surface relaxation on the pore wall. It should be pointed out that the dense packing of nanoparticles in a

monolayer on the pore surface may not be achieved, as it is possible that nanoparticles attach to some sites of pore surface preferentially due to heterogeneity and localized driving forces. The electrostatic repulsion between nanoparticles may limit the maximum amount of nanoparticles that can adsorb on the pore walls below the theoretical maximum predicted for hexagonal packing. In addition, the hydration layer on nanoparticles and the pore surface may also affect adsorption. Further experiments should be performed to study the effects of hydration layers.

Experimental results indicated that pH of nanoparticle dispersions played a role in interactions with Boise sandstone surface. Acid could increase Boise sandstone surface relaxivity by reacting with impurities such as Fe_2O_3 and FeO on mineral surface (Pettijohn, 1963). HNO_3 at pH 3.1 increased Boise sandstone surface relaxivity from 5.05 μm/s to 5.7 μm/s. Alkali can alter Boise sandstone surface relaxivity by mineral surface dissolution and exposure of paramagnetic impurities to pore fluid. Such alteration can remain for long period as long as pore fluid condition remains alkaline. TMAH at pH 13.4 increased Boise sandstone surface relaxivity to higher than 6 μm/s.

After contact with Boise sandstone, zirconia nanoparticles with positive and negative surface charges both showed increased relaxivity. Positively charged nanoparticles relaxivity increased from 1.43 μm/s to 4.3 μm/s ~10 μm/s. Nanoparticles with negative surface charge displayed increased relaxivity from 1.10 μm/s to 12 μm/s ~ 19 μm/s after contact with TMAH treated Boise sandstone. Such increase in relaxivity were possibly due to less stabilizer in dispersions after interactions with sandstone surface. Less stabilizers were ionically bounded with nanoparticles, leaving more specific area of nanoparticles exposure to bulk fluid and increasing chance of protons to get close to paramagnetic sites and relaxed faster. Hence increased the effective relaxivity of nanoparticles. Attachment of iron ions on negatively charged nanoparticles further

enhanced nanoparticle relaxivity. Our work helps to understand the behavior of nanoparticles in porous media through NMR measurements and will be used in future studies on the pore-scale characteristics in rocks. This work will help advance nanoparticle-based analyses of fluid-solid or fluid-fluid interfaces through adsorption of nanoparticles. Applications of this work include imaging oil-water contacts, and determining interfacial surface areas for many petrophysical and reservoir engineering needs. However, the differences in temperature and pressure conditions between oilfield subsurface and the laboratory may lead to different properties of nanoparticles and interactions between nanoparticles and pores.

Chapter 5

Altering nuclear magnetic resonance surface relaxation on nanoparticles by adsorption of Fe(III)

5.1 INTRODUCTION

Many applications of nuclear magnetic resonance (NMR) have been explored in recent decades. In the biological and medical areas, NMR is used to obtain images of anatomy and physiological processes of bodies, which helps in the diagnosis and treatment of diseases (Mansfield and Pykett, 1978). In the oil and gas industry, NMR is employed to determine porosity, pore size, permeability, tortuosity, water saturation, and wettability of reservoir rocks (Hinedi et al., 1997; Freedman et al., 2003; Wang et al., 2005; Daigle and Johnson, 2016). Pore surface relaxivity is the key parameter that links the NMR signal to pore size in rock samples (Coates et al., 1999).

With the development of nanotechnology and nanomaterials having the advantage of small size and large surface area to volume ratio, paramagnetic nanoparticles and magnetic nanoparticles have been used as enhanced oil recovery agents (Ogolo et al., 2012) and applied in produced water purification (Ko et al., 2014). They have also been employed in the characterization of multiphase fluid dynamics in porous media (Prodanović et al., 2010) and pore connectivity (Cheng et al., 2014b). Their use in NMR has included application as contrast agents to highlight the pores that contribute the most to flow (Cheng et al., 2014b) and more robust determination of pore size through alteration of rock surface properties (Zhu et al., 2016).

Nanoparticles have been widely used in medical and biological sciences as magnetic resonance imaging (MRI) contrast agents (Na et al., 2009), which help identification of disease-specific biomarkers at molecular and cellular levels. Coating of these nanoparticles with various polymers or functional groups is introduced to generate

shells that bring compatibility in biological environments and to attach to specific human tissue (Oh et al., 2006) and other applications. The behavior of these surface coatings often depends on having precise control on fluid chemistry (Petri-Fink et al., 2008). However, when nanoparticles are injected into subsurface reservoir rocks, the pore fluid chemistry cannot be controlled or predicted as easily as in medical applications. The chemistry of pore fluid and behavior of nanoparticles can vary from site to site. The behavior and stability of nanoparticles affect NMR response and limit their application in downhole environments (Carter et al., 2005). Polymer coatings are often used to stabilize nanoparticles in harsh reservoir conditions (ShamsiJazeyi et al., 2014). While providing the dispersion stability that is necessary for subsurface applications, the surface properties of the nanoparticles can take on the properties of those polymers themselves, potentially completely masking the properties of the nanoparticle core (Gupta and Gupta, 2004).

In the subsurface, anions and cations in the pore fluid can interact with the solid pore surface. If more paramagnetic ions are present on the pore surface, the relaxivity of pore surface will increase, which will reduce the NMR relaxation time. Following adsorption of paramagnetic cations such as Fe(III) and Mn(II), increases in mineral surface relaxivity have been observed that follow predictions from theory (Kenyon and Kolleeny, 1995; Bryar et al., 2000). Previous studies also indicated that cations could similarly adsorb onto nanoparticles (Hu et al., 2005) or the surface coating driven by electrostatic attraction (Zhang et al., 2009). Our previous results in Chapter 4 indicates that attachment of Fe ions from Boise sandstone pore surface onto zirconia nanoparticles in pores may increase relaxivities of nanoparticles by a factor of 8 to 12. Research on how adsorbed ions on nanoparticles can change relaxivity is limited. For practical use of nanoparticles as contrast agents in the subsurface, it is crucial to understand the way magnetic and paramagnetic ions affect nanoparticles and corresponding NMR signals.

5.2 RELAXATION THEORY

5.2.1 Relaxivity of nanoparticles in dispersions

Relaxation of hydrogen nuclei in nanoparticle dispersions is similar to the relaxation behavior of a very dilute porous medium in which solid nanoparticles are the matrix providing surface relaxation (Korb et al., 1997; McDonald et al., 2005; Zhu et al., 2015), and the bulk fluid in which the nanoparticles are dispersed provides the bulk fluid relaxation. The overall longitudinal relaxation rate $1/T_1$ of a nanoparticle dispersion is the sum of the contributions from bulk relaxation rate $1/T_{1,\mathrm{Fluid}}$ and nanoparticle surface relaxation rate $1/T_{1,\mathrm{NP}}$ (e.g., Carr and Purcell, 1954):

$$\frac{1}{T_1} = \frac{1}{T_{1,\mathrm{Fluid}}} + \frac{1}{T_{1,\mathrm{NP}}} . \quad (5.1)$$

The bulk fluid relaxation rate is easy to obtain from experiments by measuring the relaxation time of pure dispersing fluid.

When diffusion of water molecules across the pores is fast enough to maintain uniform magnetization in the pores during signal decay, the longitudinal surface relaxivity ρ_1 can be used to link $1/T_{1,\mathrm{NP}}$ to S/V, the ratio of total nanoparticle surface area to total fluid volume in the dispersion (Senturia and Robinson, 1970). In Equation (5.2), S_{pore} is nanoparticles' surface area, which can be calculated from nanoparticles' volume V_{NP} and radius r_{NP} assuming that the nanoparticles are spherical. V_{pore} is fluid volume which equals total dispersion volume V_{Total} minus the nanoparticles' volume V_{NP}. The parameter v is the ratio of the nanoparticles' volume to the fluid volume in the dispersion (Zhu et al., 2015).

$$\frac{1}{T_{1,\mathrm{NP}}} = \rho_{1,\mathrm{NP}} \left(\frac{S}{V}\right)_{pore} = \rho_{1,\mathrm{NP}} \left(\frac{V_{NP} \dfrac{3}{r_{NP}}}{V_{Total} - V_{NP}} \right) = \rho_{1,\mathrm{NP}} \left(\frac{3v}{r_{NP}}\right) . \quad (5.2)$$

5.2.2 Relaxivity of Fe cations in solution

For paramagnetic ions in solution, the NMR relaxation theory was first developed by Solomon (1955) and extended by Bloembergen and Morgan (1961). The overall longitudinal relaxation rate of aqueous solutions with paramagnetic ions $1/T_{1,Fluid}$ contains contributions from the paramagnetic species' relaxation rates and the pure water bulk relaxation rate $1/T_{1,W}$ (Bryar et al., 2000), as indicated in Equation (5.3):

$$\frac{1}{T_{1,Fluid}} = \frac{\chi}{T_{1,M} + \tau_M} + \frac{1}{T_{1,W}} \quad , (5.3)$$

where $T_{1,M}$ is relaxation time of a hydrogen nucleus in the hydration shell around the paramagnetic ion, τ_M is the residence time of water molecules in the hydration sphere that are close enough to the paramagnetic ion to be relaxed, and χ is the molar fraction of water molecules in the paramagnetic ions' hydration shells. The value of χ is proportional to paramagnetic ion concentration in the fluid. Therefore, since the relaxation time $T_{1,W}$ is an intrinsic property of pure water, there is a linear relationship between the overall relaxation rate $1/T_{1,Fluid}$ and paramagnetic ion concentrations and number of water molecules in the hydration shell of a paramagnetic ion.

5.2.3 Relaxivity of Fe(III) adsorbed on solid surface

Given different paramagnetic surface sites, such as surface ions in a crystal lattice, adsorbed paramagnetic ions, or paramagnetic crystal defects, the surface relaxation rate of solid nanoparticles, $1/T_{1,S}$, contains contributions from paramagnetic relaxation, as well as from non-magnetic relaxation due for example to homonuclear dipolar interactions (Pfeifer, 1972). Paramagnetic relaxation is associated with various paramagnetic species on the surface (Kleinberg et al., 1994) as shown in the middle terms of Equation (5.4), where χ_i is molar fraction of water molecules located in the inner coordination sphere of the i^{th} species of adsorbed paramagnetic ion, $T_{1,N}$ is relaxation time of water molecules not

interacting with paramagnetic sites, and τ_N is the residence time of water molecules at the solid surface. There is assumed to be a background of nonmagnetic relaxation on the solid surface that causes the relaxation of protons not interacting with the paramagnetic sites. As indicated in the right-hand side of Equation (5.4), surface relaxivity ρ, the parameter characterizing effectiveness of pore surface relaxation, links surface relaxation rate $1/T_{1,S}$ with surface area to volume of the pore $(S/V)_{pore}$ when all water molecules can be relaxed with the solid surface during lifetime of decay.

$$\frac{1}{T_{1,S}} = \sum_{i=1}^{n} \frac{\chi_i}{(T_{1,M} + \tau_M)_i} + \frac{1 - \sum_{i=1}^{n} \chi_i}{T_{1,N} + \tau_N} = \rho \left(\frac{S}{V} \right)_{pore} . \quad (5.4)$$

Adsorption of Fe(III) brings more paramagnetic sites to the solid surface, so relaxivity increases with the fraction of surface occupied by magnetic sites n_i, ρ_i is the inherent relaxivity of different kind of magnetic site on solid surface (Bryar et al., 2000) as shown in Equation (5.5):

$$\rho = \sum_{i=1}^{n} n_i \rho_i + (1 - \sum_{i=1}^{n} n_i) \rho_N = \rho_N + \sum_{i=1}^{n} n_i (\rho_i - \rho_N) . \quad (5.5)$$

The molar fraction of water molecules coordinated with paramagnetic sites, χ_i, is related to the surface fraction n_i, with the assumption that the maximum distance at which a proton spin can be relaxed by a paramagnetic ion is the thickness of one monolayer of water h:

$$\chi_i = n_i h \left(\frac{S}{V} \right)_{pore} . \quad (5.6)$$

Combining Equations (5.4), (5.5) and (5.6) gives the surface relaxivity of the i^{th} paramagnetic species on the solid surface ρ_i:

$$\rho_i = \frac{h}{(T_{1M} + \tau_M)_i} . \quad (5.7)$$

5.3 MATERIALS AND METHODS

We used zirconia nanoparticles dispersed in water (ZR-30AL) with 30 wt% of colloidal zirconium oxide (ZrO_2) stabilized with 0.9 wt% HNO_3 from Nissan Chemical America Corporation. The pH value was measured as 3.1. The original ZR-30AL was diluted with DI water to 6 wt% of ZrO_2 in dispersion with pH value of 3.13 for further usage. The nanoparticles have no surface coating and had positive surface charge, with an average zeta potential of +32.5 mV. Nanoparticle diameters were between 110 and 130 nm measured by a Dynamic Light Scattering (DLS) ZetaSizer (Malvern Nano ZS).

We also used a 40 wt% dispersion of colloidal ZrO_2 (ZR-40BL) from Nissan Chemical America Corporation. These nanoparticles were dispersed in water and stabilized with 1 wt% $C_4H_{12}N.HO$. The pH was 9.2. The original ZR-40BL dispersion was diluted with DI water to reduce the weight concentration of zirconia nanoparticles to 6 wt%, and pH was measured as 9.1. No surface coating attached on the nanoparticles, they had negative surface charge with average zeta potential of -38.8 mV. Nanoparticle diameters were between 70 and 90 nm.

Silica nanoparticle dispersion with poly(ethylene glycol) (PEG) coating was diluted with DI water to obtain 4 wt% of silica nanoparticles and labeled as Si-4B. The pH value was 8.8 for the diluted silica nanoparticle dispersion. Nanoparticle size was determined by DLS Zeta Sizer as 30 nm, and the average zeta potentials of Si-4B was -28.1 mV.

Iron standard solution with Fe(III) concentration of 1000 mg/L in 2% HNO_3 was purchased from ACROS Organics. DI water was used to dilute the Fe standard solution to different concentrations: 100mg/L, 50mg/L, 18mg/L, and 8mg/L. We used 2% HNO_3 to serially dilute the Fe standard solution to build a calibration curve for inductively coupled plasma optical emission spectroscopy (ICP-OES) measurements. NMR measurements

were performed to obtain Fe^{3+} relaxation rates with Fe concentrations of 50mg/L, 25mg/L, 9mg/L, and 4mg/L.

15 ml of Fe(III) solutions with different concentrations: 100 mg/L, 50 mg/L, 18 mg/L, and 0 mg/L were mixed with 15 ml of different groups of nanoparticle dispersions: ZR-6AL, ZR-6BL, Si-4B, and DI water separately. We also introduced a control group of NaOH solution at pH 9 to isolate the effects of alkaline conditions. All mixtures were kept for overnight at ambient conditions before further measurements were performed. Measurements and treatments to different mixtures and solutions are listed in Table 5.1.

A Malvern Nano ZS was used to measure size distribution of nanoparticles mixed with different concentrations of Fe(III) in ZR-AL and ZR-BL. Size calibrations were performed with calibration standard dispersions before each measurement. 0.450 mL of zirconia nanoparticle dispersion was placed in a disposable cell to measure size distribution. The size distribution and average size value were recorded. Measurements of each dispersion sample were performed three times and the mean value and standard deviation were recorded.

We used Beckman Avanti J-E centrifuge and rotor JA-10 to remove nanoparticles. Zirconia nanoparticles with size 80-110 nm were easily separated from supernatant after 30 minutes of centrifuging at 9,000 RPM. 14,000 RPM is required to remove the smaller silica nanoparticles (30nm) by centrifugation. Since the maximum rotation speed of rotor JA-10 is 10,000 RPM, we could not separate the silica nanoparticles with the centrifuge in this study. After centrifuging Fe-zirconia nanoparticles mixtures and Fe-NaOH mixtures, 12 ml of the supernatants of the corresponding samples were collected for further NMR and ICP-OES measurements as shown in Table 5.1.

NMR measurements were performed at room temperature (20°C) using a 2 MHz GeoSpec2 benchtop NMR core analysis instrument from Oxford Instruments with an

operating frequency of 2.15 MHz The external magnetic field B_0 was 0.05047 T. We used an inversion recovery measurement to determine the distribution of longitudinal relaxation times (T_1). Samples for which we performed T_1 measurements are displayed in Table 5.1.

A Varian Liberty Series II Axial ICP-OES was employed to measure dissolved iron concentration in Fe-DI mixture and supernatants after centrifuging the Fe-nanoparticles and Fe-NaOH mixtures. Wavelengths for Fe were picked as 234.350 nm, 238.204 nm, and 259.940 nm. Calibration was generated based on 1 mg/L, 2 mg/L, 5 mg/L, 8 mg/L, 10 mg/L, 20 mg/L, and 50 mg/L iron standard solutions. Concentrations of iron in samples were measured and calculated employing standard calibration range from 0 mg/L to 50mg/L.

A Thermo Scientific Orion Versa Star pH benchtop meter was used to measure pH values of different mixtures with various Fe concentrations. The meter was calibrated with standard pH buffers at pH 4.01, 7.00 and 10.01. The pH probe was triple rinsed with DI water before and after measurements of different samples.

Table 5.1 Treatment and measurement performed of different mixture groups.

Mixture labels	Contents	NMR measurement	Centrifuge	ICP, NMR and pH measurement of pure fluid (supernatant) after centrifuge
Fe-DI solution	Fe(III) and DI water	Y	N	Y, w/o centrifuge
Fe-NaOH mixture	Fe(III) and NaOH solution	Y	Y	Y
Fe(III)-Si-2B mixture	Fe(III) and Silica NPs	Y	N	N
Fe(III)-ZR-3AL mixture	Fe(III) and Zirconia NPs	Y	Y	Y
Fe(III)-ZR-3BL mixture	Fe(III) and Zirconia NPs	Y	Y	Y

Error bars for the longitudinal relaxation rate were computed from the standard deviation of the longitudinal relaxation time obtained from the Matlab inversion. The signal and noise were extracted from the raw NMR data in the time domain. Random noise with the same properties (magnitude, mean value and standard deviation) of noise extracted from raw NMR data was added to the time domain signal. With the added noise, there was a slightly different magnetization buildup curve compared to the curve obtained directly from the raw data. A linear inversion regression was then applied to the buildup curve with added noise to compute the T_1 value. After repeating this process 100 different times, 100 buildup curves were generated and used to calculate associated T_1 values. Based on these 100 computed T_1 values, the standard deviation of T_1 was recorded and used to compute the errors in longitudinal relaxation rate.

5.4 Results and Discussions

5.4.1 Proton Relaxation by Fe(III) Ions in Solution

Longitudinal relaxation time of Fe(III) solutions with different Fe concentrations was measured and computed. The pH value was recorded as 2.4 for each sample. In nitric acid solution with Fe(III), the first hydration shell of Fe(III) contains 6 water molecules (Magini and Caminiti, 1977), while the second hydration shell is formed by 12 water molecules (Caminiti and Magini, 1979). Previous studies indicated that the relaxation rate of water molecules outside the first hydration shell of paramagnetic ions is insignificant compared to those in the first hydration shell (Koenig and Brown, 1987). At pH around 2.4, the overall relaxation rate of Fe(III) solution decreased from 18.508 s^{-1} with 50 mg/L Fe(III) ions to 0.361 s^{-1} with zero iron in solution are shown in Figure 5.1. The error bars of relaxation rate were obtained from the standard deviation of the longitudinal relaxation times of nanoparticle dispersions by linear regression of the raw data in Matlab as described

in section 5.3. Based on the slope calculated from Figure 4.1 and Equation (4.5), along with the calculated mole fraction of water in the Fe(III) hydration shell, which is 6 times Fe(III) mole fraction, $T_{1,M}+\tau_M$ associated with dissolved magnetic Fe(III) is computed to be 7.53 μs. This value is in good agreement with previous work: Bryar et al. (2000) found $T_{1,M}+\tau_M$ around 8 μs for Fe(III) ions at pH around 2.5. Smaller values of $T_{1,M}+\tau_M$ may arise from different pH values where lower pH value increases the number of exchangeable water molecules in the hydration shell and thus increases the relaxation rate (Bertini et al., 1993).

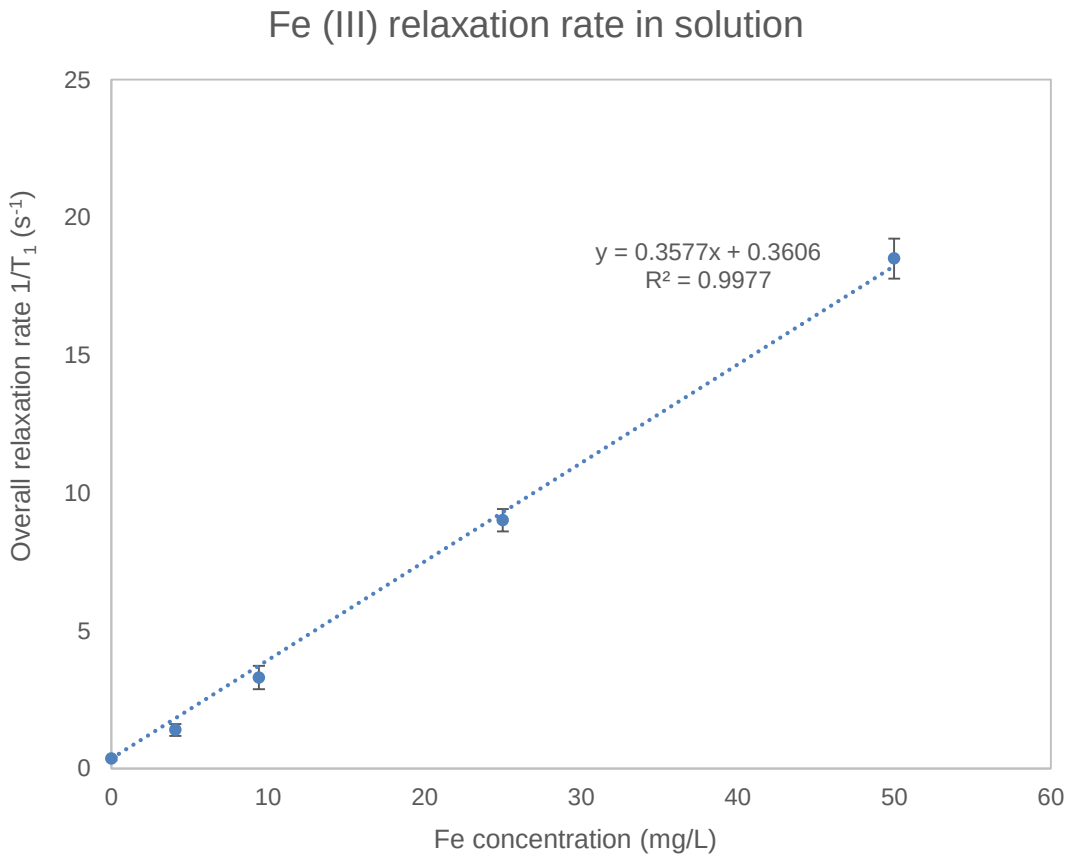

Figure 5.1 Dependence of overall relaxation rate on Fe(III) concentration in solutions.

5.4.2 Proton Relaxation in Fe- Nanoparticles mixture

As shown in Figure 5.2a), the relaxation rate of pure Fe-DI solution increased proportionally with increasing Fe concentration. This indicates that the relaxation contribution of Fe(III) ions dominates the overall relaxation rate, so hydrogen nuclei get relaxed faster with higher Fe concentrations, as demonstrated in the previous section. Error bars for the relaxation rate were obtained based on the standard deviation of the relaxation times described in section 5.3. For the Fe-NaOH mixture, the relaxation rate remained similar to that of the Fe-DI solution at the same Fe concentration. When nanoparticles were present in the Fe-zirconia nanoparticle mixtures, at relatively high Fe concentrations such as 50 mg/L and 25 mg/L, relaxation rate was lower than that of pure Fe solutions at same concentrations even with additional surface relaxivity brought from nanoparticles. In contrast, at low Fe concentration (9 mg/L), Fe-Zirconia nanoparticle mixtures showed faster relaxation rate than those of pure Fe-DI solutions. The observed amount of change in relaxation rate in this case cannot be simply explained by the additional contribution of the nanoparticle surface relaxation rate. For example, with 9 mg/L of Fe in mixture, the relaxation rate of Fe(III)-ZR-3AL was 3.631 s^{-1}, while the relaxation rate of Fe(III) in solution at 9 mg/L was 3.252 s^{-1}. The increase from 3.252 s^{-1} to 3.782 s^{-1} (0.379 s^{-1}) is smaller than surface relaxation of pure zirconia nanoparticles in ZR-3AL, which is 0.419 s^{-1}. This may indicate that Fe(III) and nanoparticles interact with each other and the overall relaxation rate of Fe and nanoparticles is not simply the sum of the relaxation rate of aqueous Fe(III) in solution and the pure zirconia nanoparticle surface relaxation rate as indicated by lines in Figure 5.2b).

For Fe-Silica nanoparticle mixtures, the relaxation rate was much slower than that of pure Fe-DI solution with the same Fe concentrations. This suggests that the addition of silica nanoparticles causes the Fe(III) in the mixtures to relax proton spins less efficiently

so that the overall relaxation rate decreased in the Fe-nanoparticles mixture. From Equation (5.4), this suggests that the value of χ decreased after adding silica nanoparticles. A possible explanation for this is that Fe ions were removed from the aqueous phase and adsorbed to the nanoparticle surfaces (Zhu et al., 2016), thus altering both the bulk fluid and surface relaxations. In both types of nanoparticles (silica and zirconia, with and without surface coating), the overall relaxation rate showed similar trend at high Fe concentration (25 mg/L ~ 50 mg/L): with presence of nanoparticles, relaxation rate decreased.

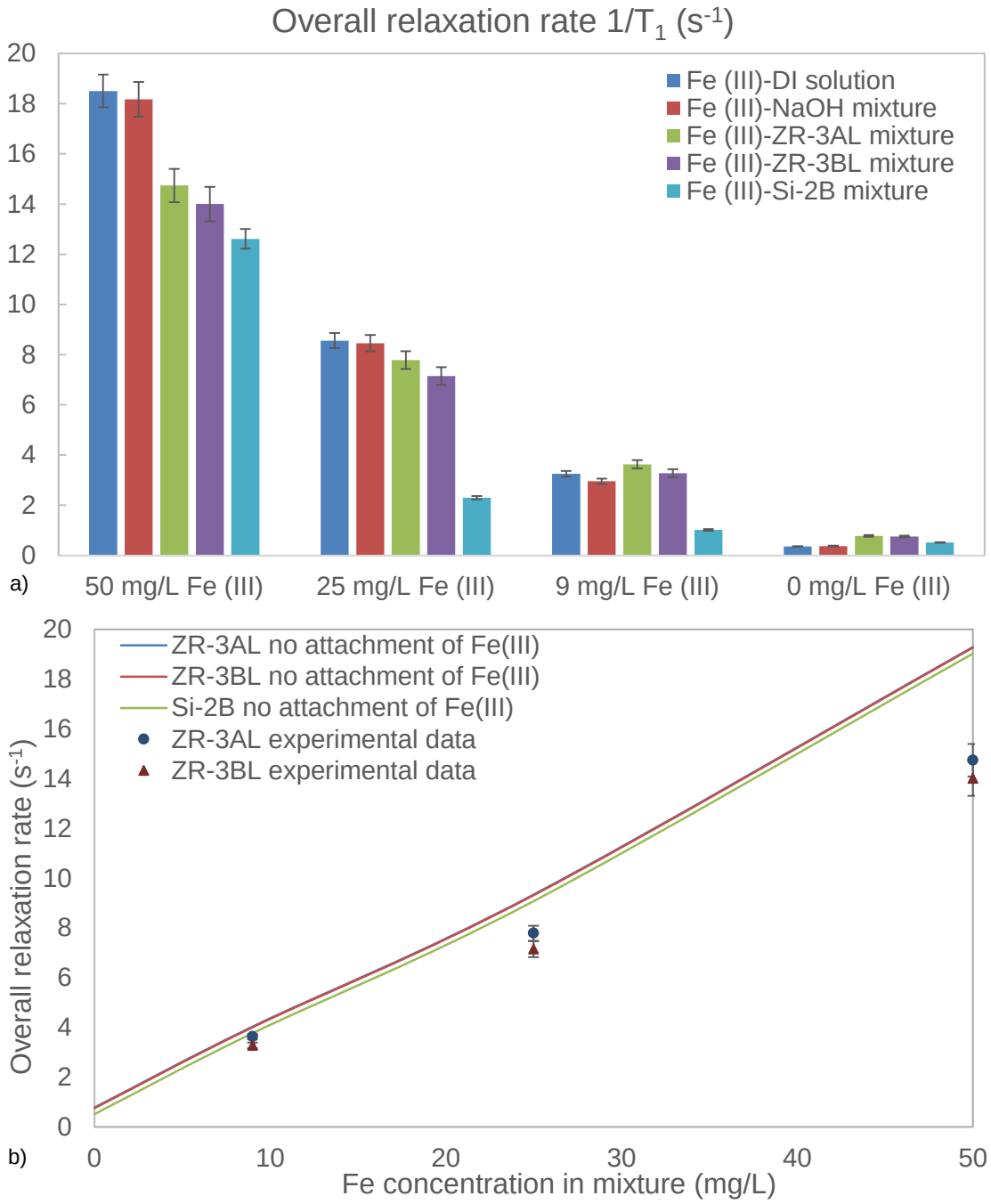

Figure 5.2 Longitudinal relaxation rate of Fe-DI solution and Fe(III)-nanoparticles mixtures with different Fe(III) concentrations. a) Grouping of relaxation rates of different mixtures with same Fe concentration; b) Comparison of measured mixture overall relaxation rate with values assuming no Fe(III) adsorption onto nanoparticles.

5.4.3 Fe(III) and pH in supernatants

To separate the relaxation contribution of nanoparticles in the mixture, we centrifuged the Fe-Zirconia nanoparticles, collected the supernatant, measured the Fe concentration with ICP-OES and recorded the NMR results of the supernatant. In the meantime, Fe-NaOH mixture was used as a control group to isolate effects of pH on Fe concentrations and relaxation rate in supernatants. However, due to the speed limit of centrifuge rotor, silica nanoparticles with smaller size (21 nm ~ 35 nm) could not be removed from the mixture, so we only further studied the Fe-Zirconia nanoparticles mixture and supernatants in this work.

Table 5.2 ICP measured Fe concentration in supernatants of Fe-NaOH mixtures and Fe-Zirconia nanoparticles after centrifuging.

Fe conc. in mixture (mg/L)	Fe conc. in Fe-NaOH supernatant (mg/L)	Fe conc. in Fe(III) - ZR-3AL supernatant (mg/L)	Fe conc. in Fe(III) -ZR-3BL supernatant (mg/L)
50	49.03	0.9603	0.9019
25	24.89	0.5179	0.5095
9	8.516	0.1043	0.09675
0	0.0366	0.02094	0.02630

We also centrifuged the group of Fe-NaOH mixture at 10,000 RPM for 30 minutes. As shown in Table 5.2, the supernatant collected from Fe-NaOH mixture contained a similar Fe concentration to the mixture before centrifuging and we determined that 98% of the original Fe(III) remained in the supernatant after centrifuging. According to the ICP-OES results for Fe concentration in Fe-Zirconia nanoparticle mixtures and supernatants after centrifuging displayed in Table 5.2, there was much less iron remaining in the supernatant, indicating that Fe(III) was retained on the zirconia nanoparticles' solid surface. Adsorption of Fe(III) onto nanoparticles may also explain the decrease in overall relaxation rate observed with the addition of silica nanoparticles to Fe solutions.

Relaxation rates of supernatants from Fe-NaOH and Fe-Zirconia nanoparticle mixtures are shown in Figure 5.3a). The relaxation rates of the supernatants after removal of zirconia nanoparticles were smaller than 0.8 s^{-1}, indicating that less Fe(III) was in the supernatant. This suggests that most of the Fe(III) was attached to the zirconia nanoparticles' surface. Figure 5.3b) shows the bounds on overall relaxation rate assuming no adsorption of Fe(III) (upper bound) and full adsorption of Fe(III) (lower bound). The measured data for NaOH fall along the upper bound, indicating that all Fe(III) remained in the supernatant as expected. The data for the two nanoparticle dispersions fall along the lower bound, indicating that all of the Fe(III) was attached to the nanoparticles. Error bars for the longitudinal relaxation rate were computed from the standard deviation of relaxation times as described in section 5.3.

Table 5.3 pH of supernatant from Fe-Zirconia nanoparticles mixtures and Fe-NaOH mixtures, and Fe-Silica nanoparticles mixtures.

Fe conc. in mixture (mg/L)	pH of Fe-NaOH supernatant	pH of Fe(III)-ZR-3AL supernatant	pH of Fe(III)-ZR-3BL supernatant	pH of Fe-DI solutions	pH of Fe(III)- Si-2B mixtures
50	3.0	2.4	3.0	2.4	2.6
25	3.4	2.5	3.4	2.4	7.1
9	7.2	2.8	7.0	2.4	8.0
0	9.0	3.1	8.7	6.7	9.2

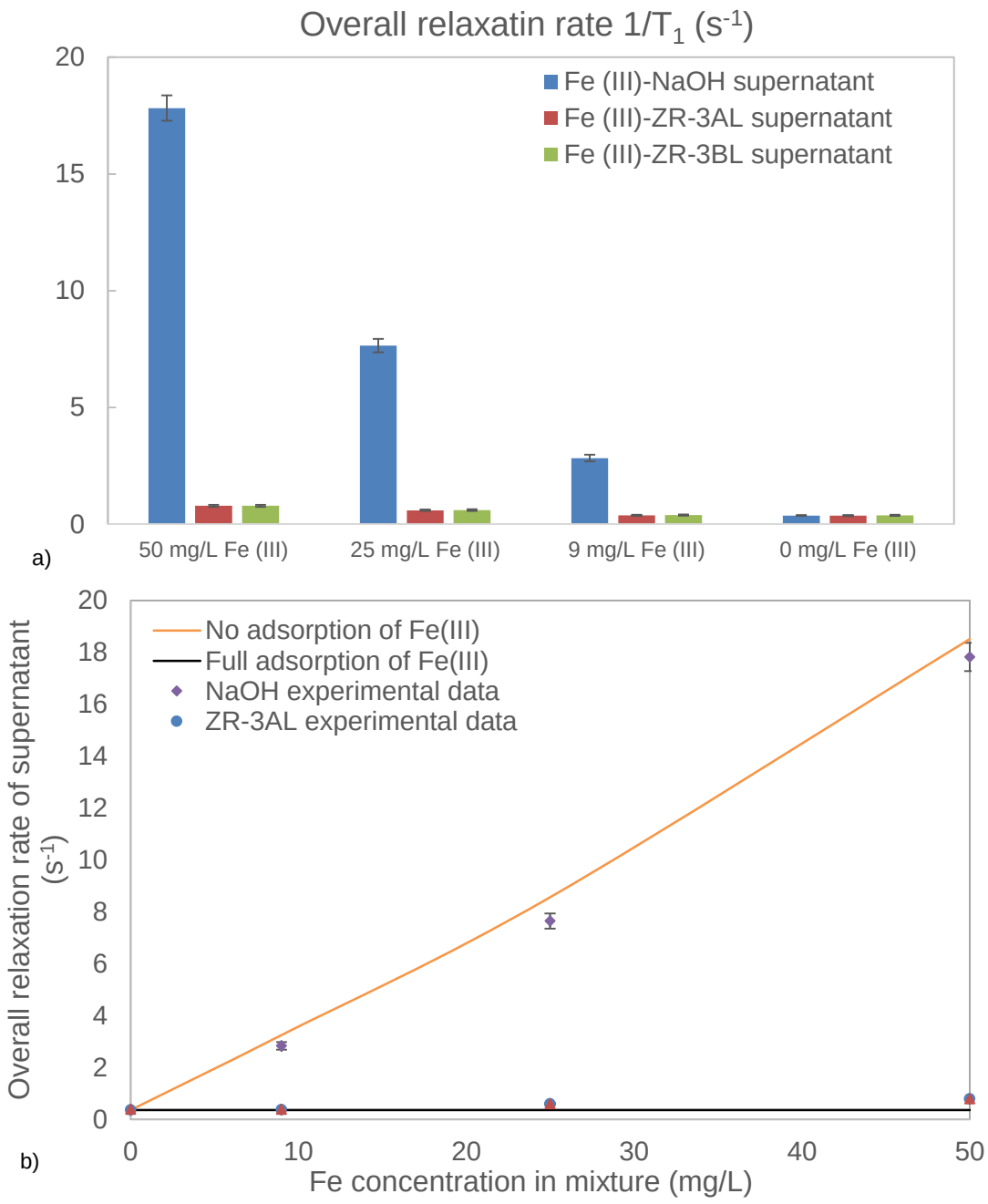

Figure 5.3 Relaxation rates of supernatants from Fe-Zirconia nanoparticles mixtures and Fe-NaOH mixtures. 5.3a) Grouping of relaxation rates of supernatants collected from different mixtures with same original Fe concentration; 5.3b) Comparison of measured supernatant relaxation rate of mixtures with theoretical values assuming no Fe(III) attached onto nanoparticles.

The pH values of the supernatants and Fe-DI solution are displayed in Table 5.3. At low Fe concentration (9 mg/L) the pH value of each mixture group varies from 2.4 in pure Fe(III) solution to 7.5 in the Fe-NaOH mixture because the Fe standard solution is significantly diluted. To isolate the effect of pH on Fe(III) relaxivity, the Fe(III)-ZR-3BL group was compared to the Fe-NaOH group for Fe concentrations ranging from 9 mg/L to 50 mg/L; the Fe(III)-ZR-3AL group was compared to the Fe-DI solution for Fe concentrations at 25 mg/L and 50 mg/L.

5.4.4 Proton Relaxation by Zirconia Nanoparticles with adsorbed Fe(III)

Table 5.4 Surface relaxivity of zirconia nanoparticles with increased amount of adsorbed Fe(III) under different iron concentrations.

Fe conc. in mixture (mg/L)	ZR-3AL radius in mixture (nm)	Surface relaxivity of ZR-3AL (μm/s)	Adsorbed Fe(III) onto ZR-3AL (mg)	ZR-3BL radius in mixture (nm)	Adsorbed Fe(III) onto ZR-3BL (mg)	Surface relaxivity of ZR-3BL (μm/s)	Si-2B radius in mixture (nm)
50	58.2	50.17	1.345	42.9	1.342	35.13	10.35
25	59.7	27.17	0.5974	42.5	0.5976	17.77	17.45
9	57.8	12.27	0.2088	44.0	0.2078	8.430	13.95
0*	59.6	1.427	N.A.	43.3	N.A.	1.095	10.94

Based on Fe concentration measured by ICP-OES in the Fe-Zirconia nanoparticle mixtures and corresponding supernatants, a mass balance calculation indicates that Fe(III) adsorbed onto the zirconia nanoparticles (Table 5.4). Before adsorption of Fe, pure zirconia nanoparticles in dispersion have surface relaxivities of 1.427 μm/s for ZR-3AL and 1.095 μm/s for ZR-3BL (Zhu, et al., 2015). Relaxation rates of zirconia nanoparticles in the mixtures were computed using Equation (5.1) by subtracting the supernatant relaxation rate from the overall relaxation rate of the Fe-Zirconia nanoparticle mixture. We assumed that the supernatant represented the composition of the dispersing fluid in the presence of

nanoparticles. The nanoparticle surface relaxivity was then determined using Equation (5.2) with nanoparticle sizes obtained from DLS measurements.

As shown in Table 5.4, relaxivity of zirconia nanoparticles increased with the amount of adsorbed Fe(III). The relaxivity of positively-charged zirconia nanoparticles increased about 40 fold after exposure to 50 mg/L Fe(III) at pH around 2.4; at pH around 3, the relaxivity of negatively-charged zirconia nanoparticles increased by a factor of 36. The results indicate that with Fe(III) in solution, even at disparate pH values and nanoparticle surface charges, adsorption of Fe ions onto nanoparticles increased nanoparticles relaxivity.

When pH value was above 6, with no surface coating, zirconia nanoparticles in dispersion were negatively charged (Tang et al., 2000), and the driving force for adsorption of Fe(III) onto ZR-3BL was likely due to electrostatic attraction between negatively charged nanoparticle and iron cations (Stuart et al., 1991). Under acidic conditions where pH value was lower than 6, zirconia nanoparticles with positive surface charge also acted as a Fe(III) sink, which suggests that electrostatic attraction was not the driving force of adsorption in these cases. Hydrolysis of Fe^{3+} in solution builds $Fe(OH)_3$ and polymers of Fe(III) could have been precipitated at pH values ranging from 1.8 to 3.4 (Dousma and De Bruyn, 1976). These polymers tend to precipitate on solid surfaces under acidic conditions (Dai and Hu, 2014).

Although we were not able to perform any measurements on supernatants from the silica nanoparticle solutions, the behavior observed with the negatively charged zirconia nanoparticles can be used to inform some interpretations of our measurements. At pH from 5.5 to 9, the PEG coated silica nanoparticles were negatively charged. Therefore, the increase in relaxation rate can probably be attributed to electrostatically-driven adsorption of Fe ions onto the nanoparticles.

With the assumption that the values of surface relaxivities (ρi) for pure solid surface and paramagnetic sites are constant, the surface relaxivity of adsorbed Fe(III) ions can be computed according to Equations (5.4-5.7). Adsorbed Fe(III) relaxivity on zirconia nanoparticles was computed as 68 μm/s to 78 μm/s when assuming there are 3 water molecules remaining in a hemisphere around Fe(III) after their adsorption on the solid surface. Similar values with 80 μm/s to 120 μm/s for surface relaxivity of adsorbed Fe(III) ions on silica gel surface were obtain by previous studies (Bryar et al., 2000).

To compute the theoretical highest amount of Fe(III) that can be adsorbed onto nanoparticles, we assume all the conditions such as temperature, viscosity, pressure, pH value, zeta potential will favor each Fe(III) ions to attach onto nanoparticle surface. We employ a geometric method where Fe(III) ions and their associated hydration shells are assumed to be spheres. The attached Fe(III) spheres form a monolayer, and each Fe(III) sphere makes a project area of $\pi r_{Fe(III)}^2$ on the nanoparticle surface. The radius can be computed from Fe^{3+}'s ionic radius (0.66 Å), the Fe-O distance (2.00 Å) (Persson, 2010), and the O-H distance in water molecules (0.942 Å) (Csaszar et al., 2005). This yields $r_{Fe(III)}$ of 0.3602 nm. Since zirconia nanoparticles are a very dilute matrix compared to rock, the volume fraction of zirconia nanoparticles in dispersion is 0.557%. We compute the volume of Fe(III)-ZR3AL mixture that contains only 1 zirconia nanoparticle with radius of 58.56 nm (mean value computed based on Table 5.4) as 0.151 μm^3. Given Fe(III) molecular weight of 55.845 g/mol, theoretically up to 95,883 Fe(III) ions can attach onto the nanoparticle surface to cover 90.69% of the surface. This would increase the nanoparticle surface relaxivity to 68.15 μm/s. With Fe(III) concentration of 50 mg/L, there are 81,426 Fe(III) atoms in this volume. As indicated in Figure 5.4, if all 81,426 Fe(III) atoms get adsorbed onto the surface of spherical nanoparticles with radius of 58.56 nm, 3.14×10^{-6} mol/m^2 Fe(III) would be attached on the nanoparticle. With the radius of Fe(III) being

0.3602 nm, the nanoparticle surface fraction occupied by Fe(III) is 0.77, according to Equations (5.4 and 5.5), and the corresponding surface relaxivity is calculated as 58.1 μm/s based on experimental results assuming a linear relationship between nanoparticle relaxivity and adsorbed Fe(III) amount. Similarly, the maximum number of Fe(III) ions that can be adsorbed onto ZR-3BL is 52,011, which would cover 90.69% of the nanoparticle surface and increase the relaxivity as 63.58 μm/s. In this study, in the Fe(III)-ZR3BL mixture with 50 mg/L initial Fe(III) concentration, there was 2.36×10^{-6} mol/m^2 Fe(III) attached onto the nanoparticle. The surface fraction occupied by the Fe(III) monolayer is 0.564, and the corresponding nanoparticle relaxivity is 40.1 μm/s.

In Figure 5.4, assuming monolayer attachment as described in Equations (5.4-5.7), the relaxivities of ZR-3AL and ZR-3BL should increase linearly with quantity of adsorbed Fe(III). Experimental data with errors in nanoparticle relaxivity are displayed and compared with the two theoretical bounds. Errors bars for nanoparticle relaxivity were determined from the standard deviations of nanoparticle size and relaxation times of mixture and effluents as described in section 5.3 and equations in Appendix A. The deviation from linearity observed at lower adsorbed Fe(III) quantities could be caused by variable relaxivity among different Fe(III) species. We did not consider Fe(III) adsorption dynamics or mechanisms in the monolayer attachment, and it is possible and that at different pH values, different Fe(III) species with various inherent relaxivities are preferentially adsorbed on nanoparticles. The relaxivity of adsorbed Fe(III) used to compute the theoretical nanoparticle relaxivity is the average value derived from calculations based on 3 samples in each group with different pH values (pH values shown in Table 5.3). Differences between this value and the specific values for different Fe(III) complexes (Bertini et al.,1993; Bryar et al., 2000) may lead to deviation of the experimental data from the predicted lines. Additionally, the radius of the zirconia nanoparticles used to

compute the theoretical lines is the averaged value obtained from 3 samples of each group shown in Table 5.4. Differences between the measured radius in the experimental data and the mean value used here also contributes to the deviation of the experimental data from the trend. Note that the iron concentration in the supernatant of the Si-2B mixtures was not determined due to the inability of those mixtures to be separated by centrifuge. For this reason, the surface relaxivity as a function of iron concentration was not determined for the silica nanoparticles.

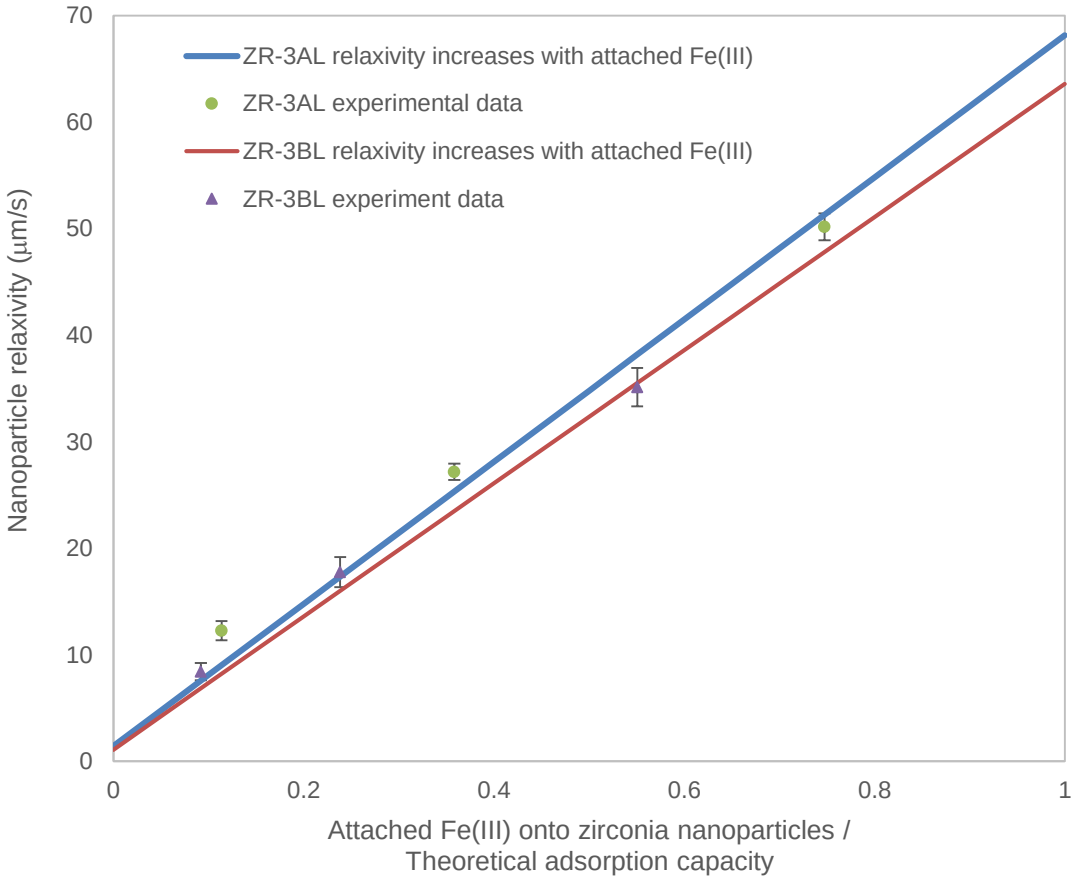

Figure 5.4 Zirconia nanoparticles relaxivity increases with attached Fe(III). Blue and Red lines display computed ZR-3AL and ZR-3BL relaxivity with attached Fe(III), respectively; green dots exhibit the experimental results from this work for ZR-3AL, purple triangles show experimental data for ZR-3BL.

According to Figure 5.4, assuming a constant nanoparticle radius of 10.35 nm and a nanoparticle volume fraction of 0.76%, the maximum percentage of 50 mg/L Fe(III) in the mixture that can attach onto silica nanoparticle surface is 100%. The attached 1.45×10^{-6} mol/m^2 Fe(III) covers 0.309 of silica nanoparticle surface, and the resulting relaxivity increased from 0.0722 μm/s to around 22 μm/s ~ 23 μm/s (giving the adsorbed Fe(III) relaxivity of 68 μm/s ~ 78 μm/s from previous results).

We were not able to separate Si-2B nanoparticles from mixtures via centrifuge, and thus were unable to obtain the necessary properties of the supernatant. The measured size of the silica nanoparticles varies by more than 50% among tested mixtures, as indicated in Table 5.2. This further complicates computation of silica nanoparticle surface relaxivity with fractions of attached Fe(III), which requires a relatively constant and representative value of nanoparticle radius. Hence, the theoretical relaxation rate with full adsorption of Fe(III) onto the silica surface with different initial Fe(III) concentrations cannot be determined. The relaxation rate of zirconia nanoparticle and Fe(III) mixture as a function of Fe concentration are shown in Figure 5.5, along with upper and lower bounds determined by assuming monolayer adsorption of Fe(III) in hexagonal packing. When there is no adsorption of Fe(III) onto nanoparticles, the overall relaxation rate is simply the sum of the nanoparticle surface relaxation rate and the relaxation rate of aqueous Fe(III) solution. In zirconia nanoparticles and Fe(III) mixtures with different Fe(III) concentration, when Fe(III) is fully adsorbed onto nanoparticles, the fraction of adsorption capacity can be determined, and the corresponding value of nanoparticle relaxivity in Figure 5.4 were used to compute the relaxation rate. As expected, the experimental data fall inside the envelope between no adsorption and full adsorption of Fe(III). At higher Fe(III) concentration, the experimental points for ZR-3AL and ZR-3BL are closer to the lower bound, indicating significant, but not full, Fe(III) adsorption.

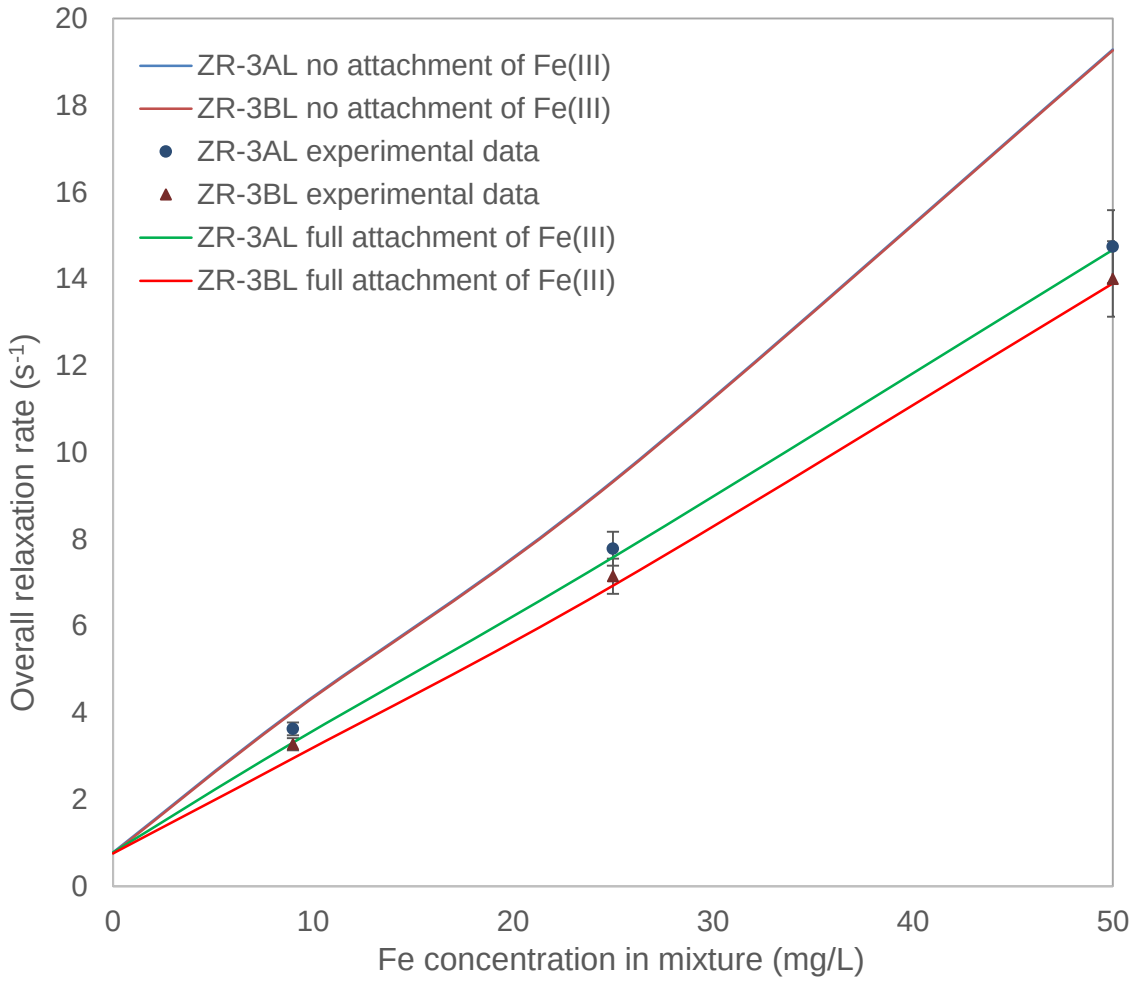

Figure 5.5 Comparison of theoretical relaxation rates with fully attached of Fe(III) and none adsorbed Fe(III) from aqueous solution to nanoparticles. Experimental data falls between the boundaries, indicating occurrence of adsorption but not to full capacity.

5.5 CONCLUSIONS

This work has shown that paramagnetic ions such as Fe(III) can adsorb onto nanoparticles regardless of surface coating and surface charge of nanoparticles. Our work suggests that the silica nanoparticles with PEG surface coating can remove Fe(III) from aqueous solution, since the relaxation rates of silica nanoparticles dispersed in Fe(III) solutions is not a simple sum of the nanoparticle and iron solution relaxation rates. Zirconia

nanoparticles with positive and negative surface charge can remove more than 90% of Fe(III) from solutions. Slightly alkaline conditions (pH between 7 and 8) do not play an important role in precipitating Fe(III) ions. Adsorbed Fe(III) significantly increased the zirconia nanoparticles' surface relaxivity. Surface relaxivity of positively charged zirconia nanoparticles increased from 1.427 μm/s to 50.17 μm/s with 2.80×10^{-6} mol/m^2 adsorbed Fe(III) at pH around 2.4. Zirconia nanoparticles with negative surface charge at pH around 3.0 had surface relaxivity increased from 1.095 μm/s to 35.13 μm/s when 2.07×10^{-6} mol/m^2 Fe(III) was adsorbed. The results show that under various pH conditions ranging from 2.4 to 7.5, adsorption of Fe(III) species onto nanoparticle surfaces occurred and increased the relaxivity of the nanoparticles.

Our research indicates that, in natural porous media with pore fluid containing paramagnetic ions, sorption of these ions to the surface of nanoparticles can significantly alter the NMR relaxation behavior of the nanoparticles. The phenomenon affects nanoparticles regardless of surface charge or whether the nanoparticles are coated with polymers or not. Care must therefore be taken when using nanoparticles as NMR contrast agents in rock samples both in the laboratory and the subsurface. With the assumption that attached Fe(III) forms a monolayer packing, the nanoparticle surface has the geometrical capacity to adsorb all the Fe(III) in the mixture. However, at laboratory conditions, we did not observe full adsorption of Fe(III) in the tested Fe(III) concentrations. It is possible that the mixture conditions are not optimized for adsorption of all Fe(III); for example, an adsorbed Fe cation may prevent other Fe cations from settling next to it due to electrostatic repulsion. We did not analyze how the hydration layer on nanoparticles affects the adsorption of Fe(III), and it is possible that the existence of a hydration layer which has higher density and viscosity than bulk water (Israelachvili and Wennerstrom, 1996) may play a role in affecting adsorption of hydrated Fe(III). In addition, in the subsurface,

temperature, pressure, pH values are different from the conditions in our experiments, which were performed at room temperature and pressure. The interactions between Fe(III) and nanoparticles in this case may be different from what we observed in this study.

Chapter 6

NMR relaxation of surface-functionalized Fe_3O_4 nanoparticles

6.1 INTRODUCTION

As indicated in Chapter 5, adsorption of paramagnetic ions onto nanoparticles with and without surface coating will increase the nanoparticles' surface relaxivity. On the other hand, presence of surface coating with low relaxivity may also affect relaxivities of paramagnetic nanoparticles. With superior magnetic properties, nanoscale dimensions and nontoxic characteristics, iron oxide nanoparticles are of high interest in nanoscience and nanotechnology. As superparamagnetic nanoparticles (MNPs), Fe_3O_4 nanoparticles have been widely applied in biomedical areas such as magnetic resonance imaging (MRI) techniques (Babes et al., 1999), tissue repair (Jordan et al., 2001) and targeted drug delivery (Chertok et al., 2008). In the petroleum industry, applications of Fe_3O_4 nanoparticles include use as a nuclear magnetic resonance (NMR) contrast agent (Ogolo et al., 2012), stabilization of magnetic Pickering emulsions (Zhou et al., 2011), remediation of oil spills in oceans (Ko et al., 2014), flow assurance in subsea pipelines (Mehta et al., 2014), and characterization of multiphase fluid dynamics in porous media (Prodanović et al., 2010).

To provide the desired chemical functionality while maintaining dispersion stability in vivo or in the subsurface, different surface coatings are usually employed in applications of iron oxide nanoparticles. In natural reservoirs, the environmental conditions are complicated, and the chemical components are not as well controlled as in biomedical research. Interactions between nanoparticles, pore fluid and rocks may take place, and various surface coatings must be used. The properties of nanoparticle cores may be influenced by the presence of these surface coatings (Lu et al., 2010; Issa et al., 2011).

In the subsurface, NMR logging is widely used to characterize properties of reservoir rocks such as porosity, pore size, permeability, tortuosity, water saturation, and wettability (Hinedi et al., 1997; Freedman et al., 2003; Wang et al., 2005; Daigle and Johnson, 2016;). In studies on the use of iron oxide nanoparticles as a contrast agent, investigation of how surface coatings of Fe_3O_4 nanoparticles affect NMR properties is limited. Thus it is crucial to understand the way and to what extent surface coating affects iron oxide nanoparticles and corresponding NMR signals.

6.1.1 Proton relaxation by dipole-dipole interactions

In NMR, the object of interest is typically a molecule, atom, nucleus, or subatomic particle. The objects (such as protons, electrons, and NMR-active nuclei) can be thought of as tiny magnets with north and south poles (dipoles) whose electromagnetic fields interact through space. This interaction is called dipole-dipole interaction; it is the most important single mechanism responsible for longitudinal (T_1) and transverse (T_2) relaxation in our studies.

In ^1H NMR as typically used in downhole applications, dipole-dipole interactions may be either proton-proton (H-H) or electron-proton (e-H). These are referred to as homonuclear and heteronuclear dipolar interactions, respectively. A dipolar interaction is the interaction of the fields from two such spinning particles. If the spins reside on the same molecule, it is called an intramolecular dipolar interaction; if on different molecules, an intermolecular interaction (Diehl et al., 1969).

Proton-proton relaxation

In pure water, the principal relaxation mechanism of protons is proton-proton relaxation. The strength of this homonuclear dipolar interaction is inversely proportional to the sixth power of distance ($1/r^6$). Hence, short-range intramolecular dipole-dipole

interactions are more powerful than long-range intermolecular ones. This generally means that two ^{1}H nuclei must approach to within about 0.3 nm of each other for their spins to be relaxed. In pure water, it is estimated that about 70% of the dipolar interactions are intramolecular while 30% are intermolecular (Bloembergen, 1956).

Electron-proton relaxation

With the presence of paramagnetic materials, electron-proton relaxation may occur. Due to its small size, an electron has a much larger gyromagnetic ratio (γ) than a proton, so electron-proton dipolar interactions are much stronger than proton-proton interactions. In natural porous media, electron-proton interactions are the dominant surface relaxation mechanism (Kleinberg et al., 1994).

6.1.2 Relaxivity of nanoparticles in dispersions

We may treat nanoparticle dispersions as dilute porous media in which solid nanoparticles are the matrix providing surface relaxation (Korb et al., 1997; McDonald et al., 2005; Zhu et al., 2015), and the bulk fluid in which the nanoparticles are dispersed provides the bulk fluid relaxation. In this study, we focus on longitudinal relaxation because it is not affected by diffusion in internal magnetic field gradients generated by the iron oxide nanoparticles (Anand and Hirasaki, 2008). The insights however are relevant and transferable to transverse surface relaxation, however. The overall longitudinal relaxation rate $1/T_1$ of a nanoparticle dispersion is the sum of the contributions from the bulk relaxation rate $1/T_{1,\text{Fluid}}$ and the nanoparticle surface relaxation rate $1/T_{1,\text{NP}}$ (e.g., Carr and Purcell, 1954), as displayed in Equation (6.1):

$$\frac{1}{T_1} = \frac{1}{T_{1,\text{Fluid}}} + \frac{1}{T_{1,\text{NP}}} \quad . \quad (6.1)$$

$1/T_{1,\mathrm{Fluid}}$ can be calculated from experiments by measuring the relaxation time of the pure dispersing fluid. When diffusion of water molecules is fast enough to maintain uniform magnetization in the pores during signal decay, $1/T_{1,\mathrm{NP}}$ is proportional to S/V, the ratio of total nanoparticle surface area (S) to total fluid volume (V) in the dispersion (Senturia and Robinson, 1970), with the constant of proportionality being the nanoparticles' surface relaxivity $\rho_{1,NP}$. In Equation (6.2), S_{pore} can be calculated from nanoparticles' volume V_{NP} and radius r_{NP} assuming that the nanoparticles are spherical. V_{pore} is fluid volume, which equals total volume of suspension V_{Total} minus the nanoparticles' volume V_{NP}. The parameter χ is the ratio of the nanoparticles' volume to the fluid volume in the dispersion (Zhu et al., 2015):

$$\frac{1}{T_{1,NP}} = \rho_{1,NP}\left(\frac{S}{V}\right)_{pore} = \rho_{1,NP}\left(\frac{V_{NP}\dfrac{3}{r_{NP}}}{V_{Total}-V_{NP}}\right) = \rho_{1,NP}\left(\frac{3\chi}{r_{NP}}\right) \quad . (6.2)$$

With various types of paramagnetic sites (surface ions in crystals, paramagnetic crystal defects, or adsorbed paramagnetic ions) on nanoparticle surfaces, the relaxation rate of nanoparticles includes contributions from paramagnetic and non-paramagnetic parts (Kleinberg et al., 1994) as shown in Equation (6.3):

$$\frac{1}{T_{1,NP}} = \rho_{1,NP}\left(\frac{S}{V}\right)_{pore} = \sum_{i=1}^{n}\frac{c_i}{(T_{1M}+\tau_M)_i} + \frac{1-\sum_{i=1}^{n}c_i}{T_{1N}+\tau_N}$$

$$= h\left(\frac{S}{V}\right)_{pore}\left(\sum_{i=1}^{n}\frac{n_i}{(T_{1M}+\tau_M)_i} + \frac{1-\sum_{i=1}^{n}n_i}{T_{1N}+\tau_N}\right) \quad . (6.3)$$

Here, c_i is the fraction of water molecules close enough to be relaxed by paramagnetic locations on the surface, T_{1M} is the intrinsic relaxation time for each paramagnetic site, τ_M is the corresponding residence time of water molecules, h is thickness of one monolayer of water molecules, and n_i is the fraction of surface sites occupied by paramagnetic relaxation centers on the nanoparticle surface. T_{1N} is the intrinsic relaxation time for each non-paramagnetic site and τ_N is the surface residence time of water molecules at the non-paramagnetic sites. When the surface concentration of paramagnetic sites n_i increases, the overall relaxation rate of the nanoparticle will increase accordingly.

If ρ_i is the inherent relaxivity of the different kinds of paramagnetic relaxation sites on the solid surface, n_i is surface concentration of paramagnetic species (Bryar et al., 2000) and ρ_N is the relaxivity of the non-paramagnetic sites, the overall relaxivity $\rho_{1,NP}$ of nanoparticles with surface coating can be computed using Equation (6.4):

$$\rho_{1,NP} = \sum_{i=1}^{n} n_i \rho_i + \left(1 - \sum_{i=1}^{n} n_i\right)\rho_N = \rho_N + \sum_{i=1}^{n} n_i \left(\rho_i - \rho_N\right) \quad . \quad (6.4)$$

As indicated in Equations (6.3 and 6.4), the nanoparticle's surface relaxation rate is determined by a combination of the relaxation rates of paramagnetic species via e-H interactions and H-H interactions from non-paramagnetic sites. Since e-H relaxation is much faster than H-H relaxation, with sufficient surface concentration of paramagnetic sites n_i and a high value of ρ_i, the nanoparticle's relaxation rate is dominated by e-H relaxation associated with paramagnetic sites. When a surface coating is present, some of the paramagnetic sites on nanoparticle surfaces may be occupied, buried or masked by the surface coating molecules, decreasing the fraction of paramagnetic sites on surface n_i. When the value of n_i is small enough that the influence of the paramagnetic sites is negligible, the overall relaxation rate may be dominated by non-paramagnetic locations via H-H relaxation.

6.1.3 Relaxation mechanism in A-MNPs

When D_2O is present in the bulk fluid phase along with H_2O, the presence of deuterium changes the relaxation characteristics at the nanoparticle surfaces. The replacement of covalently bonded hydrogen atoms with deuterium can generate partially deuterated adsorbate molecules, which will tend to change the rate of ^1H-^1H dipolar interactions but not electron-^1H dipolar interactions. This phenomenon can be used to distinguish the relative importance of the different relaxation mechanisms on the nanoparticle surface. The comparison of relaxation rates as illustrated in Figure 6.1 helps identify relaxation mechanisms involved in nanoparticle suspensions.

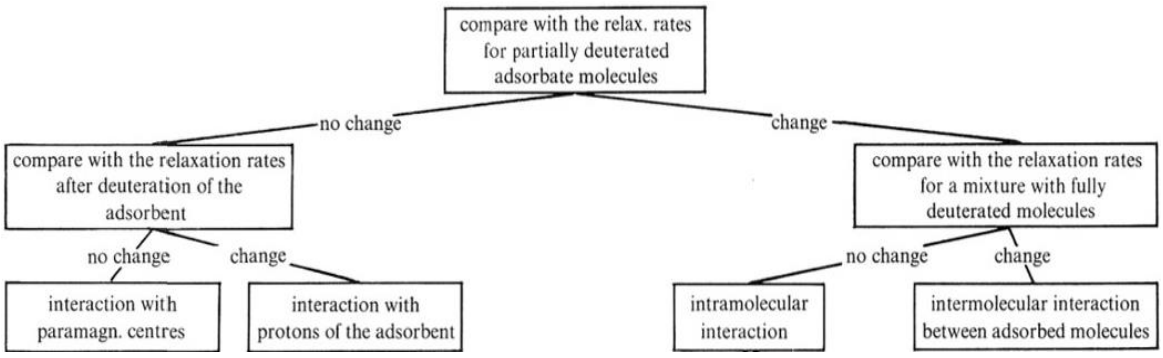

Figure 6.1 Relaxation analysis of NMR via comparing relaxation rates before and after adding D_2O. (Modified from Pfeifer, 1972).

6.2 MATERIALS AND METHODS

The method of Ko et al. (2016) was used to produce amine-functionalized Fe_3O_4 nanoparticles. A co-precipitation method was used to generate Fe_3O_4 nanoparticles (Bee et al., 1995); the general steps are shown in Figure 6.2. In the presence of citric acid, $FeCl_2 \bullet 4H_2O$ and $FeCl_3 \bullet 6H_2O$ at a molar ratio of 1:2 were mixed and heated to 90°C. With vigorous stirring under a N_2 atmosphere, ammonium hydroxide was added to induce nucleation of Fe_3O_4 nanoparticles. After 2 hours of growth, the mixture was placed in an

ice bath to stop the growth of the particles. Deionized (DI) water was used to wash and disperse the generated Fe_3O_4 nanoparticles (MNP) for further study and modification.

We used the 3-aminopropyltriethoxysilane (3-APTES) coating process (Bagaria et al., 2013; Xue et al., 2014) to coat Fe_3O_4 nanoparticles with amine functional groups. Hydrolysis of APTES at pH around 4 was performed for 1 hour, then pH was adjusted to around 8. 20 mL of Fe_3O_4 nanoparticle dispersion with nanoparticle concentration around 42 g/L (equivalent to 30 g/L Fe) was added slowly to 180 mL of APTES solution. The mixture was kept at 65°C for 24 hours, and then cooled to room temperature while stirring. Magnets were used to separate and collect the APTES-coated nanoparticles (A-MNPs) during the washing steps, and DI water was used to wash and re-suspend A-MNPs back to 20 mL volume (Wang et al., 2014). The process is illustrated in Figure 6.2.

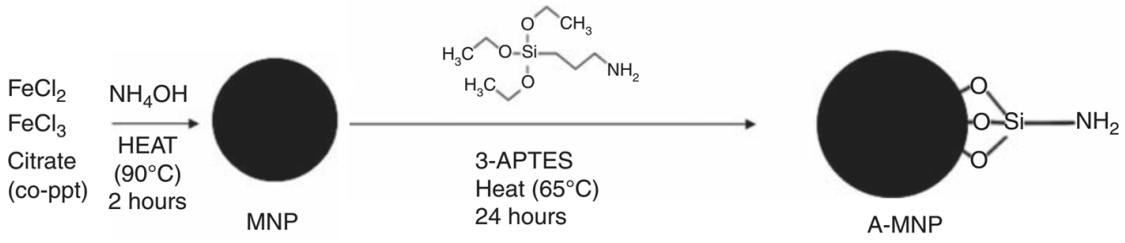

Figure 6.2. Procedures of generating Fe_3O_4 nanoparticles with different APTES coating

5.6 g, 7.5 g, and 9.8 g of APTES were hydrolyzed in 180 mL solution. After reaction with 20 mL of MNP dispersion, the corresponding A-MNPs were labeled as 5.6A-MNPs, 7.5A-MNPs and 9.8A-MNPs. The Fe concentration in the A-MNPs was around 30 g/L. DI water was used to dilute different A-MNP suspensions to 1.0 g/L Fe concentration. Serial dilution was performed to obtain different Fe concentrations: 0.07 g/L Fe, 0.05 g/L Fe, 0.025 g/L Fe, 0.01 g/L Fe, 0.007 g/L Fe, 0.005 g/L Fe, 0.0025 g/L Fe, and 0.001 g/L Fe. The corresponding NMR and dynamic light scattering (DLS) size measurements were used

to compute the relaxivity of A-MNPs with different coating amounts following the procedure of Zhu et al. (2015).

To study the possible effect that surface coating may have on the MNPs' surface relaxation rate, A-MNPs with the least and most surface coating were compared: 5.6A-MNPs and 9.8A-MNPs. These two samples were diluted with H_2O to obtain 0.1 g/L 0.02 g/L Fe concentration. Each 1 mL of 5.6A-MNPs dispersed in H_2O with those two Fe concentrations was diluted to a total of 10 mL to obtain 0.01 g/L Fe and 0.002 g/L Fe with different D_2O volume fractions of 0 vol%, 30 vol%, 50 vol%, and 70 vol%. The same procedure was repeated for the 9.8A-MNPs group. We also used mixtures of H_2O and D_2O with the same volume fractions as above to obtain the T_1 of the bulk fluid in each dispersion. NMR and DLS measurements were used to calculate normalized T_1 values of MNPs and to study how APTES coating reduces the surface relaxivities of MNPs.

A-MNPs samples were oven-dried at 80^{o}C for 24 hours to obtain nanoparticle powder. A Mettler Thermogravimetric Analyzer (model number TGA/DSC 1) was used to measure and calculate the weight of attached APTES on the nanoparticles in each sample. To prevent oxidation of Fe_3O_4, we used a N_2 stream at 50 mL/min and heated the dried nanoparticle samples from 30^{o}C to 500^{o}C with a temperature increase of 20^{o}C per minute. Before and after the TGA measurement, a Kratos X-ray Photoelectron Spectrometer (XPS) experiment was performed to make sure that there were no amine groups remaining in the burned samples. The mass percentage of APTES coated on each A-MNP sample was calculated by the weight loss of each dried A-MNP sample after heating to 500^{o}C under N_2 flow.

A Malvern Nano ZetaSizer was used to measure the size distribution of A-MNPs with different surface coating amounts, Fe concentrations, and D_2O volume fractions. Size calibrations were performed with calibration standard dispersions before each

measurement. 0.45 mL of A-MNP dispersion was placed in a disposable cell to measure size distribution. The size distribution and average size value were recorded. Measurements of each sample were performed three times and the mean value and standard deviation were recorded.

NMR measurements were performed at ambient temperature (20°C) using a 2 MHz GeoSpec2 benchtop NMR core analysis instrument from Oxford Instruments with an operating frequency of 2.15 MHz. The external magnetic field B_0 was 0.05047 T. We used an inversion recovery measurement to determine the distribution of longitudinal relaxation times (T_1).

Error bars for the longitudinal relaxation rate were computed from the standard deviation of the longitudinal relaxation time obtained from the Matlab inversion. The signal and noise were extracted from the raw NMR data in the time domain. Random noise with the same properties (magnitude, mean value and standard deviation) of noise extracted from raw NMR data was added to the time domain signal. With the added noise, there was a slightly different magnetization buildup curve compared to the curve obtained directly from the raw data. A linear inversion regression was then applied to the buildup curve with added noise to compute the T_1 value. After repeating this process 100 different times, 100 buildup curves were generated and used to calculate associated T_1 values. Based on these 100 computed T_1 values, the standard deviation of T_1 was recorded and used to compute the errors in longitudinal relaxation rate.

6.3 RESULTS

6.3.1 Relaxivities of A-MNPs with different APTES coating amount

According to the TGA results, after subtraction of the baseline, the weight percentages of APTES coating for A-MNPs were 1.60 wt% for 5.6A-MNPs, 1.99 wt% for 7.5A-MNPs, and 2.80 wt% for 9.8A-MNPs. We expected to have more APTES coated on nanoparticles with higher initial added amount of APTES in the MNP suspensions. T_1 values of A-MNPs with Fe concentration ranging from 0.001 g/L to 0.07 g/L were measured and recorded. The T_1 of DI water was used to compute $1/T_{1,NP}$ for each sample of A-MNPs using Equation (6.1). According to Equation (6.2), with the calculated nanoparticle relaxation rate $1/T_{1,NP}$ and values of $3\chi/r_{NP}$ the relaxivities of A-MNPs can be determined using the slope of a regression lines. As shown in Figure 6.3, error bars indicate the errors in longitudinal relaxation rate $1/T_1$ when linear regression of raw data was performed. Relaxivities of A-MNPs are 105,000 ± 2,110 μm/s, 94,100 ± 1,660 μm/s, and 78,300 ± 846 μm/s for 5.6-A-MNPs, 7.8A-MNPs and 9.8 A-MNPs respectively. Raw NMR data for A-MNPs dispersions are displayed in the Appendix B. Error bars associated with each $1/T_{1,NP}$ point were obtained based on the standard deviation of the relaxation times T_1 and $T_{1,Fluid}$ obtained after linear regression as described in section 6.2 and Appendix A. Weighted least squares linear regression was used to compute the relaxivity and standard deviation for each A-MNP group.

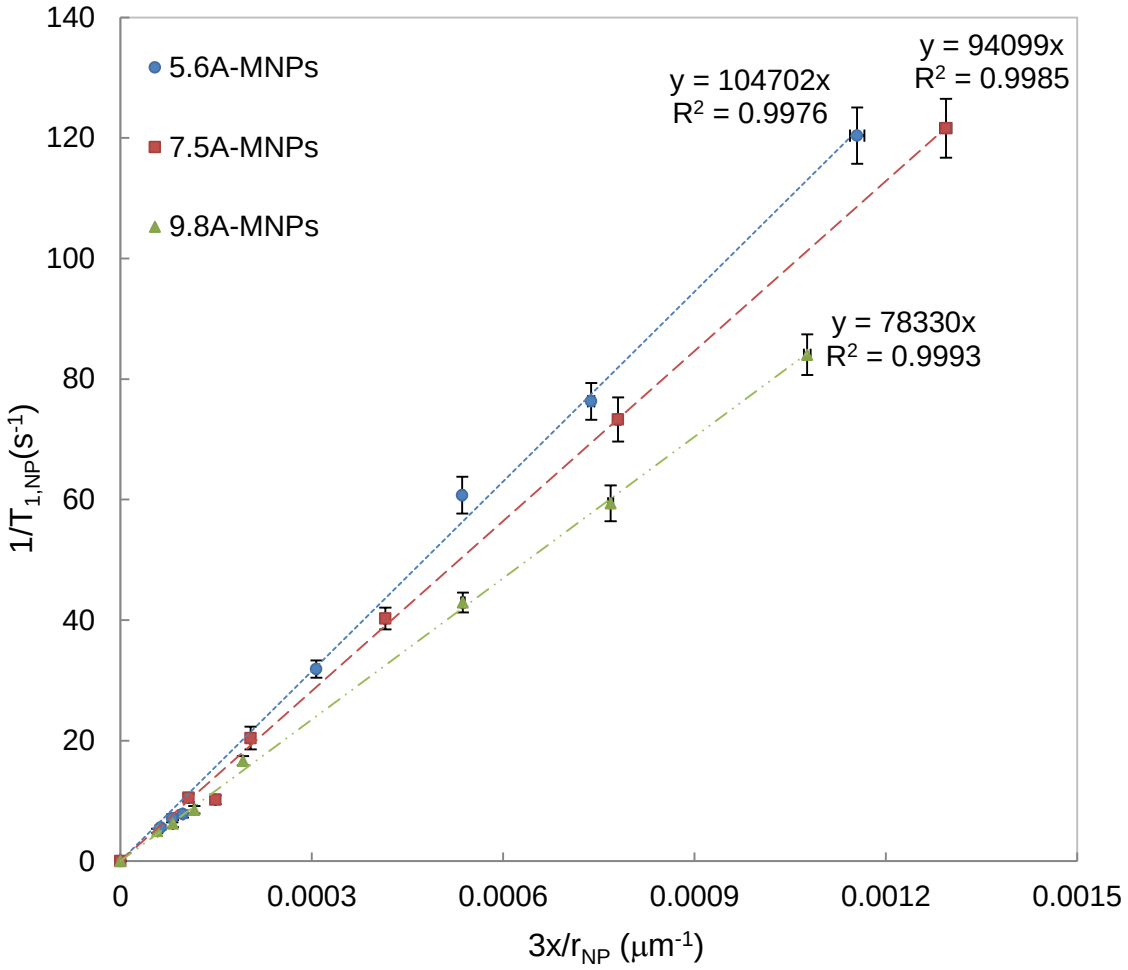

Figure 6.3 Computed $1/T_{1,NP}$ of APTES-coated Fe_3O_4 nanoparticles from Equation (6.1) with different nanoparticle fluid volume ratios χ and sizes r_{NP} in 5.6A-MNPs, 7.5A-MNPs, and 9.8A-MNPs dispersions fit using Equation (6.2). Relaxivity (slope of linear regression using weighted least squares) of each group decreases with more extent of APTES coating.

6.3.2 Variations in relaxation rate of A-MNPs with added D_2O

We measured the T_1 of bulk DI water mixed with different volumes of D_2O. T_1 increased from 2,590 ms to 5,340 ms when the percentage of D_2O increased from 0 to 70%, as displayed in Table 6.1.

Table 6.1 T_1 of water with different D_2O volume fractions.

D_2O volume fraction in water (vol%)	T_1(ms)
0	2,590
30	3,450
50	3,660
70	5,340

Table 6.2 DLS measured A-MNP radius with different D_2O volume fractions.

Nanoparticles radius of A-MNPs	0 vol% D_2O	30 vol% D_2O	50 vol% D_2O	70 vol% D_2O
r_{NP} of 5.6A-MNPs with 0.01 g/L Fe (nm)	54.5	58.0	62.0	64.0
r_{NP} of 9.8A-MNPs with 0.01 g/L Fe (nm)	40.8	42.3	45.3	43.0
r_{NP} of 5.6A-MNPs with 0.002 g/L Fe (nm)	49.6	51.0	52.0	54.5
r_{NP} of 9.8A-MNPs with 0.002 g/L Fe (nm)	51.5	39.2	36.8	41.6
Normalized r_{NP} of 5.6A-MNPs with 0.01 g/L Fe (Dimensionless)	1	1.06	1.13	1.17
Normalized r_{NP} of 9.8A-MNPs with 0.01 g/L Fe (Dimensionless)	1	1.04	1.11	1.06
Normalized r_{NP} of 5.6A-MNPs with 0.002 g/L Fe (Dimensionless)	1	1.03	1.04	1.10
Normalized r_{NP} of 9.8A-MNPs with 0.002 g/L Fe (Dimensionless)	1	0.763	0.715	0.810

With the same volume percentage of D_2O, the diluted 5.6A-MNPs and 9.8A-MNPs with Fe concentrations of 0.01 g/L and 0.002 g/L were tested with NMR to obtain A-MNP nanoparticle surface relaxation rates $1/T_{1,NP}$ according to Equation (6.1). The DLS results of A-MNP samples also indicated a slight size change of the same A-MNPs with the same Fe concentration with different D_2O volume fractions, as displayed in Table 6.2. Nanoparticle size was normalized to the value obtained for the A-MNP dispersion in DI water.

Based on Equation (6.2), with same nanoparticle concentration and constant nanoparticle relaxivity, the nanoparticles' surface relaxation rates are inversely proportional their size. To isolate the change of surface relaxation rate only brought about by the addition of D_2O, we normalized A-MNP surface relaxation rate by dividing $1/T_{1,NP}$

obtained from Equation 1 by the corresponding normalized A-MNP size calculated in Table 6.2. Normalized surface relaxation rates of two A-MNPs groups with different Fe concentrations and D_2O volume fractions are displayed in Figure 6.4. Error bars were calculated from the standard deviations of the longitudinal relaxation times T_1 and $T_{1,Fluid}$ via linear regression as described in section 6.2 and equations in Appendix A. Figure 6.4a) shows that, at relatively higher concentration of 0.01 g/L Fe, the normalized relaxation rate of A-MNPs remained similar with variation of D_2O volume fraction: 11.5 s^{-1} - 11.7 s^{-1} for 5.6A-MNPs and 9.66 s^{-1} - 9.73 s^{-1} for 9.8A-MNPs. As indicated in Figure 6.4b, at lower Fe concentration (0.002 g/L), when volume percentage of D_2O in dispersions increased from 0% to 30% to 50%, and to 70%, relaxation rate of 5.6A-MNPs dropped from 2.48 s^{-1} to 2.24 s^{-1}, to 2.29 s^{-1} and to 2.17 s^{-1}, and from 2.20 s^{-1} decreased to 1.59 s^{-1}, to 1.45 s^{-1}, and to 1.49 s^{-1} for 9.8A-MNPs.

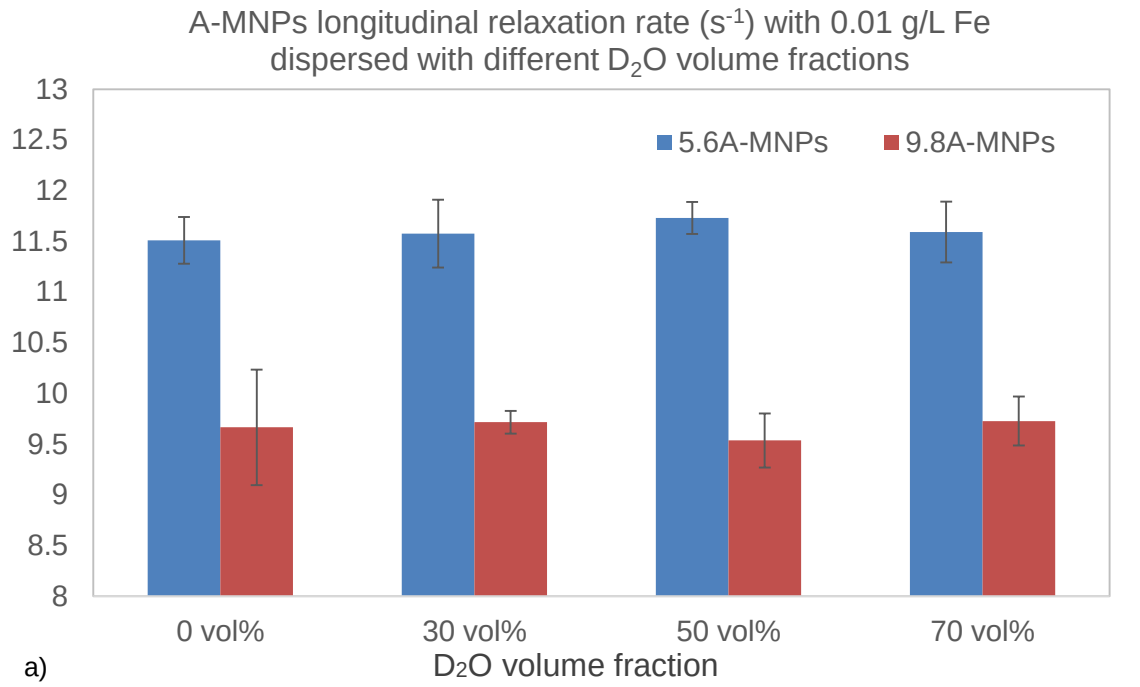

a)

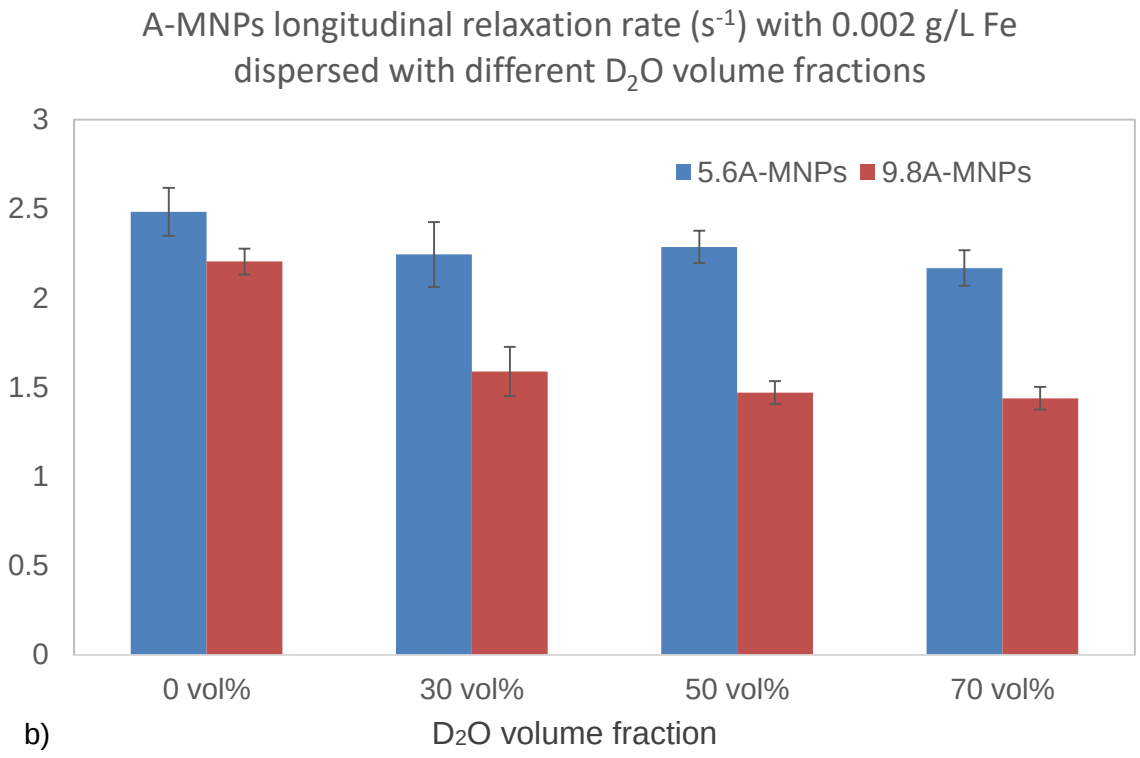

b)

Figure 6.4 Relaxation rate $1/T_1$ of 5.6A-MNPs and 9.8A-MNPs mixed with different volume fractions of D_2O with a) 0.01 g/L Fe and b) 0.002 g/L Fe.

6.4 DISCUSSIONS

6.4.1 Relaxivities of A-MNPs with different APTES coating amount

As shown in Figure 6.5, from left to right, we expect MNPs to pick up more APTES when there is more APTES present in the mixture. More Fe on the surface of nanoparticles will be occupied by APTES branches, and thus less surface area will remain accessible to protons in water molecules. As indicated in Equation (6.3), with fewer available paramagnetic sites on the surface, the relaxivity will decrease accordingly. Among the three A-MNP samples, 5.6A-MNPs have the least APTES coating with 1.60 wt%, while 9.8A-MNPs have the most APTES with 2.80 wt%. With the additional 1.20 wt% of surface coating on the 9.8A-MNPs, the surface relaxivity of the A-MNPs decreased by 25.4% from 105,000 μm/s to 78,300 μm/s. Even with the decreased relaxivity associated with more coated APTES, the value of 78,300 μm/s is significantly higher than other studied nanoparticles such as ZrO_2 nanoparticles, which had relaxivity of 1.10 μm/s ~ 1.43 μm/s (Zhu et al., 2015). The relaxivity of other Fe(III) oxides such as Fe_2TiO_5 with size around 6881 nm was reported to be around 120 μm/s (Bryar et al., 2000), which is almost 1000 times smaller than our computed relaxivity of A-MNPs with size around 100 nm. Since Fe_2TiO_5 exhibits ferromagnetic-paramagnetic behavior (Enhessari et al., 2014), giving it smaller magnetic susceptibility than ferromagnetic Fe_3O_4, at the same nanoparticle size, concentration and temperature, we expect Fe_3O_4 to have higher relaxivity than Fe_2TiO_5. In addition, as size increases from 100 nm for Fe_3O_4 to 6881 nm for Fe_2TiO_5, the specific surface area decreases dramatically from 11.6 m^2/g to 0.1 m^2/g. Lower specific area may result in fewer surface relaxation sites accessible to water molecules and smaller surface relaxivity.

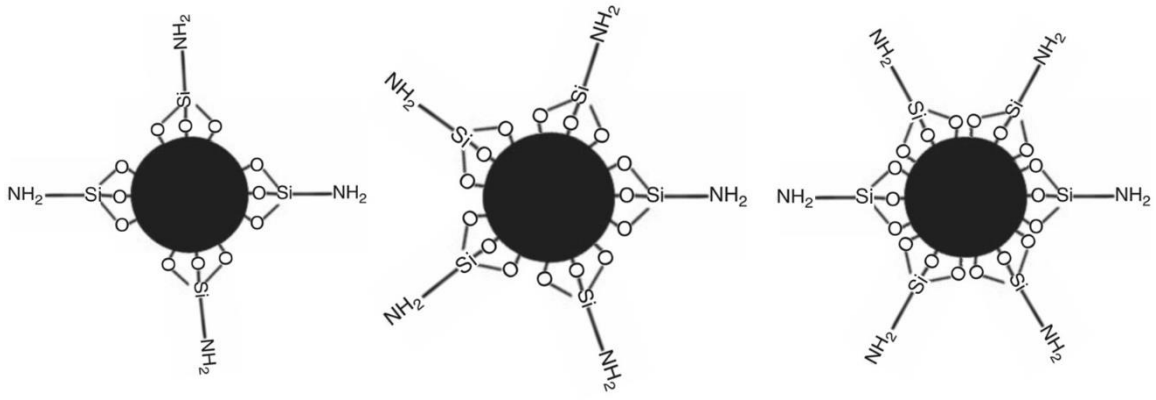

Figure 6.5 More APTES coated on MNPs with increased initial amount of 3-APTES in the mixture (from left to right) during reactions with MNPs.

Previous studies indicated that Fe_3O_4 has an inverse spinel structure where Fe_3O_4 unit cells have a face-centered cubic pattern (Hill et al., 1979), and the lattice parameter (unit cell edge length) is a=0.8396 nm, with each unit cell containing 8 Fe_3O_4 molecules (Cornell and Schwertmann, 2003). With the DLS nanoparticle sizes, along with the assumption that only Fe in the first layer of the Fe_3O_4 unit cell surface can be either accessible to water molecules as relaxation sites or bonded with APTES, we calculated the number of Fe atoms on the nanoparticle surface that can relax protons. According to Figure 6.2 and Figure 6.5, each APTES branch will covalently bond to 3 Fe atoms on the nanoparticle's surface. Given the TGA weight and the molecular weight of burned APTES, with the nanoparticle's size it is easy to obtain the number of APTES bonded to each nanoparticle. Hence the number of Fe atoms masked by APTES can be obtained by multiplying the number of APTES molecules on one nanoparticle by 3. We further calculated the fraction of Fe located on the surface of nanoparticles that were occupied by attached APTES in each A-MNPs group: 24% for 5.6A-MNPs, 30% for 7.5A-MNPs and 43% for 9.8A-MNPs. Since more than half of the surface Fe atoms remained unbonded,

surface relaxation may still be dominated by e-H relaxation: protons in the water molecules are mainly relaxed by magnetic sites (Fe) on the nanoparticle's surface.

If we assume that there is only one type of magnetic site on the MNPs, based on Equation (6.4), a linear relationship between magnetic surface site fraction n_i and the overall relaxation rate of the nanoparticles can be obtained. As shown in Figure 6.6, with more APTES on the nanoparticle surfaces, the magnetic sites fraction decreased, and the overall relaxation rate of nanoparticles decreased. According to the errors ($\pm 1\sigma$) in slope and intercept, I computed the possible relaxivity range of A-MNPs with different fraction of Fe attached with APTES, as indicated by red and blue lines. The relaxivity of bare nanoparticles falls in the range between 121,000 μm/s to 151,000 μm/s. If all magnetic sites are covered by APTES, the computed relaxivity of A-MNPs is 1,410 ± 4,670 μm/s, which is about 1.3% of the 5.6A-MNPs relaxivity (105,000 μm/s). Note that in this study, only 3 groups of A-MNPs were used to generate a linear relationship between relaxivity and fraction of occupied Fe sites on the nanoparticle surface. As a result, there are relatively large errors in the slope and intercept. More experiments with higher percentage of APTES coating are needed to better constrain the relaxivity value of MNPs fully covered by APTES.

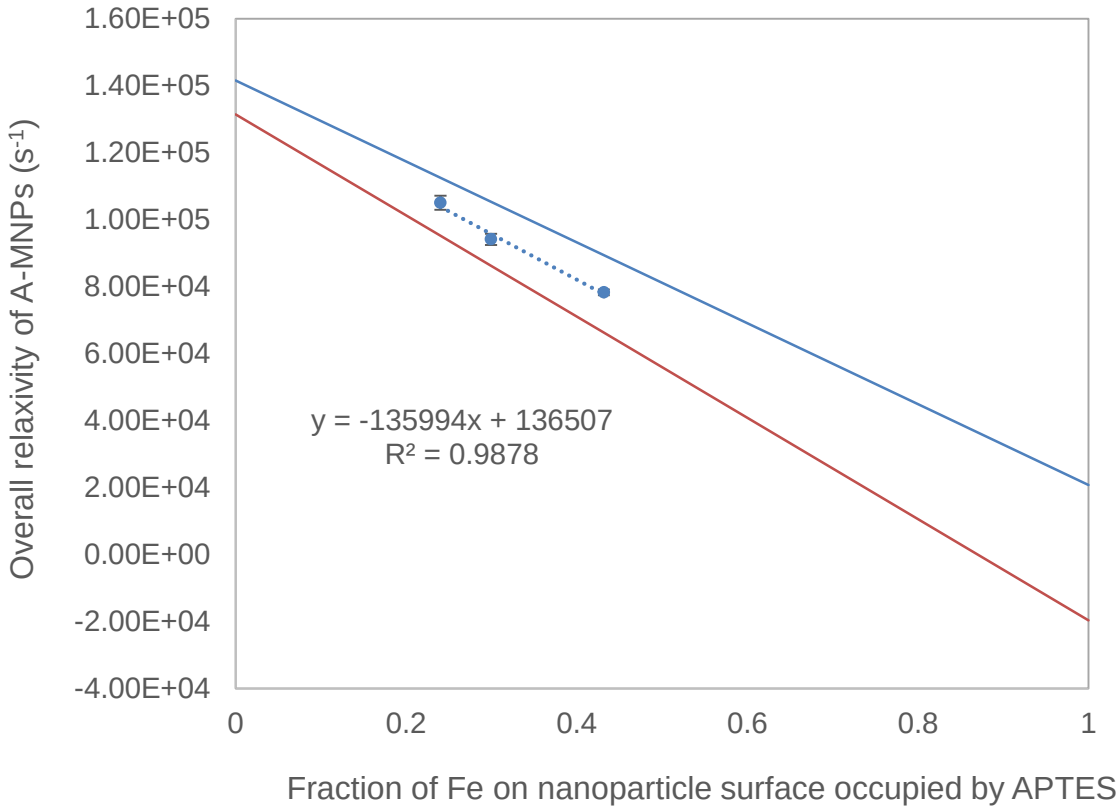

Figure 6.6 Overall relaxivity of A-MNPs decreased with less Fe accessible to protons on nanoparticle surfaces due to attached APTES coating. Red and blue lines indicate the possible range of A-MNPs relaxivity with fraction of Fe attached by APTES due to errors in slope and intercept (±1σ) obtained by linear regression of measured 3 samples.

6.4.2 Change in relaxation rate of A-MNPs with D_2O

The T_1 of H_2O-D_2O mixtures increased with higher volume fraction of D_2O. Since the intermolecular H-H relaxation contributes 30% of the overall H-H relaxation in bulk water, with more D_2O, the intermolecular H-H relaxation is hindered by the presence of D_2O and decreases the overall relaxation rate, i.e., elongates the relaxation time.

During the process of obtaining normalized surface relaxivity of A-MNPs at the same concentration with different D_2O volume fractions, the relaxation brought by bulk fluid was deducted and effects from nanoparticle size were filtered by dividing $1/T_{1,NP}$ by

the normalized nanoparticle size. At relatively higher Fe concentration (0.01 g/L), normalized surface relaxation rates of 5.6A-MNPs and 9.8A-MNPs did not vary much with the change of D_2O volume fraction. This situation indicates that nanoparticle surface relaxation was dominated by e-^{1}H relaxation. With a sufficient amount of Fe_3O_4, which relaxes protons by e-^{1}H relaxation, the surface relaxation is not significantly affected by the presence of D_2O. At lower Fe concentration (0.002 g/L), when D_2O concentration increased generally from 0 vol% to 70 vol%, the surface relaxation rate of 5.6A-MNPs decreased correspondingly from 2.48 s^{-1} to 2.17 s^{-1}, which is a 12.5% drop; the 9.8A-MNPs' surface relaxation rate dropped from 2.20 s^{-1} to 1.44 s^{-1}, a decrease of 34.5%. With more APTES coating, the effect of D_2O in reducing the surface relaxation rate became more obvious. With the attachment of APTES, more magnetic sites of Fe are occupied by APTES and not available to relax ^{1}H from water molecules; in addition, the ^{1}H in APTES functional groups such as $–NH_2$ may introduce proton-proton relaxation (Ganesan et al., 1990) which also contributes to the overall surface relaxation of A-MNPs. With more APTES on the Fe_3O_4 surface, there is less e-H relaxation on the nanoparticles' surface; with lower Fe concentration, e-H relaxation becomes less dominant, so the contribution of H-H brought from APTES becomes more significant. With the large range of chemical shift values of $–NH_2$, –H in the amine group of APTES can be exchanged with –D in D_2O. Since D cannot be seen by ^{1}H-NMR, with higher D_2O volume fraction, more of the amine groups in APTES contain deuterium, so the NMR signal and relaxation rate would be reduced due to the interrupted H-H relaxation. A-MNPs with more APTES attached have surface relaxation rates more sensitive to the presence and amount of D_2O.

6.5 CONCLUSIONS

In this work, we computed and compared 3 groups of APTES-coated Fe_3O_4 nanoparticles (A-MNPs) with different surface coating amount: 1.60 wt% for 5.6A-MNPs, 1.99 wt% for 7.5A-MNPs, and 2.80 wt% for 9.8A-MNPs. The corresponding surface relaxivities decreased from 105,000 μm/s to 94,100 μm/s to 78,300 μm/s. Among the 3 groups of A-MNPs, only 24% - 43% of the surface magnetic sites were occupied by APTES branches, leaving most of the surface Fe atoms accessible to water molecules and providing e-H relaxation which will dominate the overall surface relaxation rate of the nanoparticles. If all the magnetic sites on the nanoparticle surface are occupied by APTES, the resulting relaxivity is much smaller (102 μm/s). To accurately determine the correct value of A-MNPs fully covered with APTES, more measurement of A-MNPs with higher APTES coating amount are required.

The mechanisms by which surface coating reduces nanoparticles' relaxivity was studied by diluting A-MNPs with the least and most surface coating using different volume fractions of D_2O. When D_2O volume fraction increased from 0 vol% to 70 vol%, with Fe concentration of 0.002 g/L, 9.8A-MNPs with 2.80 wt% surface coating showed more reduction in surface relaxation rate (dropped by 34.5%) compared to 5.6A-MNPs with 1.60 wt% surface coating (dropped by 12.5%). This suggests that at very low nanoparticle concentration, e-H relaxation is less dominant due to the limited amount of Fe_3O_4; intermolecular H-H relaxation between ^1H in APTES braches and ^1H in water molecules contributed more to nanoparticle surface relaxation. Our results indicate that A-MNPs with various coating amounts relax protons at nanoparticle surfaces mainly by e-H relaxation and controls the overall relaxation of suspensions at higher Fe_3O_4 nanoparticles concentration. In this study, the maximum amount of APTES attached to nanoparticles was 2.80 wt%, covering only 43% of the Fe_3O_4 nanoparticle surface. In this case the effect of

APTES in reducing relaxivities of the nanoparticle was limited. However, when APTES coating amount is increased, we would expect more nanoparticle surface occupied by APTES, leaving less Fe_3O_4 exposed to water molecules. Therefore, when organic surface coating is used to add target functional groups onto nanoparticles in oilfield, the presence of surface coating may affect the NMR signal of porous media, and care should be taken when using nanoparticles with extensive surface coating. We caution that this experiment was performed at room temperature and pressure, and the relaxivity of these same A-MNPS may change when applied in field conditions.

Chapter 7

Synthesis, Conclusions, and Future Work

7.1 SYNTHESIS

Recent work focused on NMR measurements of porous media saturated with nanofluids (e.g., Anand and Hirasaki, 2008; Yu, 2012; Cheng et al., 2014a,b) did not study how and to what extent the pore surface relaxivity will be altered by adsorbed paramagnetic nanoparticles. In the meantime, when applying nanoparticles in the oilfield where natural porous media have more complicated fluid and surface chemistry, there are several factors such as interactions between natural rock surfaces, pore fluid and nanofluids, attachment of paramagnetic species, and coating of surface polymers that may affect nanoparticles' relaxivity (Keating and Knight, 2008; Issa et al., 2011). How the attachment of paramagnetic species and surface coatings onto nanoparticles change nanoparticles' surface relaxivity and the NMR signal of nanofluids in porous media remains to be studied.

7.1.1 Attachment of nanoparticles onto pore surface and modified pore surface relaxivity

In this work, I chose zirconia (ZrO_2) nanoparticles without surface coating. There were two dispersions of zirconia nanoparticles with similar size but different surface charge: ZR-AL, with positively charged nanoparticles, and ZR-BL, with negatively charged nanoparticles. I used ZR-6AL and ZR-6BL nanofluids, with 6 wt% nanoparticles, and ZR-7.5AL and ZR-7.5BL, with 7.5 wt% nanoparticles.

Nanoparticle retention limit in porous media

With the assumption that nanoparticles are spheres, attached nanoparticles will form a densely packed monolayer, and each adsorbed nanoparticle occupying its projected area (πr_{NP}^2) on pore walls. The highest surface fraction that can be occupied by a monolayer

of equal spheres is 0.9069. In the 2 mm glass bead pack with pore radius as 613 μm, the maximum possible adsorption fraction of ZR-6AL is about 30%. In Boise sandstone cores, with much smaller pore radius of 10.6 μm, there is much more pore surface provided for adsorption of nanoparticles. In ZR-6AL saturated Boise sandstone cores, up to 65.8% of nanoparticles can be adsorbed to the pore walls; for ZR-7.5AL, up to 54.2% of the nanoparticles can attach to the pore surfaces. Similarly, up to 48.9% of negatively charged zirconia nanoparticles in the ZR-6BL dispersion can attach onto the pore surface; and 38.0% of nanoparticles in ZR-7.5BL can attach onto the pore surface. With these maximum extents of attached nanoparticles, the computed surface relaxivities are close to the surface relaxivity values of the nanoparticles themselves.

Retained nanoparticles and the modified pore surface relaxivity

Density measurement of effluents from Boise sandstone cores indicated that negatively charged zirconia nanoparticles were trapped in Boise sandstone cores but not in the glass bead packs. Such different results may due to differences in surface charge and other properties between the glass bead surface and Boise sandstone surface. In addition, smaller pores in Boise sandstone can play a role in retaining nanoparticles mechanically via narrow pore throats (Arawole, 2015). To maintain significant negative surface charge, a strong alkaline was used to pretreat Boise sandstone cores, and the NMR results indicated that such treatment increased Boise sandstone surface relaxivity from 5.05 μm/s to more than 6 μm/s. In Boise sandstone cores saturated with ZR-6BL and ZR-7.5BL, after flushing 2 pore volumes with DI water, 3.4% and 3.0% of nanoparticles were retained in the cores, only around 3% of pore surface is occupied by attached nanoparticles assuming monolayer packing, the resulting pore surface relaxivities were 6.4 μm/s and 6.6 μm/s. After flushing 2 pore volumes of TMAH at the same pH value as ZR-6BL and ZR-7.5BL, there were

2.8% and 2.3% of negatively charged nanoparticles left in the cores, covering about 2% of pore surface, the corresponding surface relaxivity was about 6.6 μm/s and 6.7 μm/s. The results indicated that in this study Boise sandstone pore surface relaxivity alteration was mainly due to strong alkali condition: with pH higher than 10, dissolution of silica surface (Revil et al., 1999a, b) may expose buried paramagnetic species and speed up the relaxation. Since both the nanoparticles and pore surface were negatively charged, electrical repulsion may prevent the attachment of nanoparticles onto the silica surface, resulting in very little percentage (around 2% ~ 3%) of negatively charged nanoparticles being retained in the sandstone. The small retention value is in good agreement with previous work in which less than 10% of 20 nm silica nanoparticles were retained in Boise sandstone (Caldelas, 2010). These values do not approach the maximum adsorption limits calculated above (48.9% for ZR-6BL and 38.0% for ZR-7.5BL). Such retention may due to van del Waals attractions and mechanical straining.

As indicated in my experiment results, 11.6% of positively charged zirconia nanoparticles in ZR-6AL were retained in the 2 mm glass bead pack with pore radius as 613 μm. The bead surface relaxivity was correspondingly altered from 10.42 μm/s to 7.27 μm/s. With a calculated maximum fraction of attached nanoparticles of 30%, the resulting glass bead surface relaxivity would be 2.265 μm/s. In contrast, in Boise sandstone, the smaller pore size (10.6 μm) provided more surface area for attached nanoparticles. I observed that 40% of ZR-6AL and 37% of ZR-7.5AL were left in Boise sandstone cores after flushing with 2 pore volumes of DI water, pore surface covered by attached nanoparticles assuming monolayer packing are 23.38% and 26.42%, respectively. If homogeneous adsorption is assumed, the changed pore surface relaxivities are computed to be 5.8 μm/s and 5.9 μm/s respectively. When flushing with 2 pore volumes of HNO_3 under same pH value of nanofluids, there were 35% of ZR-6AL and 31% of ZR-7.5AL

trapped in Boise sandstone cores, occupying 20.45% and 21.99% of pore surface. The altered pore surface relaxivities were 6.4 μm/s and 6.5 μm/s. The adsorption may be the result of a force balance between electrostatic attraction and van del Waals attraction. I did not find the evidence that nanoparticles attached onto pore surface to the full coverage capacity, so it is possible that my experimental conditions such as zeta potential difference between surface of nanoparticles and pore walls, electrostatic repulsion between each nanoparticle, pH values, viscosity, temperature cannot drive the full 100% (for ZR-6AL) or 100% (for ZR-7.5AL) of nanoparticles' attachment. The results suggested that there is a way to control pore surface relaxivity by adsorbed paramagnetic nanoparticles, and serve as the foundation to generate a model to link relaxation time distribution and pore size by altered pore surface relaxivity.

My work helps to understand the behavior of nanoparticles in porous media through NMR measurements and will be used in future studies on the pore-scale characteristics in rocks. This research part will help advance nanoparticle-based analyses of fluid-solid or fluid-fluid interfaces through adsorption of nanoparticles. Applications of this work include imaging oil-water contacts, and determining interfacial surface areas for many petrophysical and reservoir engineering needs.

7.1.2 Attachment of iron species onto nanoparticle surface

Another interesting finding in the Boise sandstone cores experiments is that the relaxivity of effluents increased after contact with Boise sandstone cores, and nanofluid effluents showed a higher increase relative to pure fluid effluents. I measured the iron concentrations in the original fluids and effluents, and showed that the increased iron concentration in effluents helps to explain speeded up relaxation (Revil et al., 1999a,b) in the pure fluid effluents. In the case of nanofluids, the comparison of iron concentration in

supernatants of original nanofluids and effluents indicated that the gain in iron concentration was not enough to support the observed increase in relaxation rate of the nanofluid effluents. I determined the nanoparticle relaxivity in each effluent: positively charged nanoparticles increased relaxivity from 1.43 μm/s to 4 μm/s ~ 10 μm/s; negatively charged nanoparticle relaxivity increased from 1.10 μm/s to 12 μm/s ~ 19 μm/s. I proposed that paramagnetic species from Boise sandstone cores (Pettijohn, 1963) might also attach to nanoparticles and increase nanoparticle relaxivity, which also contributed to speeding up the overall relaxation in effluents.

To testify the hypothesis that iron can attach onto nanoparticles and increase surface relaxivity. I further conducted the experiments by mixing Fe(III) solution with same volume of ZR-6AL and ZR-6BL nanofluids. To see if surface coating can help shield nanoparticles from attachment of iron species, I employed polyethylene glycol (PEG)-coated silica nanofluids labeled as Si-4B with 4 wt% of silica nanoparticles to mix with Fe(III) solutions, too. The experiments showed that at as high as 50 mg/L Fe(III) in the mixture, more than 90% of iron in the aqueous solution can be picked up by nanoparticles regardless of surface charge sign and the presence of surface coating. Relaxivities of positively charge nanoparticles increased from 1.43 μm/s to 50.17 μm/s after 2.80×10^{-6} mol/m^2 attached Fe(III), and negatively charged nanoparticles with original relaxivity of 1.10 μm/s showed a modified relaxivity of 35.13 μm/s after adsorption of 2.07×10^{-6} mol/m^2 Fe(III). A previous study (Bryar et al, 2000) found that after equilibrating with 5 mg/L Fe, silica gel showed an increased relaxivity from 0.0012 μm/s to 0.020 μm/s with 1×10^{-9} mol/m^2 Fe adsorbed. Such attachment of Fe in their results is much more efficient than our findings for Fe(III) attached onto zirconia nanoparticles. It may be explained by the difference between types of nanoparticle surface that results in different rotational correlation times.

With the assumption of dense monolayer packing of attached Fe(III) onto nanoparticles surface, up to 3.14×10^{-6} mol/m^2 Fe(III) can be attached onto ZR-3AL, 2.36×10^{-6} mol/m^2 Fe(III) adsorbed on to ZR-3BL, and 1.45×10^{-6} mol/m^2 Fe(III) onto Si-2B nanoparticles. In this experiment, the attachment of Fe(III) did not reach the calculated limit which would be 100% of Fe(III), so it is possible that the pH value, viscosity, temperature, electrostatic repulsion between each cations and other properties were not able to support 100% adsorption.

The results provided a hint of the possible interactions between nanoparticles and paramagnetic species in natural porous media: attachment of nanoparticles may affect pore surface relaxivity, and adsorption of paramagnetic materials onto nanoparticles will dramatically increase nanoparticle relaxivity and further affect NMR signal of nanofluids saturated porous media. Attached iron species can speed up nanoparticles' relaxivity to about 36 ~ 40 fold, such increase is comparable with previous reported study which claimed increased by 6 to 50 fold with attached paramagnetic materials (Kenyon and Kolleeny, 1995). When using nanoparticles as NMR contrast agents, the sorption of paramagnetic species should be considered before interpretation of NMR results.

7.1.3 Attachment of organic surface coatings on nanoparticles

Given the results that adsorption of paramagnetic materials causes the relaxivity of nanoparticles with initially low relaxivity to increase dramatically, another question arises: since adsorbed iron species onto nanoparticles significantly increased the relaxivity of nanoparticles in porous media, what will happen if organic surface coating with low relaxivity is attached to iron oxide nanoparticles with initially high relaxivity? To what extent will the surface coating modify the iron oxide nanoparticle relaxivity?

To answer the above questions, I studied three groups of 3-aminopropyl triethoxysilane (APTES) coated Fe_3O_4 nanoparticles (A-MNPs) with different surface coating amounts: 5.6A-MNPs, 7.5A-MNPs and 9.8A-MNPs. Fe sites that relax protons via electron-proton relaxation can be occupied by APTES branches and cannot relax protons any more. The results showed that nanoparticle relaxivity decreased from 105,000 μm/s for 5.6A-AMNPs to 94,100 μm/s for 7.5A-MNPs to 78,300 μm/s for 9.8A-MNPs with as surface coating amount increased. Previous work has reported decreased relaxivity with increased PEG surface coating on $Mn_{0.5}Zn_{0.5}Gd_{0.02}Fe_{1.98}O_4$ nanoparticles (Issa et al., 2011). The fraction of Fe sites taken by APTES are 24%, 30%, and 43% respectively for 5.6A-MNPs, 7.5A-MNPs and 9.8A-MNPs. With the assumption that nanoparticle surface relaxivity has a linear relationship with the fraction of available Fe sites accessible to water molecules, we computed that with no APTES coating, the nanoparticles have surface relaxivity of 136,656 μm/s; with 100% of APTES coating, the resulting relaxivity is 101 μm/s. These determined values with 0% and 100% surface coating may be differ from the true values due to large uncertainties caused by the use of only 3 groups of A-MNPs. Studies of more groups of A-MNPs with higher surface coating are required to obtain more accurate estimation of relaxivity for bare and fully covered nanoparticles.

To identify the relaxation mechanisms of A-MNPs, I used D_2O in the mixture. The presence of D will change the fraction of H and hence the proton-proton relaxation brought by APTES, while electron-proton relaxation will not be affected. The results showed that, with relatively high nanoparticle concentration (0.01 g/L Fe), 5.6A-MNPs and 9.8A-MNPs relax protons mainly by electron-proton relaxation, since the presence of D_2O and change in D_2O volume fraction did not vary relaxation rate of nanoparticles. In contrast, at relatively low nanoparticle concentration (0.002 g/L Fe), 5.6A-MNPs and 9.8A-MNPs exhibited lowered relaxation rates with increased D_2O volume fraction. With the higher

surface coating in 9.8A-MNPs, the decrease was more significant, indicating that at low nanoparticle concentration, nanoparticles relax protons also via proton-proton relaxation. Hence, the presence of APTES coating decreased iron oxide nanoparticle relaxivity by occupying Fe relaxation sites, but due to the small surface coverage fraction of APTES, Fe_3O_4 can still relax protons mostly via electron-proton relaxation. Only in very dilute A-MNPs will proton-proton relaxation brought from APTES also play a role in relaxing protons.

In sum, my project studied the possible interactions between nanoparticles and pores in porous media saturated with nanofluids (as shown in Figure 7.1): adsorption of nanoparticles onto the pore surface will modify the pore surface relaxivity, while attachment of paramagnetic species and organic surface coating may affect the relaxivity of nanoparticles. Pore fluid chemistry is therefore necessary to characterize in any application of nanoparticles as NMR contrast agents in rocks.

In the course of my experiments, I did not observe full adsorption of nanoparticles on pore surfaces, of iron on nanoparticle surfaces, or of organic surface coating on nanoparticle surfaces. Therefore, all the observed behavior lies between two endmembers. It is possible that in my project, the fluid properties, local surface chemistry, and laboratory conditions are not sufficient to support full attachment of adsorbates onto surfaces. Given the variation in behavior between the fully adsorbed and completely desorbed conditions I computed, constraining and controlling the degree of adsorption of any material described in this dissertation is essential for any subsurface application of nanoparticles as NMR contrast agents.

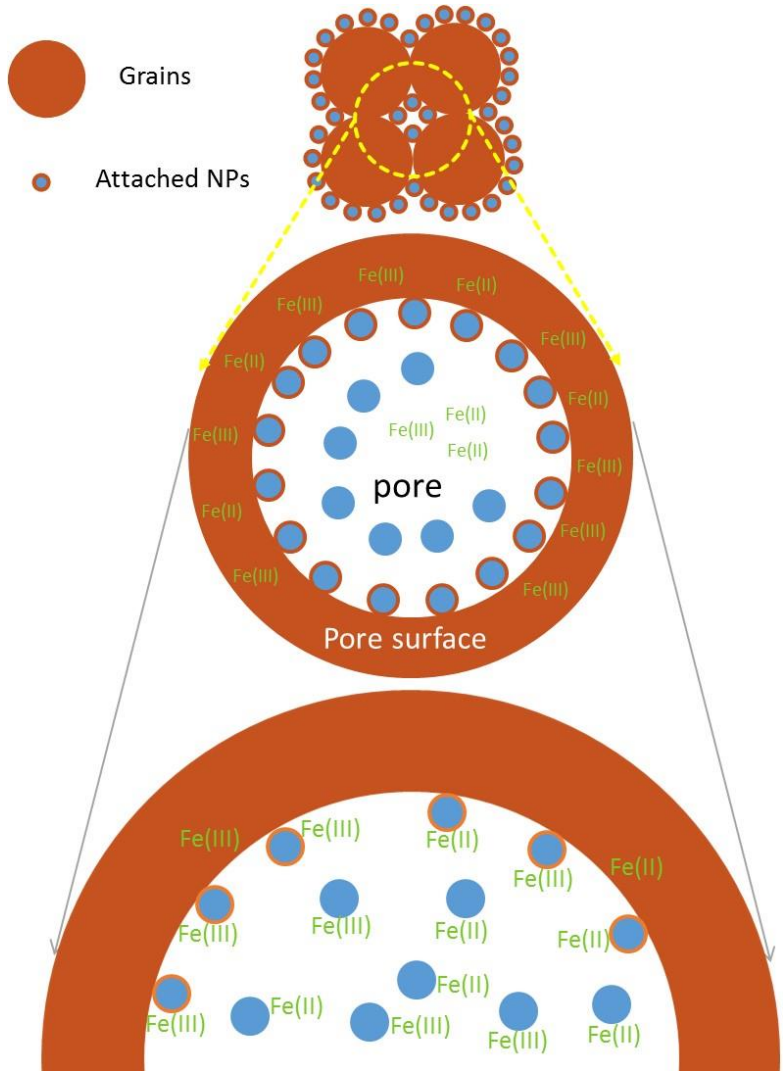

Figure 7.1 Different adsorption mechanisms affecting NMR response of nanoparticles in porous media. Top: idealized depiction of nanoparticles adsorbed on grain surfaces. Middle: in reality, some nanoparticles remain in dispersion while others are adsorbed. Paramagnetic species on the pore surface additional provide some surface relaxation. Bottom: in even more detail, paramagnetic species present in the pore fluid and/or desorbed from the grain surface due to the nanoparticle dispersion chemistry can attach to nanoparticles, further complicating the NMR response.

7.2 CONCLUSIONS

To understand the effect of nanoparticles on pore surface relaxivity, I performed experiments by adding different paramagnetic nanoparticles in pore fluid, and made three measurements: i) a nanoparticle-free fluid measurement (DI water) to get the pore wall effect; ii) the fluid-saturated measurement under conditions for which the change in aqueous concentration is the dominant effect (this demonstrates surface adsorption occurred); iii) displacing the nanoparticle dispersion with DI water and isolating the effect of the controlled relaxivity of the pore walls.

The bulk relaxation rate of the nanoparticle dispersions is proportional to nanoparticle-pure fluid volume ratio, and inversely proportional to nanoparticle size. In nanofluid-saturated porous media (glass bead packs, outcrop sandstone), electrostatic attraction between grain surfaces and nanoparticles was the main driving force for adsorption of nanoparticles onto grain surfaces. The two types of zirconia nanoparticles used in this study differed only in their zeta potential (one being positive, the other negative), and only the positively charge particles adsorbed appreciably onto the negatively charged silica surfaces of the porous medium. Porous media surface relaxivities were altered only by the presence of adsorbed paramagnetic nanoparticles. When 1.114 vol. % positively charged zirconia nanoparticles dispersion was used to saturate a glass bead pack, 11.6% of the nanoparticles were adsorbed to the bead surfaces and modified the glass bead surface relaxivity from 10.42 μm/s to 7.27 μm/s. DI water flushing was able to wash out 14% of adsorbed nanoparticles from siliceous surface, change of surface relaxivity due to core flushing was 15.4%. In contrast, negatively charged zirconia nanoparticles did not alter the relaxivity of the beads.

Zirconia nanoparticle dispersions in Boise sandstone cores altered sandstone surface relaxivity, in a complicated way depending on nanoparticles' surface charge and

pH condition of the dispersions. During contact with 6 wt% and 7.5 wt% positively charged zirconia nanoparticles at pH 3.1, Boise sandstone surface relaxivity changed from 5.05 μm/s to 5.8 μm/s ~ 6.5 μm/s due to 31% ~ 40% adsorbed nanoparticles onto pore surface. In Boise sandstone pores with pore walls pretreated with TMAH at pH 13.4, sandstone surface relaxivity increased to 6.3 μm/s due to strong alkaline condition. With 2.3% ~ 3.4% retained negatively charged nanoparticles, the sandstone surface relaxivity remained higher than 6 μm/s.

Experimental results indicated that pH of nanoparticle dispersions played a role in interactions with Boise sandstone surface. Acid could increase Boise sandstone surface relaxivity by reacting with impurities such as Fe_2O_3 and FeO on mineral surface (Pettijohn, 1963). HNO_3 at pH 3.1 increased Boise sandstone surface relaxivity from 5.05 μm/s to 5.7 μm/s. Alkali can alter Boise sandstone surface relaxivity by mineral surface dissolution and exposure of paramagnetic impurities to pore fluid. Such alteration can remain for long period as long as pore fluid condition remains alkaline. TMAH at pH 13.4 increased Boise sandstone surface relaxivity to 6.3 μm/s.

After contact with Boise sandstone, zirconia nanoparticles with positive and negative surface charges both showed increased relaxivity. Positively charged nanoparticles relaxivity increased from 1.43 μm/s to 4 μm/s ~ 9 μm/s. Nanoparticles with negative surface charge displayed increased relaxivity from 1.10 μm/s to 12 μm/s ~ 19 μm/s after contact with TMAH treated Boise sandstone. Such increase in relaxivity were possibly due to less stabilizer in dispersions after interactions with sandstone surface. Less stabilizer was ionically bonded with the nanoparticles, leaving more surface area of the nanoparticles exposed to bulk fluid and increased the chances for protons to get close to paramagnetic sites and be relaxed faster. Hence, the effective relaxivity of nanoparticles

increased. Attachment of iron ions on negatively charged nanoparticles further enhanced nanoparticle relaxivity.

After contact with Boise sandstone, the relaxivities of negatively charged zirconia nanoparticles increased dramatically, indicating attachment of paramagnetic species such as Fe onto nanoparticles from pore surface. In order to understand the role of Fe ions in altering nanoparticle surface relaxivity, I designed my experiments by mixing nanoparticles with and without surface coating into Fe(III) solutions with various Fe(III) concentrations: i) measure relaxation times of the mixtures and pure Fe (III) solutions at same concentration (to isolate relaxivity of nanoparticles); ii) measure relaxation time and Fe(III) concentration of supernatants after centrifuge of nanoparticles (to calculate the adsorption of Fe(III) onto nanoparticles); iii) compare surface relaxivity of nanoparticles before and after attachment of Fe(III) to get relationship between adsorbed Fe(III) and alteration in nanoparticles surface relaxivities.

The results indicate that paramagnetic ions such as Fe(III) can adsorb onto nanoparticles regardless of surface coating and surface charge of nanoparticles. My work suggests that the silica nanoparticles with PEG surface coating can remove Fe(III) from aqueous solution, since the relaxation rates of silica nanoparticles dispersed in Fe(III) solutions is not a simple sum of the nanoparticle and iron solution relaxation rates. Zirconia nanoparticles with positive and negative surface charge can remove more than 90% of Fe(III) from solutions. Slightly alkaline conditions (pH between 7 and 8) do not play an important role in precipitating Fe(III) ions.

When pH value was above 6, with no surface coating, zirconia nanoparticles in dispersion were negatively charged (Tang et al., 2000), and the driving force for adsorption of Fe(III) onto ZR-3BL was likely due to electrostatic attraction between negatively charged nanoparticle and iron cations (Stuart et al., 1991). Under acidic conditions where

pH value was lower than 6, zirconia nanoparticles with positive surface charge also acted as a Fe(III) sink, which suggests that electrostatic attraction was not the driving force of adsorption in these cases. Hydrolysis of Fe^{3+} in solution builds $Fe(OH)_3$ and polymers of Fe(III) could have been precipitated at pH values ranging from 1.8 to 3.4 (Dousma and De Bruyn, 1976). These polymers tend to precipitate on solid surfaces under acidic conditions (Dai and Hu, 2014). Although I was not able to perform any measurements on supernatants from the silica nanoparticle solutions, the behavior observed with the negatively charged zirconia nanoparticles can be used to inform some interpretations of our measurements. At pH from 5.5 to 9, the PEG coated silica nanoparticles were negatively charged. Therefore, the increase in relaxation rate can probably be attributed to electrostatically-driven adsorption of Fe ions onto the nanoparticles.

Adsorbed Fe(III) significantly increased the zirconia nanoparticles' surface relaxivity. Surface relaxivity of positively charged zirconia nanoparticles increased from 1.427 μm/s to 50.17 μm/s with 2.80×10^{-6} mol/m^2 adsorbed Fe(III) at pH around 2.4. Zirconia nanoparticles with negative surface charge at pH around 3.0 had surface relaxivity increased from 1.095 μm/s to 35.13 μm/s when 2.07×10^{-6} mol/m^2 Fe(III) was adsorbed. The results show that under various pH conditions ranging from 2.4 to 7.5, adsorption of Fe(III) species onto nanoparticle surfaces occurred and increased the relaxivity of the nanoparticles. My research indicates that, in natural porous media with pore fluid containing paramagnetic ions, sorption of these ions to the surface of nanoparticles can significantly alter the NMR relaxation behavior of the nanoparticles. The phenomenon affects nanoparticles regardless of surface charge or whether the nanoparticles are coated with polymers or not. Care must therefore be taken when using nanoparticles as NMR contrast agents in rock samples both in the laboratory and the subsurface.

With the observed confirmation that attached Fe onto nanoparticles increases nanoparticle relaxivity. It leads to another question: whether and how organic surface coating with low relaxivity will affect iron oxides nanoparticle's relaxivity. To identify the effect of surface coating to iron oxides nanoparticles, I employed 3 groups of amine functionalized Fe_3O_4 nanoparticles (A-MNPs) designed to attach with different amount of ATPES. I i) measured coating weight percentage and calculated relaxivities of the 3 samples; ii) added D_2O to nanoparticles dispersions to check NMR relaxation mechanisms of A-MNPs.

The three groups of A-MNPs are coated with different surface coating amount: 1.60 wt% for 5.6A-MNPs, 1.99 wt% for 7.5A-MNPs, and 2.80 wt% for 9.8A-MNPs. The corresponding surface relaxivities decreased from 105,000 μm/s to 94,100 μm/s to 78,300 μm/s. Among the 3 groups of A-MNPs, only 24% ~ 43% of the surface magnetic sites was occupied by APTES branches, leaving more than half of the surface Fe atoms accessible to water molecules and providing e-H relaxation which will dominate the overall surface relaxation rate of the nanoparticles.

The mechanisms by which surface coating reduces nanoparticles' relaxivity was studied by diluting A-MNPs with the least and most surface coating using different volume fractions of D_2O. When D_2O volume fraction increased from 0 vol% to 70 vol%, with Fe concentration of 0.002 g/L, 9.8A-MNPs with 2.80 wt% surface coating showed more reduction in surface relaxation rate (dropped by 34.5%) compared to 5.6A-MNPs with 1.60 wt% surface coating (dropped by 12.5%). It suggested that at very low nanoparticle concentration, e-H relaxation is less dominant due to the limited amount of Fe_3O_4; intermolecular H-H relaxation between ^1H in APTES braches and ^1H in water molecules contributed more to nanoparticle surface relaxation. My results indicate that A-MNPs with various coating amounts relax protons at nanoparticle surfaces mainly by e-H relaxation

and controls the overall relaxation of suspensions at higher Fe_3O_4 nanoparticles concentration. In this study, the maximum amount of APTES attached to nanoparticles was 2.80 wt%, covering only 43% of the Fe_3O_4 nanoparticle surface. In this case the effect of APTES in reducing relaxivities of the nanoparticle was limited. However, when APTES coating amount is increased, we would expect more nanoparticle surface occupied by APTES, leaving less Fe_3O_4 exposed to water molecules. Therefore, care should be taken when using nanoparticles with extensive surface coating.

To sum up, this project was intended to coat silica surfaces with a known quantity of nanoparticles and thus control the pore surface relaxivity. 30% ~ 40% retention of positively charged zirconia nanoparticles were observed in Boise sandstone cores after flushing with 2 pore volumes of DI water and HNO_3. Assuming a monolayer packing of nanoparticles on the pore walls, the maximum surface fraction that can be achieved by attached nanoparticles is 90.69%. With 30% ~ 40% of nanoparticles captured in sandstone cores, only 20.5% ~ 26.4% of pore surface were covered by attached nanoparticle via monolayer packing, the pore surface was not covered by nanoparticles to full capacity. Electrostatic repulsion between nanoparticles may prevent nanoparticles from getting too close to each other on the pore surface and thus limit the adsorption amount. Due to interactions between nanofluids and pore surfaces, nanoparticles picked up paramagnetic ions from the pore surface, causing the nanoparticles' relaxivities to increase and thus making the calculation and prediction of altered sandstone surface relaxivity more complicated. Based on my results, it is currently not practical to coat pore surfaces completely with a nanoparticle monolayer. Further study on how to prevent adsorption of paramagnetic species onto nanoparticles, and how to increase nanoparticle attachment to pore surfaces, is necessary to ensure constant nanoparticle relaxivity and predictable value of pore surface with attached nanoparticles.

Table 7.1 Property summary of four nanoparticle dispersions studied in this project.

Nanoparticles	Label	Size (nm)	Surface charge	Relaxivity (μm/s)
zirconia	ZR-AL	90~110	positive	1.427
zirconia	ZR-BL	70~80	negative	1.095
PEG coated Silica	Si-B	20~30	negative	0.0722
APTES coated Fe_3O_4	A-MNPs	70~100	negative	78,300~105,000

In this study, as displayed in Table 7.1, four groups of nanoparticles were studied: ZR-AL, ZR-BL, Si-B, and A-MNPs. Among those samples, A-MNPs with high relaxivity will help increase the pore surface relaxivity if attached on to pore surface. However, with negative surface charge of silica under natural conditions (Revil, 1999a, b), it is not easy for the negatively charged A-MNPs to adsorb onto pore surface. However, it is possible that A-MNPs can be employed to attach onto positive pore surfaces and control surface relaxivity such as calcite. With low relaxivity and negative surface charge, Si-4B is not a good candidate to coat silica pore surface or control pore surface relaxivity. For zirconia nanoparticles, ZR-BL nanoparticles were observed to be retained in Boise sandstone at very low fraction (2% to 3%) and not at all in glass bead packs; ZR-AL was retained better in glass bead packs (11.6%) and Boise sandstone (30% to 40%), resulting in an appreciable alteration of pore surface relaxivity via adsorption onto pore surface. However, due to their relatively small relaxivities, attachment of paramagnetic ions on the zirconia nanoparticles increased their surface relaxivity, which makes it complicate to link the attached amount of nanoparticles and altered pore surface relaxivity since the nanoparticle relaxivity is variable. Hence, even with the evidence that positively charged zirconia nanoparticles can attach to silica surfaces and alter the pore surface relaxivity, due to their low relaxivity and vulnerability to the presence of paramagnetic ions, zirconia nanoparticles in this study may

need to be modified to increase relaxivity and/or to prevent adsorption of paramagnetic ions before they can be suitably applied for this purpose.

More generally, my work helps to understand factors that affect nanoparticles' surface relaxivities and the behavior of nanoparticles in porous media, and will be used in future studies of the pore-scale characteristics in rocks. In particular, my work highlights the complicated interplay between nanoparticles and rock surfaces that affect measurements of bulk properties. Understanding these complicating factors is essential to future applications that depend on coating grain surfaces or fluid interfaces with nanoparticles, such as enhanced oil recovery, imaging oil-water contacts, and determining interfacial surface areas.

7.2 FUTURE WORK

This project is a step toward the engineered control of surface relaxivity of porous media, which in turn would enable more robust inference of pore size distributions from NMR measurements, especially using logging tools. In my experiments, factors that many affect nanoparticles surface relaxivities were studied, however all the possible mechanisms of Fe(III) adsorbed onto positively charged zirconia nanoparticles were not well studied.

The known value of pore size and surface relaxivity of silica porous media enabled me to estimate adsorbed zirconia nanoparticles and modified surface relaxivity. To realize the end goal of being able to predict pore size distributions directly from NMR measurements with no prior knowledge of pore sizes, further work is necessary to understand the link between zeta potential differences between nanoparticles and substrates, quantity adsorbed, and overall relaxivity alteration.

My results indicated adsorption of positively charged nanoparticles onto silica surface. A separate experiment to study the adsorption of negatively charged nanoparticles

onto positive pore surface may broaden the applications and studies of nanoparticle-pore surface interaction and effect of adsorbed nanoparticles on pore surface relaxivity.

The experimental data showed that, even with an excess amount of nanoparticles in the pores, full coverage in a monolayer was never observed. It is possible that electrostatic repulsion between nanoparticles prevents them from settling next to each other on the pore surface. It will be useful to use DLVO theory to better analyze and predict the adsorption of nanoparticles on pore walls, and to provide guidance on suitable surface coatings that can promote this behavior.

In addition, I did not analyze how hydration layers on nanoparticles and pore surfaces will affect attachment of nanoparticles onto pore walls. Further study is required to identify the role of the hydration layer in nanoparticle adsorption and relaxation.

Appendix A

ARITHMETIC CALCULATIONS OF ERROR PROPAGATION

$$X = u \pm v$$

$$\sigma_X^2 = \sigma_{u \pm v}^2 = \sigma_u^2 \left(\frac{\partial X}{\partial u} \right)_{\bar{u}}^2 + \sigma_v^2 \left(\frac{\partial X}{\partial v} \right)_{\bar{v}}^2 = \sigma_u^2 + \sigma_v^2$$

$$X = uv$$

$$\sigma_X^2 = \sigma_{uv}^2 = \sigma_u^2 \left(\frac{\partial X}{\partial u} \right)_{\bar{u}}^2 + \sigma_v^2 \left(\frac{\partial X}{\partial v} \right)_{\bar{v}}^2 = \sigma_u^2 \bar{v}^2 + \sigma_v^2 \bar{u}^2$$

$$\left(\frac{\sigma_X}{\bar{u}\bar{v}} \right)^2 = \left(\frac{\sigma_{uv}}{\bar{u}\bar{v}} \right)^2 = \left(\frac{\sigma_u}{\bar{u}} \right)^2 + \left(\frac{\sigma_v}{\bar{v}} \right)^2$$

$$X = \frac{u}{v}$$

$$\sigma_X^2 = \sigma_{\frac{u}{v}}^2 = \sigma_u^2 \left(\frac{\partial X}{\partial u} \right)_{\bar{u}}^2 + \sigma_v^2 \left(\frac{\partial X}{\partial v} \right)_{\bar{v}}^2 = \frac{\sigma_u^2}{\bar{v}^2} + \frac{\sigma_v^2 \bar{u}^2}{\bar{v}^4}$$

$$\left(\frac{\sigma_X}{\frac{\bar{u}}{\bar{v}}} \right)^2 = \left(\frac{\sigma_{\frac{u}{v}}}{\frac{\bar{u}}{\bar{v}}} \right)^2 = \left(\frac{\sigma_u}{\bar{u}} \right)^2 + \left(\frac{\sigma_v}{\bar{v}} \right)^2$$

X: function of u and v (u and v are independent measured varibles from an experiment)

σ_X: standard deviation of X

σ_u: standard deviation of u

σ_v: standard deviation of v

Appendix B

RAW NMR DATA

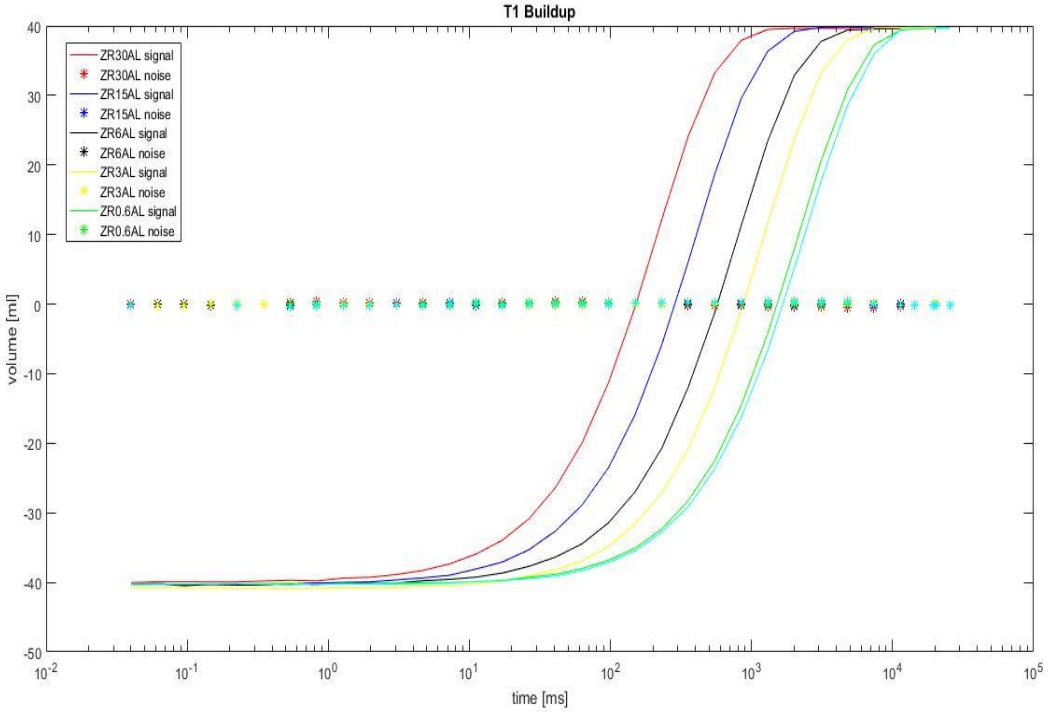

Figure B-1. T_1 relaxation of ZR-AL dispersions with different nanoparticle weight percentage. x axis is time, y axis is measured sample volume after correction with H index.

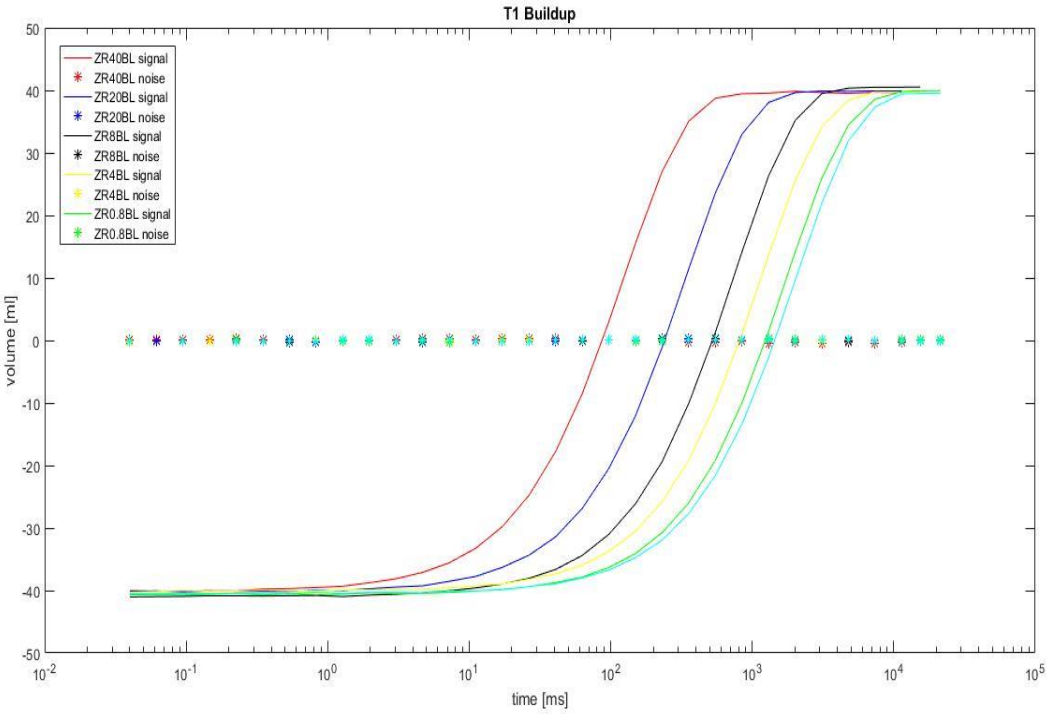

Figure B-2. T_1 relaxation of ZR-BL dispersions with different nanoparticle weight percentage. x axis is time, y axis is measured sample volume after correction with H index.

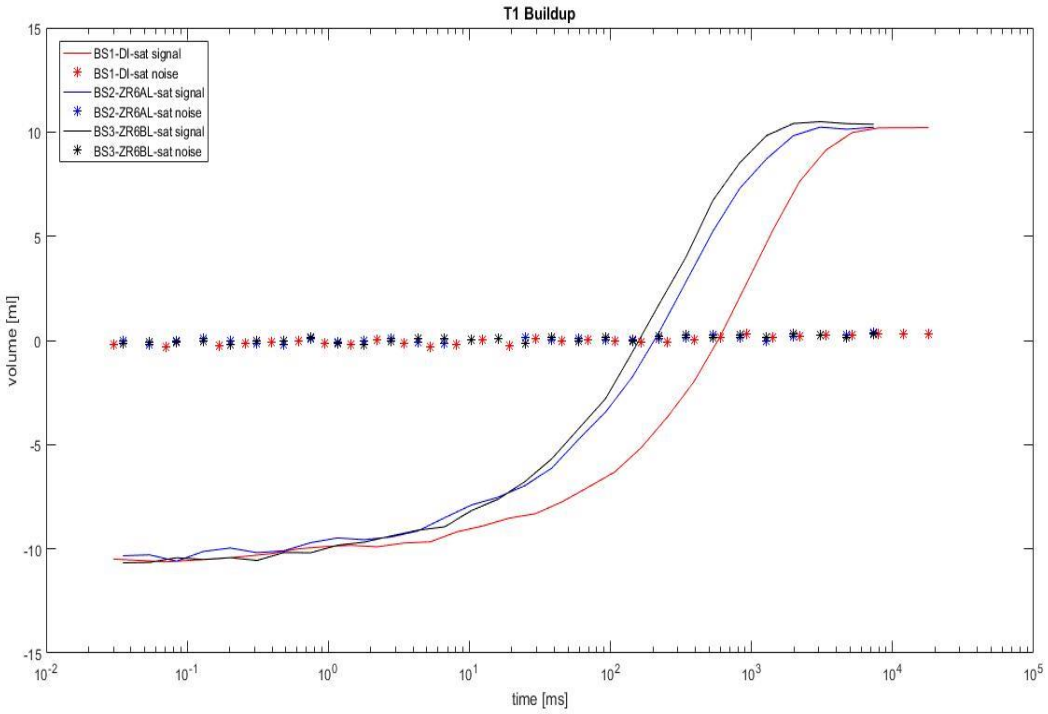

Figure B-3. T_1 relaxation of 3 saturated Boise sandstone cores: BS1, BS2, BS3. They are saturated with DI water, ZR-6AL, and ZR-6BL nanoparticle dispersions, respectively. x axis is time, y axis is measured sample volume after correction with H index.

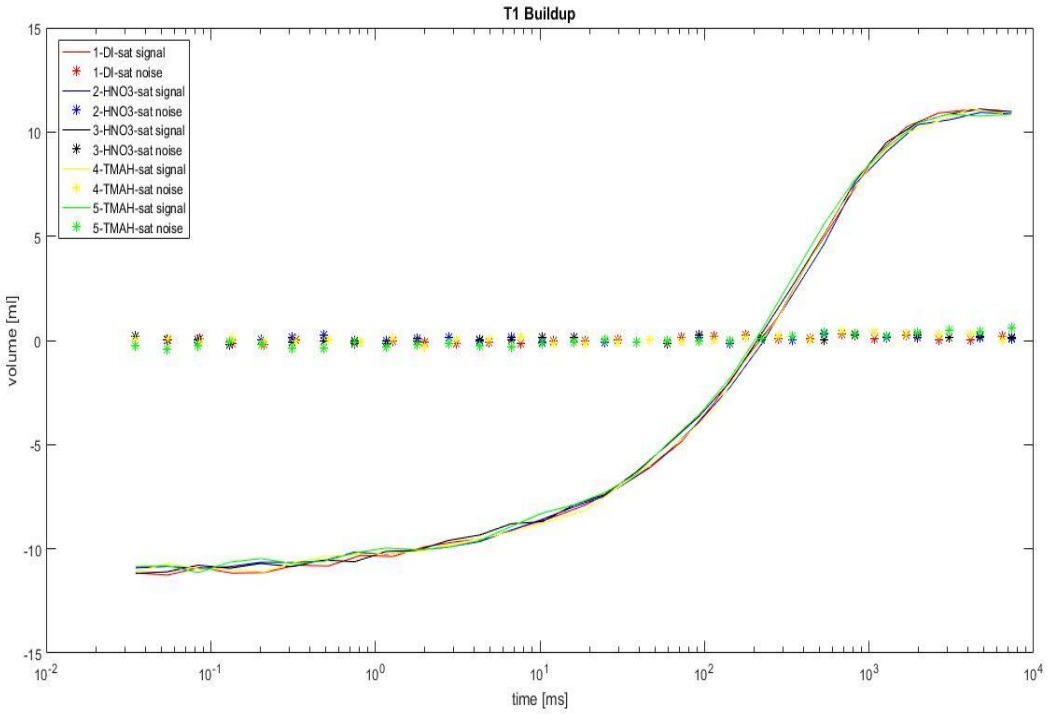

Figure B-4. T_1 relaxation of DI water, HNO_3, and TMAH saturated Boise sandstone cores for Cores #1-#5 after correction with H index. x axis is time, y axis is measured sample volume after correction with H index.

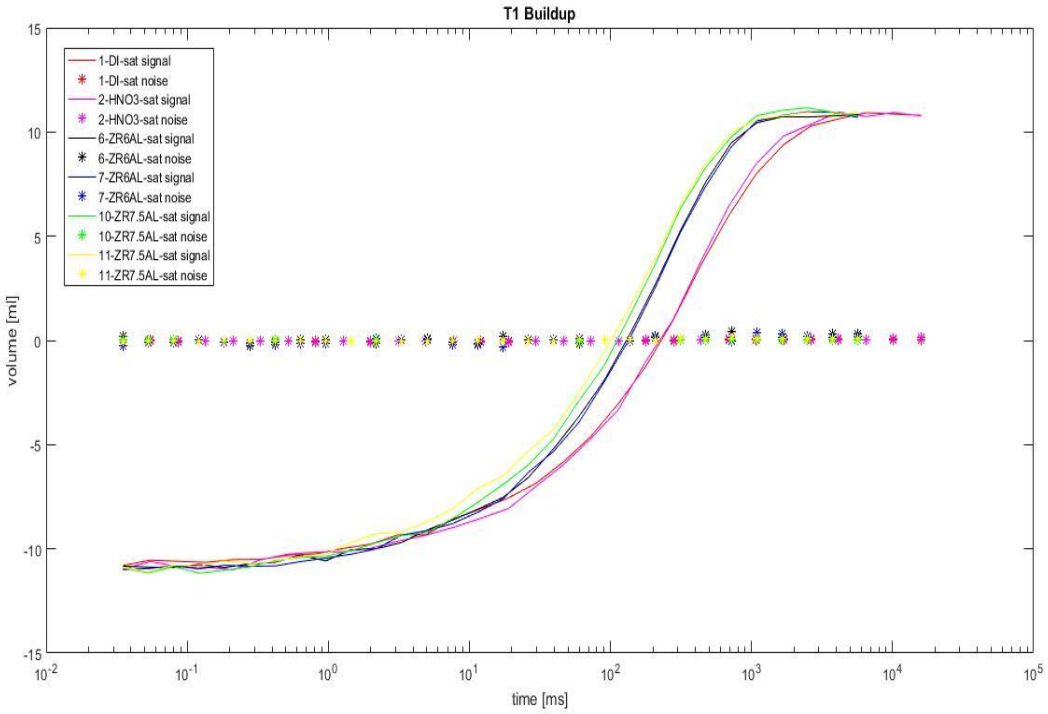

Figure B-5. T_1 relaxation of DI, HNO_3, ZR-6AL, and ZR-7.5AL dispersions saturated Boise sandstone cores for Cores #1, #2, #6, #7, #10, and #11 after correction with H index. x axis is time, y axis is measured sample volume after correction with H index.

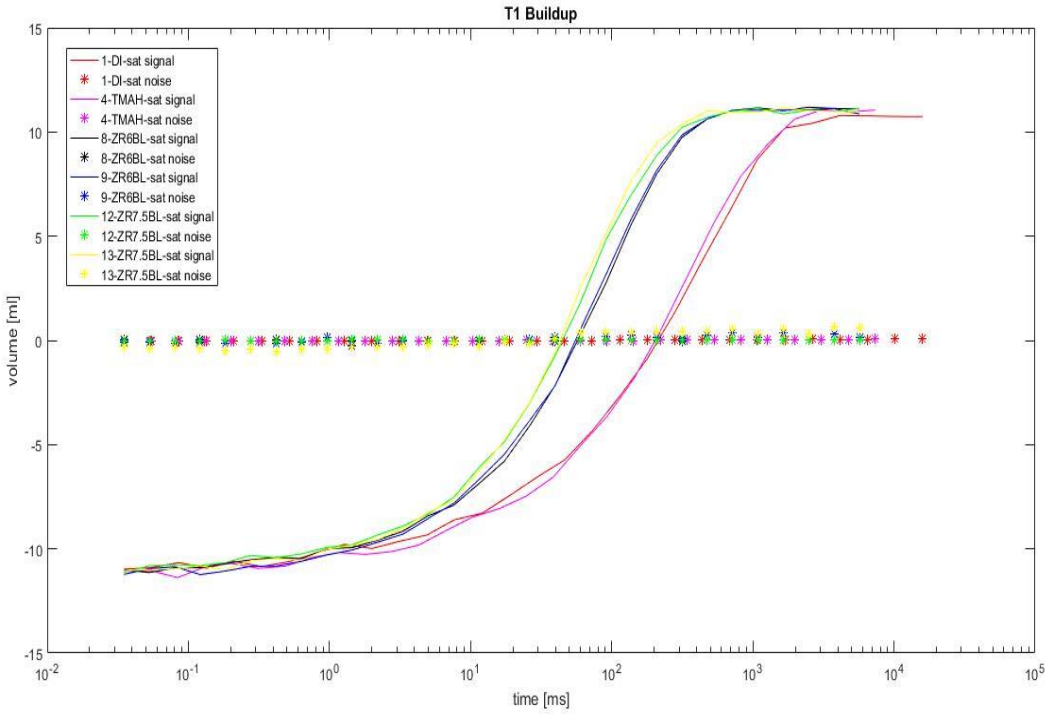

Figure B-6. T_1 relaxation of DI, TMAH, ZR-6BL, and ZR-7.5BL dispersions saturated Boise sandstone cores for Cores #1, #4, #8, #9, #12, and #13. x axis is time, y axis is measured sample volume after correction with H index.

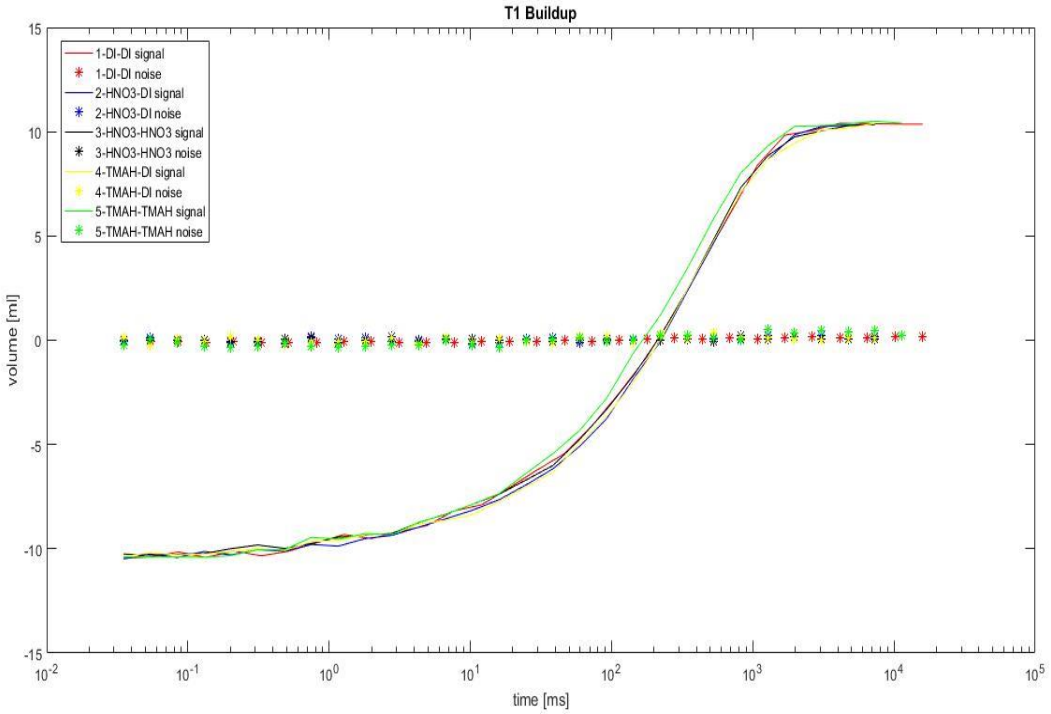

Figure B-7. T_1 relaxation of DI water, HNO_3, and TMAH saturated Boise sandstone cores for Cores #1-#5 after core flooding with pre-selected pure fluid for 2 pore volume. x axis is time, y axis is measured sample volume after correction with H index.

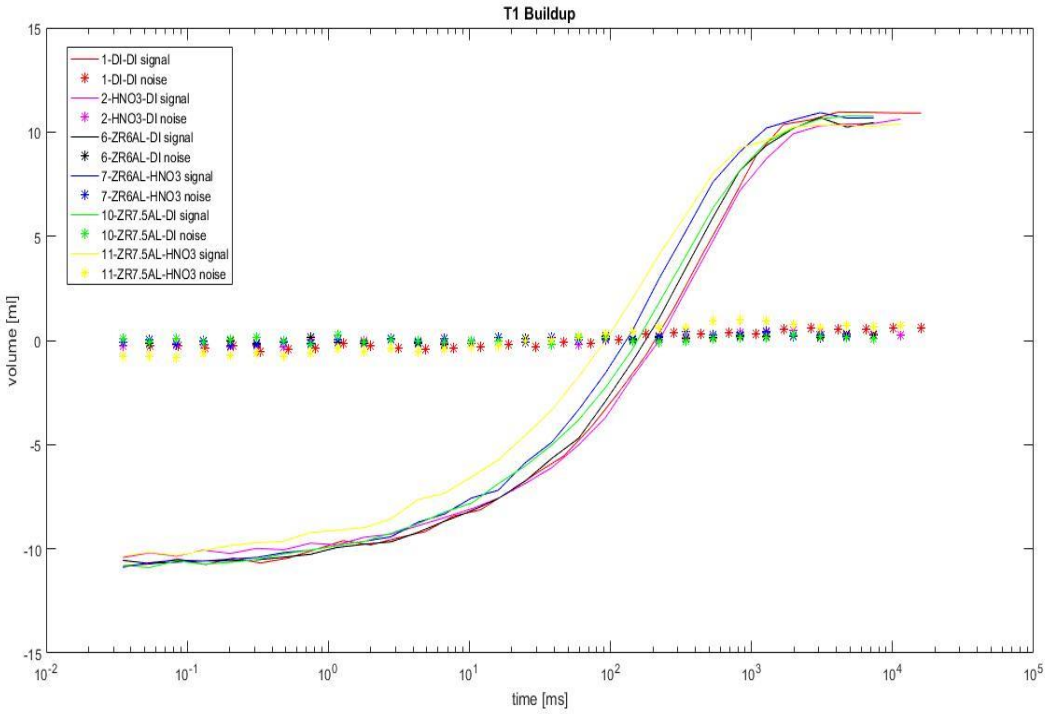

Figure B-8. T_1 relaxation of DI, HNO_3, ZR-6AL, and ZR-7.5AL saturated Boise sandstone cores for Cores #1, #2, #6, #7, #10, and #11 after core flooding with pre-selected pure fluid for 2 pore volume. x axis is time, y axis is measured sample volume after correction with H index.

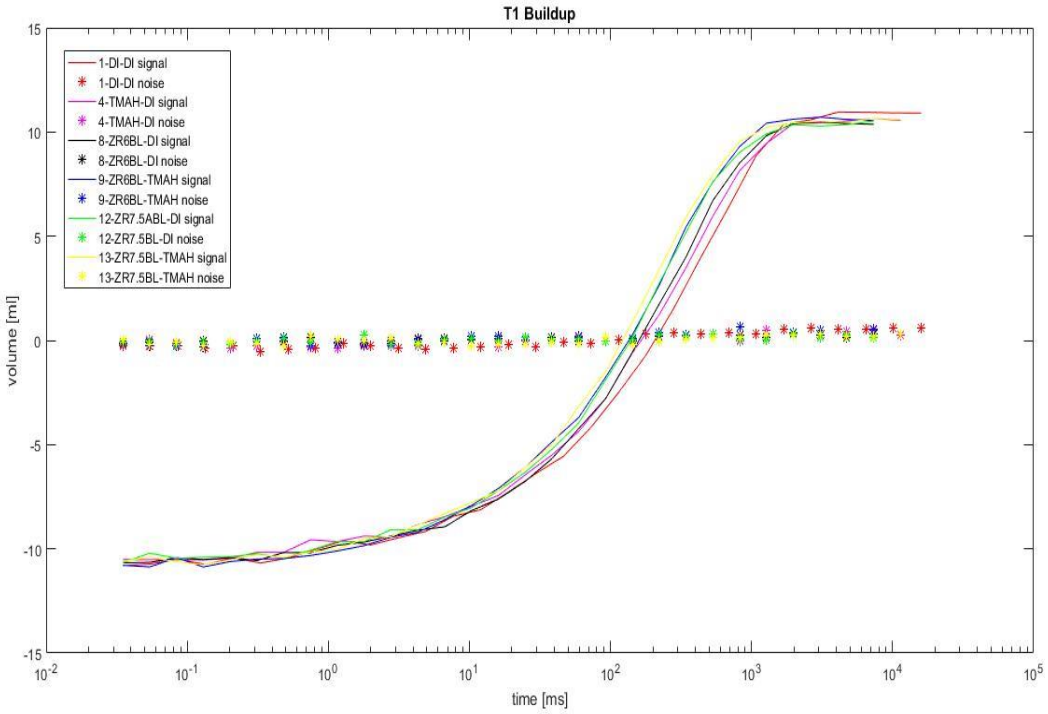

Figure B-9. T_1 relaxation of DI, TMAH, ZR-6BL, and ZR-7.5BL saturated Boise sandstone cores for Cores #1, #4, #8, #9, #12, and #13 after core flooding with pre-selected pure fluid for 2 pore volume. x axis is time, y axis is measured sample volume after correction with H index.

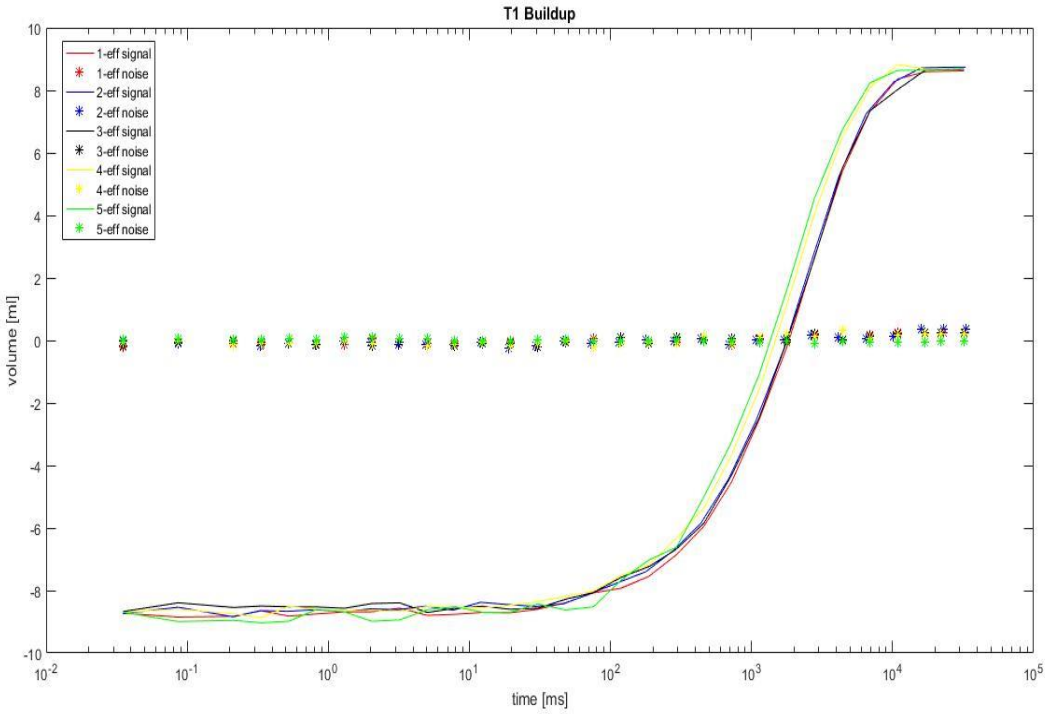

Figure B-10. T_1 relaxation of first 0.7 pore volume effluents from DI water, HNO_3, and TMAH saturated Boise sandstone cores for Cores #1-#5. x axis is time, y axis is measured sample volume after correction with H index.

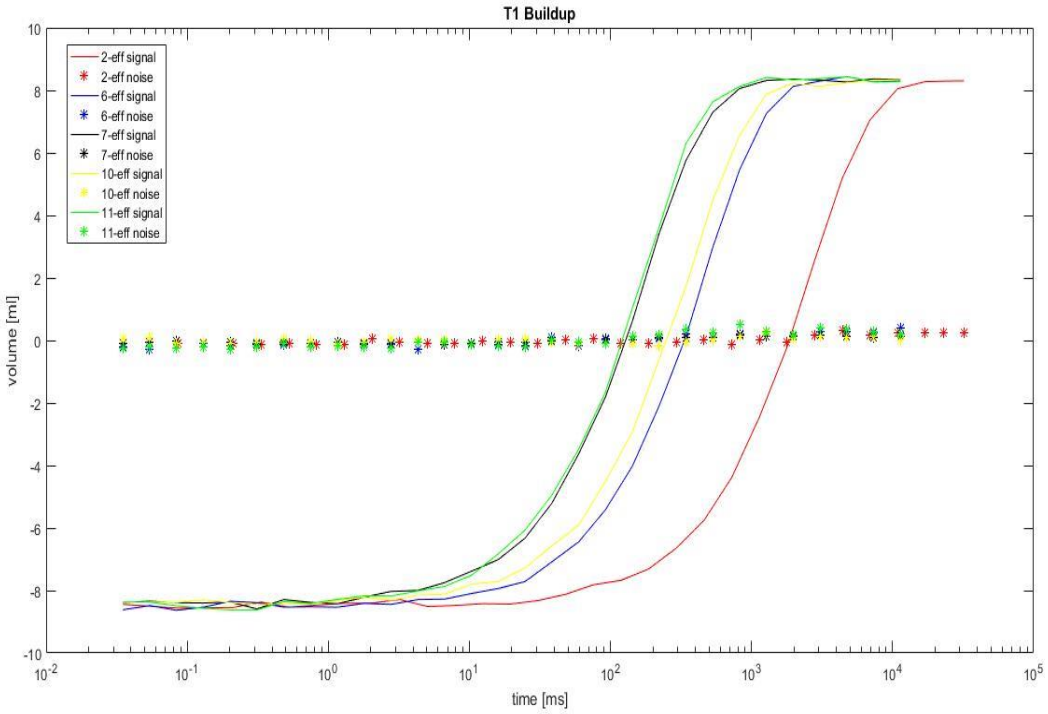

Figure B-11. T_1 relaxation of first 0.7 pore volume effluents from HNO_3, ZR-6AL, and ZR-7.5AL saturated Boise sandstone cores for Cores #2, #6, #7, #10, and #11. x axis is time, y axis is measured sample volume after correction with H index.

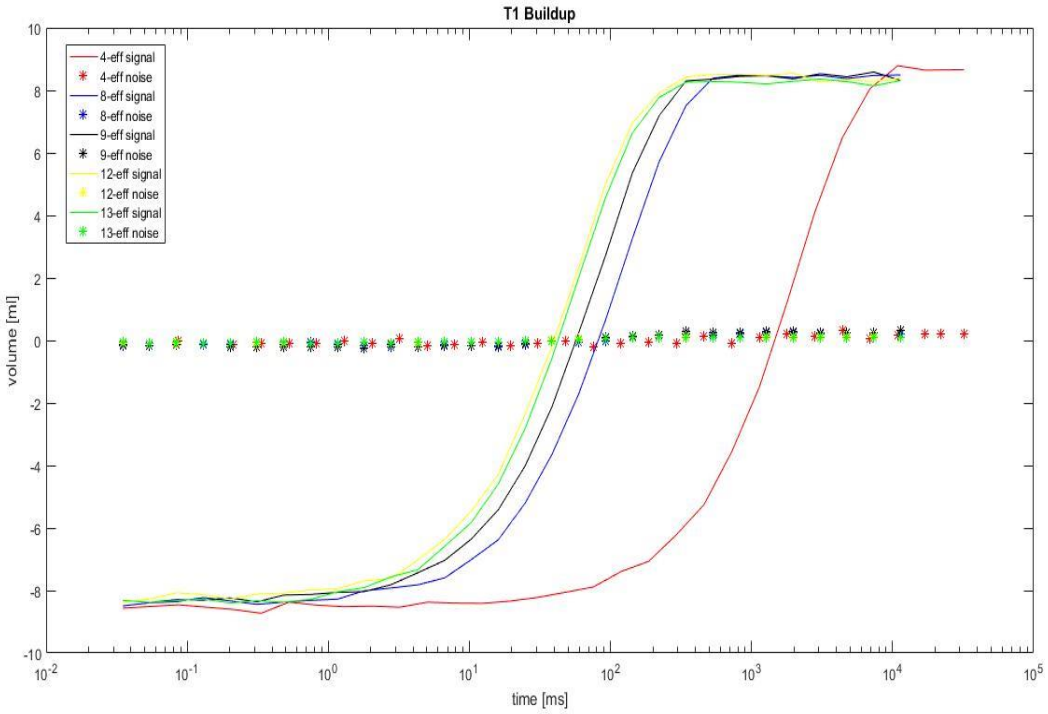

Figure B-12. T_1 relaxation of first 0.7 pore volume effluents from TMAH, ZR-6BL, and ZR-7.5BL saturated Boise sandstone cores for Cores #4, #8, #9, #12, and #13. x axis is time, y axis is measured sample volume after correction with H index.

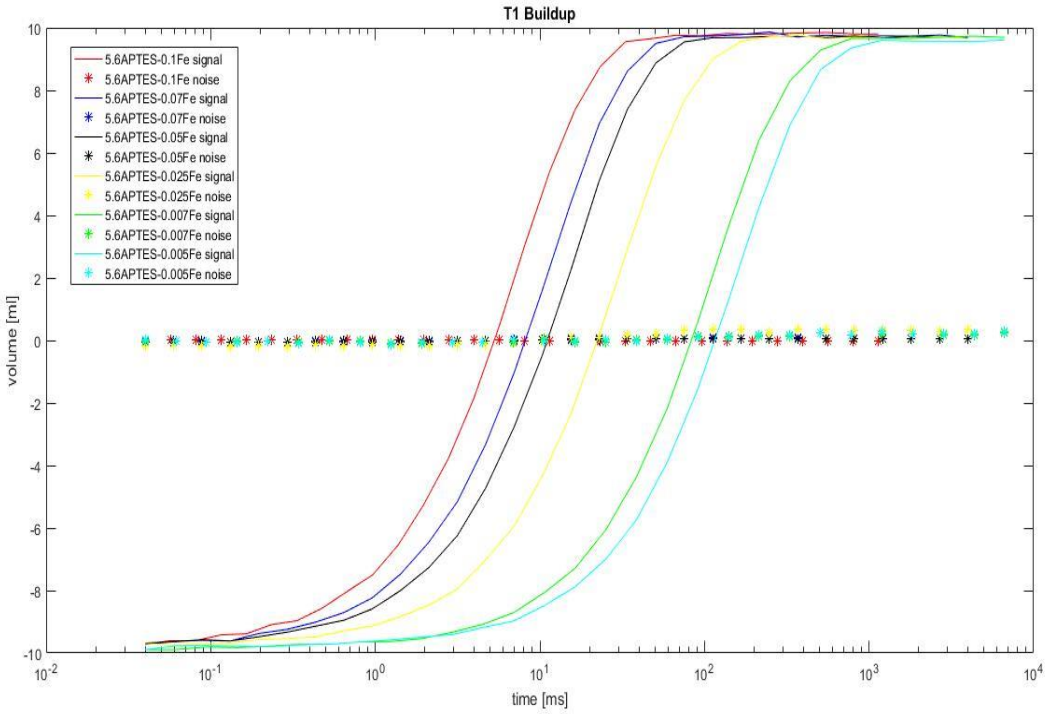

Figure B-13. T_1 relaxation of 5.6A-MNPs dispersions with different nanoparticle concentration. x axis is time, y axis is measured sample volume after correction with H index.

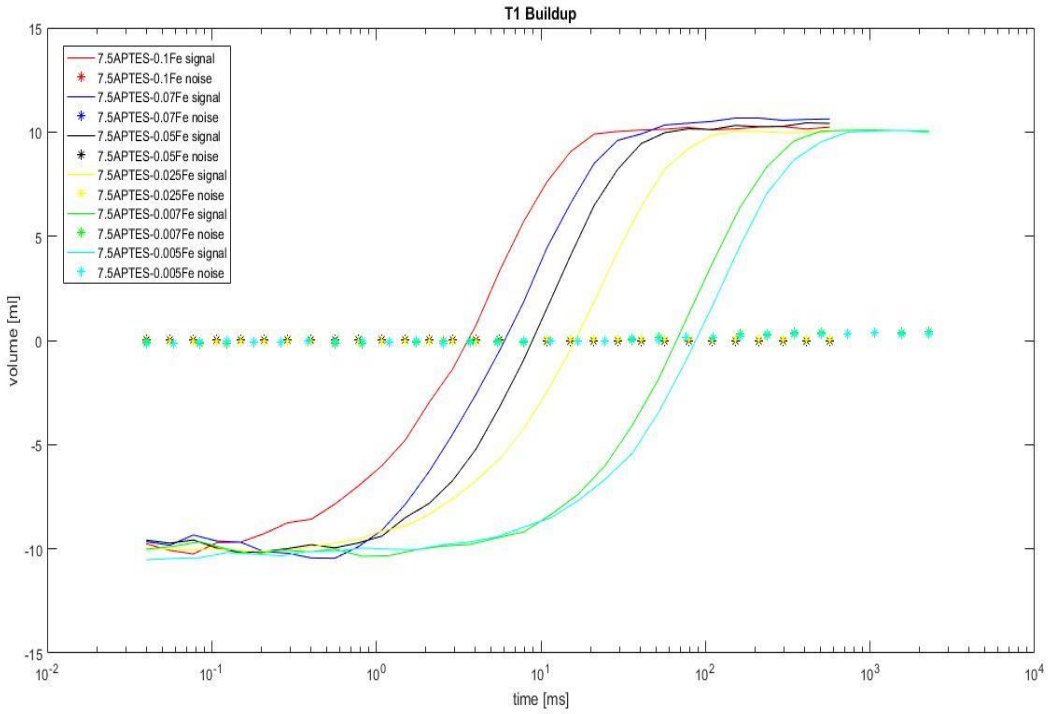

Figure B-14. T_1 relaxation of 7.5A-MNPs dispersions with different nanoparticle concentration. x axis is time, y axis is measured sample volume after correction with H index.

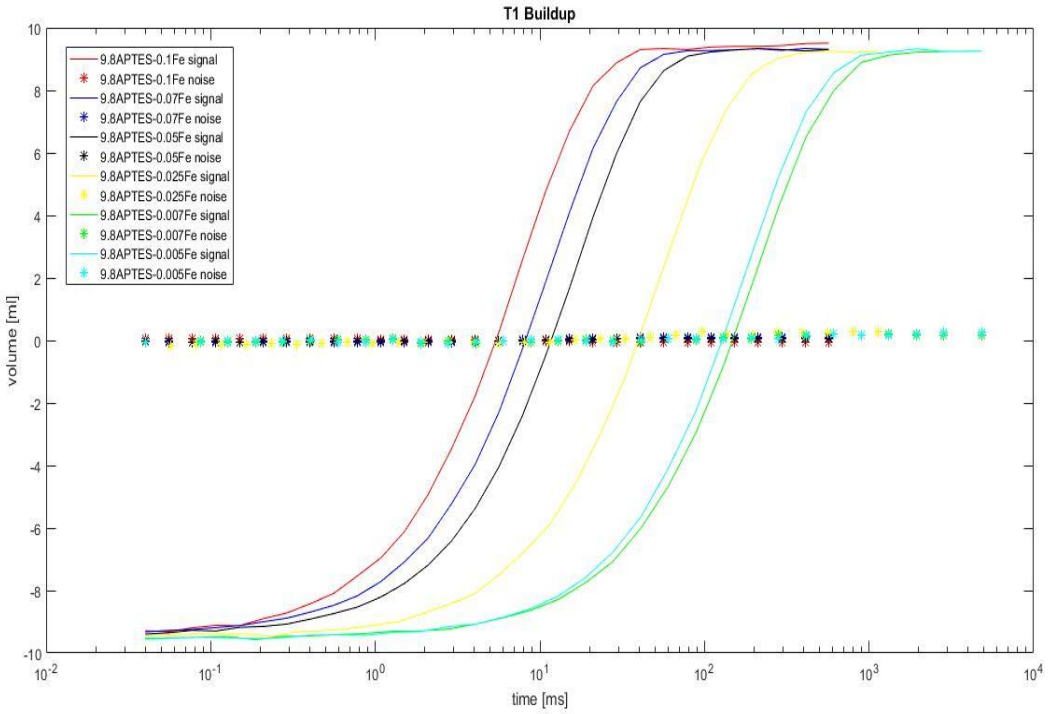

Figure B-15. T_1 relaxation of 9.8A-MNPs dispersions with different nanoparticle concentration. x axis is time, y axis is measured sample volume after correction with H index.

References

Abragam, A. (1961). *Principles of nuclear magnetism*. Oxford, UK: Oxford University Press.

Allen, D., Crary, S., & Freedman, B. (1998). How to use borehole nuclear magnetic resonance. *Oceanographic Literature Review*, *3*(45), 586-587.

Anand V., Hirasaki, G. J. (2008). Paramagnetic relaxation in sandstones: Distinguishing T_1 and T_2 dependence on Surface relaxation, Internal gradients and dependence on echo Spacing. *Journal of Magnetic Resonance*, *190*(1), 68-65.

Arawole, S. S. (2015). Multiple Approaches To Characterizing Pore Structure For A Range Of Sandstones Samples.

Babes, L., Denizot, B., Tanguy, G., Le Jeune, J. J., & Jallet, P. (1999). Synthesis of iron oxide nanoparticles used as MRI contrast agents: a parametric study. *Journal of Colloid and Interface Science*, *212*(2), 474-482.

Bagaria, H. G., Yoon, K. Y., Neilson, B. M., Cheng, V., Lee, J. H., Worthen, A. J., Xue, Z., Huh, C., Bryant, S. L., Bielawski, C. W., & Johnston, K. P. (2013). Stabilization of iron oxide nanoparticles in high sodium and calcium brine at high temperatures with adsorbed sulfonated copolymers. *Langmuir*, *29*(10), 3195-3206.

Bee, A., Massart, R., & Neveu, S. (1995). Synthesis of very fine maghemite particles. *Journal of Magnetism and Magnetic Materials*, *149*(1-2), 6-9.

Bertini, I., Capozzi, F., Luchinat, C., & Zhicheng, X. (1993). Nuclear and electron relaxation of Fe $(OH_2)_6^{3+}$. *Journal of Physical Chemistry*, *97*(6), 1134-1137.

Bloembergen, N. (1956). Spin relaxation processes in a two-proton system. *Physical Review*, *104*(6), 1542.

Bloembergen, N., & Morgan, L. O. (1961). Proton relaxation times in paramagnetic solutions. Effects of electron spin relaxation. *The Journal of Chemical Physics*, *34*(3), 842-850.

Bloembergen, N., Purcell, E. M., & Pound, R. V. (1948). Relaxation effects in nuclear magnetic resonance absorption. *Physical Review*, *73*(7), 679.

Brownstein, K. R., & Tarr, C. E. (1979). Importance of classical diffusion in NMR studies of water in biological cells. *Physical Review A*, *19*(6), 2446.

Bryar, T. R., Daughney, C. J., & Knight, R. J. (2000). Paramagnetic effects of iron (III) species on nuclear magnetic relaxation of fluid protons in porous media. *Journal of Magnetic Resonance*, *142*(1), 74-85.

Caldelas, F. M. (2010). Experimental parameter analysis of nanoparticle retention in porous media (Doctoral dissertation).

Caminiti, R., & Magini, M. (1979). An X-ray diffraction study on the first and the second hydration shell of the Fe (III) ion in nitrate solutions. *Chemical Physics Letters*, *61*(1), 40-44.

Carmichael, R. S. (1982). *CRC Handbook of Physical Properties of Rocks*. Boca Raton, FL: CRC Press, Inc.

Carr, H. Y., & Purcell, E. M. (1954). Effects of diffusion on free precession in nuclear magnetic resonance experiments. *Physical Review*, *94*(3), 630.

Carter, R. S., Harley, S. J., Power, P. P., & Augustine, M. P. (2005). Use of NMR spectroscopy in the synthesis and characterization of air-and water-stable silicon nanoparticles from porous silicon. *Chemistry of Materials*, *17*(11), 2932-2939.

Chang, H. C., & Wang, L. C. (2010). A simple proof of Thue's Theorem on circle packing. *arXiv preprint arXiv*:1009.4322.

Cheng, K., Aderibigbe, A., Alfi, M., Heidari, Z., & Killough, J. (2014a). Quantifying the impact of petrophysical properties on spatial distribution of contrasting nanoparticle agents. In *SPWLA 55th Annual Logging Symposium*. Society of Petrophysicists and Well-Log Analysts.

Cheng, K., Chi, L., & Heidari, Z. (2014b). Improved assessment of pore-size distribution and pore connectivity in multiple-porosity systems using superparamagnetic iron oxide nanoparticles and NMR measurements. In *SPE Annual Technical Conference and Exhibition*. Society of Petroleum Engineers.

Chertok, B., Moffat, B. A., David, A. E., Yu, F., Bergemann, C., Ross, B. D., & Yang, V. C. (2008). Iron oxide nanoparticles as a drug delivery vehicle for MRI monitored magnetic targeting of brain tumors. *Biomaterials*, *29*(4), 487-496.

Coates, G. R., Xiao, L., & Prammer, M. G. (1999). *NMR Logging: Principles and Applications*. Houston, TX: Gulf Professional Publishing.

Cornell, R. M., & Schwertmann, U. (2003). *The Iron Oxides: Structure, Properties, Reactions, Occurrences and Uses*. New York, NY: John Wiley & Sons.

Császár, A. G., Czakó, G., Furtenbacher, T., Tennyson, J., Szalay, V., Shirin, S. V., Zobov, N. F. & Polyansky, O. L. (2005). On equilibrium structures of the water molecule. The Journal of chemical physics, 122(21), 214305.

Dai, C., & Hu, Y. (2014). Fe (III) hydroxide nucleation and growth on quartz in the presence of Cu (II), Pb (II), and Cr (III): metal hydrolysis and adsorption. *Environmental Science & Technology*, *49*(1), 292-300.

Daigle, H., & Dugan, B. (2011). An improved technique for computing permeability from NMR measurements in mudstones. *Journal of Geophysical Research: Solid Earth*, *116*(B8), B08101.

Daigle, H., & Johnson, A. (2016). Combining mercury intrusion and nuclear magnetic resonance measurements using percolation theory. *Transport in Porous Media*, *111*(3), 669-679.

Daigle, H., Thomas, B., Rowe, H., & Nieto, M. (2014). Nuclear magnetic resonance characterization of shallow marine sediments from the Nankai Trough, Integrated Ocean Drilling Program Expedition 333. *Journal of Geophysical Research: Solid Earth*, *119*(4), 2631-2650.

Diehl, P. S., Fluck, E., & Kosfeld, R. (1969). *NMR: Basic Principles and Progress*. Berlin: Springer-Verlag.

Dousma, J., & De Bruyn, P. L. (1976). Hydrolysis-precipitation studies of iron solutions. I. Model for hydrolysis and precipitation from Fe (III) nitrate solutions. *Journal of Colloid and Interface Science*, *56*(3), 527-539.

Enhessari, M., Razi, M. K., Etemad, L., Parviz, A., & Sakhaei, M. (2014). Structural, optical and magnetic properties of the Fe2TiO5 nanopowders. *Journal of Experimental Nanoscience*, *9*(2), 167-176.

Fernández-Toledano, J. C., Moncho-Jordá, A., Martínez-López, F., & Hidalgo-Álvarez, R. (2006). Theory for interactions between particles in monolayers. In *Colloidal Particles at Liquid Interfaces*, edited by B. P. Binks & T. S. Horozov, pp. 108-151.

Fleury, M. (2007). NMR surface relaxivity determination using NMR apparent diffusion curves and BET measurements. In *International Symposium of the Society of Core Analysts, Calgary, Canada*.

Foley, I., Farooqui, S. A., & Kleinberg, R. L. (1996). Effect of paramagnetic ions on NMR relaxation of fluids at solid surfaces. *Journal of Magnetic Resonance, Series A*, *123*(1), 95-104.

Freedman, R., Heaton, N., Flaum, M., Hirasaki, G. J., Flaum, C., & Hürlimann, M. (2003). Wettability, saturation, and viscosity from NMR measurements. *SPE Journal*, *8*(4), 317-327.

Ganesan, K., Damle, R., & Ramakrishna, J. (1990). ChemInform Abstract: Proton NMR study of molecular dynamics in hydrazinium perchlorate. *ChemInform,21*(20).

Gaudin, A. M., & Fuerstenau, D. W. (1955). Streaming potential studies. Quartz flotation with anionic collectors. *Mining Eng.*, *7*.

Godinez, I. G., & Darnault, C. J. (2011). Aggregation and transport of nano-TiO 2 in saturated porous media: effects of pH, surfactants and flow velocity. *Water Research*, *45*(2), 839-851.

Gupta, A. K., & Gupta, M. (2005). Cytotoxicity suppression and cellular uptake enhancement of surface modified magnetic nanoparticles. *Biomaterials*, *26*(13), 1565-1573.

Hill, R. J., Craig, J. R., & Gibbs, G. V. (1979). Systematics of the spinel structure type. *Physics and Chemistry of Minerals*, *4*(4), 317-339.

Hinedi, Z. R., Chang, A. C., Anderson, M. A., & Borchardt, D. B. (1997). Quantification of microporosity by nuclear magnetic resonance relaxation of water imbibed in porous media. *Water Resources Research*, *33*(12), 2697-2704.

Hu, J., Chen, G., & Lo, I. M. (2005). Removal and recovery of Cr (VI) from wastewater by maghemite nanoparticles. *Water Research*, *39*(18), 4528-4536.

Iler, R. K. (2004). *The Chemistry of Silica: Solubility, Polymerization, Colloid and Surface Properties, and Biochemistry*. New York, NY: Wiley.

Ishido, T., & Mizutani, H. (1981). Experimental and theoretical basis of electrokinetic phenomena in rock-water systems and its applications to geophysics. *Journal of Geophysical Research: Solid Earth*, *86*(B3), 1763-1775.

Israelachvili, J., & Wennerstrom, H. (1996). Role of hydration and water structure in biological and colloidal interactions. *Nature*, *379*(6562), 219.

Issa, B., Qadri, S., Obaidat, I. M., Bowtell, R. W., & Haik, Y. (2011). PEG coating reduces NMR relaxivity of $Mn_{0.5}Zn_{0.5}Gd_{0.02}Fe_{1.98}O_4$ hyperthermia nanoparticles. *Journal of Magnetic Resonance Imaging*, *34*(5), 1192-1198.

Jordan, A., Scholz, R., Maier-Hauff, K., Johannsen, M., Wust, P., Nadobny, J., ... & Lanksch, W. (2001). Presentation of a new magnetic field therapy system for the treatment of human solid tumors with magnetic fluid hyperthermia. *Journal of Magnetism and Magnetic Materials*, *225*(1), 118-126.

Keating, K., & Knight, R. (2008). A laboratory study of the effect of magnetite on NMR relaxation rates. *Journal of Applied Geophysics*, *66*(3), 188-196.

Keesom, W. H., Zelenka, R. L., & Radke, C. J. (1988). A zeta-potential model for ionic surfactant adsorption on an ionogenic hydrophobic surface. *Journal of Colloid and Interface Science*, *125*(2), 575-585.

Kenyon, W. E., & Kolleeny, J. A. (1995). NMR surface relaxivity of calcite with adsorbed Mn^{2+}. *Journal of Colloid and Interface Science*, *170*(2), 502-514.

Kim, J. K., & Lawler, D. F. (2005). Characteristics of zeta potential distribution in silica particles. *Bulletin of the Korean Chemical Society*, *26*(7), 1083-1089.

Kleinberg, R. L., & Horsfield, M. A. (1990). Transverse relaxation processes in porous sedimentary rock. *Journal of Magnetic Resonance*, *88*(1), 9-19.

Kleinberg, R. L., Kenyon, W. E., & Mitra, P. P. (1994). Mechanism of NMR relaxation of fluids in rock. *Journal of Magnetic Resonance, Series A*, *108*(2), 206-214.

Ko, S., Lee, H., & Huh, C. (2016). Efficient removal of enhanced-oil-recovery polymer from produced water with magnetic nanoparticles and regeneration/reuse of spent particles. *SPE Production & Operations*, in press.

Ko, S., Prigiobbe, V., Huh, C., Bryant, S. L., Bennetzen, M. V., & Mogensen, K. (2014). Accelerated oil droplet separation from produced water using magnetic nanoparticles. In *SPE Annual Technical Conference and Exhibition*. Society of Petroleum Engineers.

Koenig, S. H., & Brown, R. D. (1987). Relaxometry of paramagnetic-ions in tissue. *Metal Ions in Biological Systems*, *21*, 229-270.

Korb, J. P., Whaley-Hodges, M., & Bryant, R. G. (1997). Translational diffusion of liquids at surfaces of microporous materials: Theoretical analysis of field-cycling magnetic relaxation measurements. *Physical Review E*, *56*(2), 1934.

Korringa, J., Seevers, D. O., & Torrey, H. C. (1962). Theory of spin pumping and relaxation in systems with a low concentration of electron spin resonance centers. *Physical Review*, *127*(4), 1143.

Krohn, C. E. (1988). Fractal measurements of sandstones, shales, and carbonates. *Journal of Geophysical Research, 93*(B4), 3297-3305.

Li, H. C., & De Bruyn, P. L. (1966). Electrokinetic and adsorption studies on quartz. *Surface Science*, *5*(2), 203-220.

Lu, W., Senapati, D., Wang, S., Tovmachenko, O., Singh, A. K., Yu, H., & Ray, P. C. (2010). Effect of surface coating on the toxicity of silver nanomaterials on human skin keratinocytes. *Chemical Physics Letters*, *487*(1), 92-96.

Magini, M., & Caminiti, R. (1977). On the structure of highly concentrated iron (III) salt solutions. *Journal of Inorganic and Nuclear Chemistry*, *39*(1), 91-94.

Mansfield, P., & Pykett, I. L. (1978). Biological and medical imaging by NMR. *Journal of Magnetic Resonance (1969)*, *29*(2), 355-373.

McDonald, P. J., Korb, J. P., Mitchell, J., & Monteilhet, L. (2005). Surface relaxation and chemical exchange in hydrating cement pastes: a two-dimensional NMR relaxation study. *Physical Review E*, *72*(1), 011409.

Mehta, P., Huh, C., & Bryant, S. L. (2014, December). Evaluation of superparamagnetic nanoparticle-based heating for flow assurance in subsea flowlines. In *International Petroleum Technology Conference*. International Petroleum Technology Conference.

Meiboom, S., & Gill, D. (1958). Modified spin-echo method for measuring nuclear relaxation times. *Review of Scientific Instruments*, *29*(8), 688-691.

Morgan, F. D., Williams, E. R., & Madden, T. R. (1989). Streaming potential properties of westerly granite with applications. *Journal of Geophysical Research: Solid Earth*, *94*(B9), 12449-12461.Na, H. B., Song, I. C., & Hyeon, T. (2009). Inorganic nanoparticles for MRI contrast agents. *Advanced Materials*, *21*(21), 2133-2148.

Nelson, P. H. (2009). Pore-throat sizes in sandstones, tight sandstones, and shales. *AAPG Bulletin*, *93*(3), 329-340.

Ogolo, N. A., Olafuyi, O. A., & Onyekonwu, M. O. (2012, January). Enhanced oil recovery using nanoparticles. In *SPE Saudi Arabia Section Technical Symposium and Exhibition*. Society of Petroleum Engineers.

Oh, J., Feldman, M. D., Kim, J., Condit, C., Emelianov, S., & Milner, T. E. (2006). Detection of magnetic nanoparticles in tissue using magneto-motive ultrasound. *Nanotechnology*, *17*(16), 4183.

Oldenburg, C. M., Borglin, S. E., & Moridis, G. J. (2000). Numerical simulation of ferrofluid flow for subsurface environmental engineering applications. *Transport in Porous Media*, *38*(3), 319-344.

Overbeek, J. T. G. (1952). Electrochemistry of the double layer. *Colloid Science*, *1*, 115-193.

Persson, I. (2010). Hydrated metal ions in aqueous solution: how regular are their structures?. *Pure and Applied Chemistry*, *82*(10), 1901-1917.

Petri-Fink, A., Steitz, B., Finka, A., Salaklang, J., & Hofmann, H. (2008). Effect of cell media on polymer coated superparamagnetic iron oxide nanoparticles (SPIONs): colloidal stability, cytotoxicity, and cellular uptake studies. *European Journal of Pharmaceutics and Biopharmaceutics*, *68*(1), 129-137.

Pettijohn, F. J. (1963). *Data of Geochemistry: Chemical Composition of Sand-Stones--Excluding Carbonate and Volcanic Sands* (No. 440). Washington, DC: US Government Printing Office.

Pfeifer, H. (1972). Nuclear magnetic resonance and relaxation of molecules adsorbed on solids. *NMR Basic Principles and Progress, 7*, 55-153.

Pride, S. (1994). Governing equations for the coupled electromagnetics and acoustics of porous media. *Physical Review B*, *50*(21), 15678.

Prodanović, M., Ryoo, S., Rahmani, A. R., Kuranov, R. V., Kotsmar, C., Milner, T. E., & Huh, C. (2010). Effects of magnetic field on the motion of multiphase fluids containing paramagnetic nanoparticles in porous media. In *SPE Improved Oil Recovery Symposium*. Society of Petroleum Engineers.

Revil, A., Pezard, P. A., & Glover, P. W. (1999a). Streaming potential in porous media: 1. Theory of the zeta potential. *Journal of Geophysical Research: Solid Earth, 104*(B9), 20021-20031.

Revil, A., Schwaeger, H., Cathles, L. M., & Manhardt, P. D. (1999b). Streaming potential in porous media: 2. Theory and application to geothermal systems. *Journal of Geophysical Research: Solid Earth*, *104*(B9), 20033-20048.

Rodriguez Pin, E., Roberts, M., Yu, H., Huh, C., & Bryant, S. L. (2009). Enhanced migration of surface-treated nanoparticles in sedimentary rocks. In *SPE Annual Technical Conference and Exhibition*. Society of Petroleum Engineers.

Ryoo, S., Rahmani, A. R., Yoon, K. Y., Prodanović, M., Kotsmar, C., Milner, T. E., & Huh, C. (2012). Theoretical and experimental investigation of the motion of multiphase fluids containing paramagnetic nanoparticles in porous media. *Journal of Petroleum Science and Engineering*, *81*, 129-144.

Ryu, S. (2009). Effect of inhomogeneous surface relaxivity, pore geometry and internal field gradient on NMR logging: Exact and perturbative theories and numerical investigations. In *SPWLA 55th Annual Logging Symposium*. Society of Petrophysicists and Well-Log Analysts.

Senturia, S. D., & Robinson, J. D. (1970). Nuclear spin-lattice relaxation of liquids confined in porous solids. *SPE Journal*, *10*(03), 237-244.

ShamsiJazeyi, H., Miller, C. A., Wong, M. S., Tour, J. M., & Verduzco, R. (2014). Polymer-coated nanoparticles for enhanced oil recovery. *Journal of Applied Polymer Science*, *131*(15).

Sis, H., & Birinci, M. (2009). Effect of nonionic and ionic surfactants on zeta potential and dispersion properties of carbon black powders. *Colloids and Surfaces A: Physicochemical and Engineering Aspects*, *341*(1), 60-67.

Solomon, I. (1955). Relaxation processes in a system of two spins. *Physical Review*, *99*(2), 559.

Stuart, M. C., Fleer, G. J., Lyklema, J., Norde, W., & Scheutjens, J. M. H. M. (1991). Adsorption of ions, polyelectrolytes and proteins. *Advances in Colloid and Interface Science*, *34*, 477-535.

Tang, F., Huang, X., Zhang, Y., & Guo, J. (2000). Effect of dispersants on surface chemical properties of nano-zirconia suspensions. *Ceramics International*, *26*, 93-97.

Vane, L. M., & Zang, G. M. (1997). Effect of aqueous phase properties on clay particle zeta potential and electro-osmotic permeability: Implications for electro-kinetic soil remediation processes. *Journal of Hazardous Materials*, *55*(1-3), 1-22.

Vuong, Q. L., Van Doorslaer, S., Bridot, J. L., Argante, C., Alejandro, G., Hermann, R., Disch, S., Mattea, C., Stapf, S., & Gossuin, Y. (2012). Paramagnetic nanoparticles as potential MRI contrast agents: characterization, NMR relaxation, simulations and theory. *Magnetic Resonance Materials in Physics, Biology and Medicine*, *25*(6), 467-478.

Wang, Q., Prigiobbe, V., Huh, C., Bryant, S. L., Mogensen, K., & Bennetzen, M. V. (2014). Removal of divalent cations from brine using selective adsorption onto magnetic nanoparticles. In *International Petroleum Technology Conference*. International Petroleum Technology Conference.

Wang, R., Pavlin, T., Rosen, M. S., Mair, R. W., Cory, D. G., & Walsworth, R. L. (2005). Xenon NMR measurements of permeability and tortuosity in reservoir rocks. *Magnetic Resonance Imaging*, *23*(2), 329-331.

Wang, Y., Li, Y., Fortner, J. D., Hughes, J. B., Abriola, L. M., & Pennell, K. D. (2008). Transport and retention of nanoscale C60 aggregates in water-saturated porous media. *Environmental Science & Technology*, *42*(10), 3588-3594.

Washburn, K. E. (2014). Relaxation mechanisms and shales. *Concepts in Magnetic Resonance Part A*, *43*(3), 57-78.

Wong, P. (1999). *Methods in the Physics of Porous Media*. San Diego, CA: Academic Press.

Xue, Z., Foster, E., Wang, Y., Nayak, S., Cheng, V., Ngo, V. W., Pennell, K. D., Bielawski, C. W., & Johnston, K. P. (2014). Effect of grafted copolymer composition on iron oxide nanoparticle stability and transport in porous media at high salinity. *Energy & Fuels*, *28*(6), 3655-3665.

Yu, H., Kotsmar, C., Yoon, K. Y., Ingram, D. R., Johnston, K. P., Bryant, S. L., & Huh, C. (2010). Transport and retention of aqueous dispersions of paramagnetic nanoparticles in reservoir rocks. In *SPE Improved Oil Recovery Symposium*. Society of Petroleum Engineers.

Yu, H., Yoon, K. Y., Neilson, B. M., Bagaria, H. G., Worthen, A. J., Lee, J. H., Cheng, V., Bielawski, K. P., Bryant, S. L., & Huh, C. (2014). Transport and retention of aqueous dispersions of superparamagnetic nanoparticles in sandstone. *Journal of Petroleum Science and Engineering*, *116*, 115-123.

Zhang, Y., Chen, Y., Westerhoff, P., & Crittenden, J. (2009). Impact of natural organic matter and divalent cations on the stability of aqueous nanoparticles. *Water Research*, *43*(17), 4249-4257.

Zhou, J., Qiao, X., Binks, B. P., Sun, K., Bai, M., Li, Y., & Liu, Y. (2011). Magnetic Pickering emulsions stabilized by Fe3O4 nanoparticles. *Langmuir*, *27*(7), 3308-3316.

Zhu, C., Daigle, H., & Bryant, S. (2015). Nuclear magnetic resonance investigation of surface relaxivity modification by paramagnetic nanoparticles. In *SPE Annual Technical Conference and Exhibition*. Society of Petroleum Engineers.

Zhu, C., Daigle, H., & Bryant, S. L. (2016). Paramagnetic nanoparticles as nuclear magnetic resonance contrast agents in sandstone: Importance of nanofluid-rock interactions. *Interpretation*, *4*(2), SF55-SF65.